ABSTRACT

LI, LIPING. Near-Far Resistant Ultra-Wideband Communications in Multiple-Access Environments. (Under the direction of Dr. J. Keith Townsend).

Ultra-Wideband (UWB) systems promise high data rate and accurate localization capabilities for communications, imaging, sensor networks, and vehicular systems. The simple UWB receiver structure is especially attractive to applications which require low cost and low power consumption. However, the envisioned simple receiver designs are also fraught with challenges ranging from estimation of highly frequency-selective multipath channels to synchronization of received signals consisting of very narrow pulses. In this context, transmitted reference (TR) UWB systems have been proposed in the literature as one way to avoid computationally intensive channel estimation while still maintaining a relatively simple receiver structure.

In this dissertation, we investigate the performance of TR UWB communication systems in multiple-access environments. We remove the commonly invoked assumption of perfect power control and include in our analysis an additional group of users which have power levels much higher than the desired user. The detrimental effects of high-power users are suppressed by chip discrimination in this dissertation. To yield a straightforward mapping between the number of equal-power users and the variance of the resulting MAI, we incorporate the power delay profile (PDP) of the channel in the analysis, which makes the theoretical analysis tractable. This analytical technique of using PDP is also applied to analyze the MAI in frequency-shifted reference (FSR) UWB systems.

The near-far problem also arises for synchronization when high-power users are included in the network. In this dissertation, we propose and investigate a synchronization procedure which is near-far resistant. By exploiting the structure of interfering power levels, we devise an efficient suppression technique which only requires the knowledge of the spreading code of the desired user. Complex matrix operations required by other techniques found in the CDMA literature are not required in our suppression process. We also propose a new dimension-based technique for the detection of the code phase based on the suppressed signal. Simulation results validate our proposed near-far resistant synchronization technique and the superior performance is shown when compared to the current literature.

Near-Far Resistant Ultra-Wideband Communications in Multiple-Access Environments

by
Liping Li

A dissertation submitted to the Graduate Faculty of
North Carolina State University
in partial fullfillment of the
requirements for the Degree of
Doctor of Philosophy

Electrical Engineering

Raleigh, North Carolina

2009

APPROVED BY:

Dr. Bojko Bakalov	Dr. Brian Hughes
Dr. Huaiyu Dai	Dr. Robert Ulman
Dr. J. Keith Townsend Chair of Advisory Committee	

DEDICATION

To my husband and parents, only with their ever-lasting support can I go after my dreams.

BIOGRAPHY

Liping Li received her B.S. in electrical engineering from Southwest University of Science and Technology in June 2002. After the undergraduate study, she joined University of Science and Technology of China where she was involved with a large project in Ultra Wideband (UWB) communications. In June 2005, she received the M.S. in electrical engineering from University of Science and Technology of China. From August 2005, she began pursuing her PhD in electrical engineering in North Carolina State University with Dr. J. Keith Townsend. During the career in NC State University, she worked on multiple access analysis for UWB systems and published several papers. She is now working on near-far resistant synchronization techniques for UWB communications.

ACKNOWLEDGMENTS

I would like to thank my advisor, Dr. J. Keith Townsend, for his guidance during my beginning days at NC State University. He understood how difficult it was for me to face a totally different environment and gave me advices whenever I needed. I am also grateful for his supervision of my research, for all the discussions when I was frustrated, and for numerous corrections of my research papers (Imagine how painful it is for him to revise the papers given that I'm not a native speaker!)

My heartfelt thanks need to be dedicated to the other advisory committee members who have been very supportive either in classes or in research.

I am especially in debt to my husband, Wei Leng, for his encouragement at times when there seemed to be no hope. I can not thank him enough for his sacrifices to make my PhD possible.

I also appreciate the encouragement from one particular colleague from University of Science and Technology of China, Han Huang, who is a great engineer and played an important role in my engineering road.

TABLE OF CONTENTS

LIST OF TABLES

LIST OF FIGURES

Chapter 1

Introduction

Ultra Wideband (UWB) communications systems received a renewed attention in 2002 when Federal Communications Commission (FCC) allocated the $3.1 - 10.6$ GHz band for its usage [1]. The allowed power emission level for UWB wireless communications in [1] is extremely low (at the thermal noise level), which enables the coexistence of UWB systems with the legacy systems such as the Global Positioning System (GPS) and IEEE 802.11 wireless local area networks (WLANs). One type of UWB systems, known as impulse radio (IR), results in a very simple receiver structure where intermediate frequency (IF) processing is not required. This feature gives UWB systems an advantage in low-cost receiver designs. The low-power spectral density, low-cost features make UWB systems suitable in applications such as real-time, high-data-rate home entertainment systems, sensor networks, and systems that can exploit the geolocation capability of UWB.

Despite the envisioned advantages, UWB systems are also fraught with implementation challenges. Impulse radio UWB uses narrow pulses on the order of sub-nanoseconds duration, modulated either in time or in amplitude. In a multipath environment, hundreds

or thousands of echos of the narrow pulses can be resolved by the receiver. This results in a large diversity gain which can be exploited to improve the performance. It is shown that over fifty fingers in a Rake receiver are required to achieve a satisfactory performance [2]. The complexity in implementing a large number of Rake fingers and the computationally intensive estimation of the channel (required by a Rake receiver) have inspired alternative approaches such as transmitted reference (TR) signaling [3, 4, 5, 6, 7, 8, 9, 10, 11, 12, 13, 14, 15], a scheme which dates back to the 60s [16].

In this dissertation, we investigate the multiple access issues for TR UWB systems in multipath environments. Networks under consideration include both a large number of active interfering users that have power levels similar to or lower than the desired user, and a small number of users with much higher power levels than the desired user. We differentiate these two types of interference as: interference from equal-power users (the conventional multiple-access interference, MAI) and interference from high-power users. Therefore, the near-far effects are included in the analysis. With the existence of the near-far problem, we also investigate the synchronization issue for UWB systems. In the following sections, we provide essential background investigations of the subjects in this dissertation as well as our contributions to the investigated subjects.

1.1 Transmitted Reference UWB Systems

In TR UWB systems, signaling is carried out by transmitting a reference pulse before each data-bearing pulse separated by a time interval less than the coherence time of the channel. Therefore a pulse pair is transmitted in each frame as seen in Fig. 1.2 (a frame is the time period a pulse or a pulse pair is transmitted, which is different from the ‘frame’

in computer networks). In contrast, conventional UWB systems transmit one pulse in each frame (Fig. 1.1). Typically multiple pulse/pulse pairs are transmitted per symbol. The number of times a pulse (or pulse pair) is transmitted per symbol is called the repetition factor, denoted by N_s in this dissertation. In Fig. 1.1 and Fig. 1.2, $N_s = 3$.

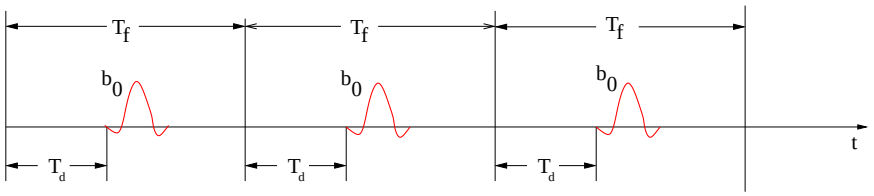

Figure 1.1: Conventional UWB systems transmit one pulse in each frame.

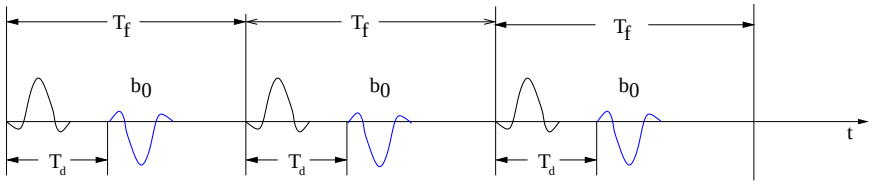

Figure 1.2: TR UWB systems transmit a pulse pair in each frame.

The separation of the two pulses, T_d, is set to be less than the coherence time of the channel so that the reference pulse and the data-bearing pulse are affected by approximately the same channel conditions. In the signaling example in Fig. 1.2, pulse amplitude modulation is used. The main advantage of TR systems over UWB systems with Rake receivers is that TR systems do no require channel estimation, while Rake receivers require channel estimation for each finger. The structure of a TR receiver is shown in Fig. 1.3. By

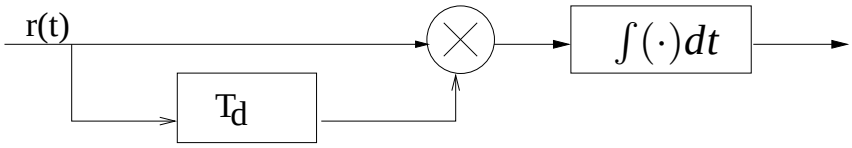

Figure 1.3: A standard TR UWB receiver has a delay element which aligns the reference signal with the data-bearing signal.

using a delay line, the reference signal is aligned with the data-bearing signal and the correlation is computed between these two signals. The reference signal serves as a template to demodulate the data-bearing signal and a large diversity gain is achieved in this way. The advantage of TR systems also comes from the more relaxed synchronization requirements [17, 18, 19] compared to UWB systems with Rake receivers [20, 21, 22].

TR systems, as any other systems, have disadvantages. One disadvantage is that the reference pulses do not convey information, thus resulting in a 3 dB energy penalty when compared to conventional UWB systems. The reference signal of TR systems is noisy since it is corrupted by at least the additive white Gaussian noise (AWGN). Just as differentially modulated systems, the noise power doubles for TR systems at high SNR. Another disadvantage of TR systems is the difficulty in implementing the analog delay line used to align the reference signal and the data-bearing signal. This difficulty is somewhat resolved by another signaling scheme, frequency-shifted reference (FSR) UWB systems which do not require analog delay lines at the receiver. Performance of FSR systems relative to TR UWB systems is studied in Chapter 3.

1.2 Multiple Access Interference in TR UWB Systems

Performance of single-link TR UWB systems is studied in [4, 5, 6, 7, 8, 9, 10, 11, 12]. Multiple-access (MA) performance of TR UWB systems is investigated in [13], [14], and [15]. In these papers, all active users in the network are assumed to have power levels equal to the desired user at the receiver side and their interference is assumed to be Gaussian distributed. The assumption that all users have the same power levels as the desired user frequently does not hold in ad-hoc wireless communications where centralized power control is not employed due to survivability and complexity constraints. Therefore in this dissertation, we consider UWB networks where transmitters in close proximity ("high-power") to a receiver cause significant interference with the desired signal due to the much larger power levels of these signals. We also include a large number of active interfering users that have power levels similar to or lower than the desired user. Performance is quantified under the combined effect of equal-power and high-power users.

1.2.1 High-power Users

In networks without power control, the received power levels from interfering users can vary over many 10's of dB. But this group of high-power users is not included in the MA analysis in the current literature [13, 14, 15]. By including the users with much higher power levels than the desired user in this dissertation, we make the MA analysis more general. The authors of [14] concluded that the optimal transmission strategy is to concentrate the transmission power in one frame for TR UWB systems. In the presence of high-power users, traditional MA suppression techniques such as in [15] do not guarantee satisfactory performance. Chip discrimination, proposed in [23, 24] for AWGN channels and studied in

[25] with multipath channels, is applied in this dissertation to achieve satisfactory performance even in environments exhibiting the so called near-far problem. Our investigation in [26] suggests that for TR UWB systems using binary PAM, the optimal transmission strategy differs from that in [14] which only included equal-power users, and we show how the optimal transmission strategy depending on the system parameters.

The constraint on TR UWB systems to have a large spacing between pulses plus the requirement of chip discrimination to have a low duty cycle results in a low data rate for TR systems. Although the data rate can be increased for TR systems by decreasing the separation time between pulses [15], the data rate is at least somewhat dependent on the delay spread of the channel. In this dissertation, we also investigate one technique, M-ary PPM, to improve the data rate for TR UWB systems in the presence of high-power users. Impulse radio using M-ary PPM has been investigated in a number of settings for UWB systems with Rake receivers [27, 28, 29, 30]. The current literature for TR UWB systems focuses on binary modulation schemes [14, 15]. Performance of the synchronization function of the receiver is investigated for M-ary TR systems in [31]. Our results in the study of high-power interference are published in [32].

1.2.2 Equal-power Users

TR UWB Systems

The work on multiple-access performance of binary TR UWB systems can be found in [13, 14, 15]. In these papers, all active users in the network are assumed to have equal power at the receiver and their interference is assumed to be Gaussian distributed. The Gaussian assumption for interference from equal-power users for UWB systems with a Rake receiver

is used in the literature, for example, [33], [27], and is evaluated in [34, 28, 35, 36, 37, 38]. For a binary TR UWB system, simulation is used to validate this Gaussian assumption of the interference from equal-power users in [14]. The noisy template and the typically longer integration time of the receiver in TR UWB systems makes the Gaussian assumption for MAI more accurate when compared to UWB systems with Rake receivers.

In this dissertation, we use the Gaussian assumption to model the effect of equal-power users and focus on providing a theoretically tractable performance evaluation for TR UWB systems with M-ary PPM. Rather than using simulations to show the bit-error-probability (BEP) performance with MAI as found in [14] and [15], we incorporate the power delay profile (PDP) of the channel, inspired by the work in [13], to derive the variance of the MAI, enabling theoretical BEP analysis. The analysis we present in this dissertation reveals a general relationship between the variance of the MAI, the shape of the transmitted pulse, and the PDP of the channel. By applying an upper bound on the BEP, the number of equal-power users that the system can support is evaluated for different modulation order M. The network throughput in terms of the total bit rate is obtained based on the number of supported equal-power users. Tradeoffs between the system performance and complexity in implementing high-order modulation schemes are discussed. This theoretical contribution can also be used to address two fundamental issues of communications for TR UWB systems using M-ary PPM: 1) To determine the achievable data rate as a function of system resources. 2) To determine the required E_b/N_0 for the system to achieve a given BEP.

Note also that in this dissertation, the combined effects of both equal-power and high-power users are quantified, including the limit in the data rate in the presence of high-power users, and the optimization of the system performance by finding the optimal operational

parameters.

FSR UWB Systems

As discussed at the beginning of this chapter, TR UWB systems have been proposed to alleviate the implementation issues of UWB Rake receivers due to channel estimation and the need for a large number of Rake fingers. However, the wideband analog delay line used in TR receivers is difficult to implement in practice as well. A slightly frequency-shifted reference (FSR) UWB system has been introduced in [39] to retain the benefits of TR UWB systems while avoiding the analog delay line of TR systems. The single-link performance of FSR systems has been investigated in [39]. A lightly loaded system with a few users is considered in [40] where the number of users is constrained by the coherence bandwidth of the channel. In this dissertation, we consider general networks with no constraints on the number of users and the MA performance of FSR UWB systems is derived under both AWGN and multipath channel conditions.

The theoretical tool developed for obtaining the MA performance of TR systems is used for FSR systems: the power delay profile (PDP) of the multipath channel is incorporated in the analysis of the MA interference power. A theoretical comparison between FSR and TR UWB systems in a multiuser environment is presented in this dissertation which contributes to the current literature.

1.3 Near-Far Resistant Synchronization

The analysis in Section 1.2 is on the detection performance where synchronization has been established. Synchronization is also impacted in environments characterized by the

near-far problem.

In the UWB literature, narrow-band, single-tone interference is considered in [41, 42, 43] and reference therein, where techniques are investigated to suppress the narrow-band interference. Synchronization for UWB systems in the presence of wide-band multiple access interference (MAI) is studied in [44, 45, 46, 47, 48, 49]. All interfering users in these works are assumed to have power levels lower than or similar to the desired user. The works in [44, 48, 49] are based on the maximal likelihood (ML) criterion for achieving acquisition in multiple-access (MA) environments. The authors in [45, 46] investigate the search orders of the divided bins in the time domain while a frequency-domain procedure for synchronization is studied in [47].

In the CDMA literature, near-far resistant synchronization is studied in [50] where the code waveforms of all users are assumed to be known by the receiver and the complexity is generally high since a global maximization is performed upon all users. In [51], blind synchronization is carried out for users with equal power levels without the knowledge of the codes from all users. Synchronization in a near-far environment which only requires knowledge of the desired user's code is investigated in [52] and [53]. However either the subspace method in [52] or the ML procedure in [53] involves matrix operations (inversions, for example) which makes the methodologies too computationally intensive for UWB communications.

In this dissertation, we investigate the coarse (symbol level) synchronization in environments where there is no power control for UWB communication networks. The power levels from interfering users at the desired receiver can vary over many tens of dB. Assuming no knowledge of interfering users' codes, we propose an easy-to-implement procedure

in this dissertation to suppress the high-power interfering signals, which uses the fact that the signs of cross correlations between received symbols are determined by dominant signal waveforms from high-power interfering users. Using the knowledge of signs of cross correlations plus the knowledge of the desired user's spreading code, the procedure retains symbols for subsequent processing only when high-power interfering waveforms are combined destructively. Due to the so-called edge effect, we find that the signals from high-power interfering users can not be completely canceled. However the dimension of interfering signals after the suppression procedure is considerably reduced.

We also propose a new dimension-based estimation technique to estimate the code phase from the suppressed signal. The issue of threshold setting is discussed for implementing the dimension detection technique. The suppression procedure and the subsequent dimension detection has low complexity compared with methods in [52] and [53] and requires no additional resources for synchronization than traditional UWB receivers.

1.4 Organization of the Dissertation

In this chapter we have given a literature review of the MAI analysis for TR UWB and FSR UWB systems and the synchronization issues faced by UWB systems. Our contributions are interleaved in the discussions of the current literature. We present the system structures and the receiver signal processing in Chapter 2, laying out the parameters and statistics which are used throughout this dissertation. Chapter 3 is the analysis of the performance in the presence of high-power users. Chip discrimination is applied in this analysis. The interfering power caused by equal-power users is analyzed in Chapter 4, where the PDP of the channel is incorporated in the analysis to yield a tractable expression of the

variance of the MAI. In Chapter 5, a near-far resistant synchronization technique is proposed which is shown to have superior performance when compared to techniques found in the current literature. Concluding remarks are given in Chapter 6 where some future work is also discussed.

Chapter 2

System Model

In this chapter, the communication environments, including the channel model and the network structure, are presented first. A key assumption used throughout this dissertation is that the network is decentralized, resulting in no power control among users. The traditional UWB signaling and the received signals are then discussed, followed by the signaling and the receiver structures of transmitted reference (TR) and slightly frequency-shifted reference (FSR) UWB systems.

The parameters and notations defined in this chapter are used throughout this dissertation. To differentiate the signals associated with different systems, we use subscript 'c' to represent signals for conventional UWB systems, subscript 's' the signals for standard TR systems (binary), and subscript 'd' the signals for differential TR systems (binary). For signals from TR systems with M-ary PPM, no subscripts are used. Unless stated otherwise, the superscript 'u' in this dissertation represents terms from user u. Among all users, user 1 is always the user of interest, or the desired user.

2.1 Communication Environments

2.1.1 Network Structure

Perfect power control is commonly assumed in UWB networks in the literature, for example by a central node, as found in [33, 54, 27, 34, 28, 35, 36, 37]. Synchronization is assumed established in these works. Although some of the papers, such as [33] and [54], have analysis with general power levels, the final results are shown assuming perfect power control and no measures are taken to suppress the effects from high-power interfering users. The near-far problem is not considered in the aforementioned works. The authors in [23, 24] assumed no power control in the network and proposed a technique, chip discrimination, to protect the desired user from the detrimental effects caused by high-power interfering users. For transmitted reference (TR) UWB systems, multiple-access analysis is found in [13, 14, 15] where users are assumed to have equal power levels. For works related to the synchronization issue in UWB systems, power control is also assumed [44, 45, 46, 47, 48, 49].

In this dissertation, we consider UWB and TR UWB networks without perfect power control. The received signals from different users can have power levels varying over many 10's of dB. We group the users as: the desired user, users with power levels similar to or lower than the desired user (group 1), and users with power levels much higher than the desired user (group 2). As pointed out in Section 1.2, the users in group 1 are called the equal-power interfering users and users in group 2 the high-power interfering users. Denote N_u as the number of users in the network, which is split as $N_u = N_e + N_h + 1$, with N_e and N_h the number of equal-power and high-power interfering users, respectively. Our inves-

tigations in TR UWB systems consider networks with both equal-power and high-power users [26, 55, 32]. Interference caused by equal-power users is called by the conventional name – multiple access interference or MAI – in this dissertation to differentiate from interference caused by high-power users. By including high-power users for both detection and synchronization, the results in this dissertation are more general.

2.1.2 Channel Model

Let $h^{(u)}(t)$ be the impulse response of the channel experienced by user u. The multipath channel used in this dissertation is based on the channel models from [56] and [57], which is written as

$$h^{(u)}(t) = X^{(u)} \sum_{l=0}^{L-1} \alpha_l^{(u)} \delta(t - \tau_l^{(u)}) \tag{2.1}$$

where $X^{(u)}$ is the log-normal shadowing factor experienced by user u. Note that the multipath channel model from [56] has the total energy contained in the multipath components normalized to be one ($\sum_{l=0}^{L-1} \left[\alpha_l^{(u)}\right]^2 = 1$) and the log-normal term $X^{(u)}$ captures the total multipath energy. The channel models presented in [56, 57] show cluster and ray arrivals. In this dissertation, we do not differentiate between clusters and rays and denote all arrivals in a unified manner.

2.2 Conventional UWB Systems

2.2.1 Signaling of UWB Systems

For impulse radio (IR) UWB systems, narrow pulses on the order of sub-nanosecond duration are transmitted [33, 54]. Multiple pulses are transmitted per symbol. As defined in Section 1.1, the number of times that a pulse is transmitted for each symbol is called the repetition factor, denoted by N_s in this dissertation unless stated otherwise. The transmitted signal of user u in conventional UWB systems is written as

$$s_c^{(u)}(t) = \sum_{i=0}^{\infty} \sum_{j=0}^{N_s-1} \sqrt{E^{(u)}} d_i^{(u)} p(t - iT_s - jT_f - c_j^{(u)} T_c) \tag{2.2}$$

where the superscript indicates user u, $E^{(u)}$ is the symbol energy of the uth user, $p(t)$ is the transmitted pulse with energy of $1/N_s$ and duration $[0,\ T_p]$, T_f is the frame time, and $T_s = N_s T_f$ is the symbol interval. Users are separated by the time-hopping sequences $\{c_j^{(u)}\}$. In this dissertation, we assume $c_j^{(u)}$ is uniformly distributed on the interval $[0,\ N_h^{(u)} - 1]$. The term T_c is the chip duration. Every N_s pulses convey one bit, $d_i^{(u)} \in \{\pm 1\}$, for user u, where i corresponds to the ith bit. Note that the data streams for different users are statistically independent.

For synchronization purposes, spreading codes are used. For codes with a block length of M, a total of M symbols are transmitted for each block, $\{d_i^{(u)}\}_{i=0}^{M-1}$. In this dissertation, Gold codes with $M = 31$ are used.

2.2.2 Received Signal

The transmitted signal in (2.2) goes through a multipath channel and is dispersed in time. Denote $h_F(t)$ as the impulse response of the front-end bandpass filter of the receiver with a bandwidth W. Let $H_F(f)$ be the Fourier transform of $h_F(t)$. Denote $g^{(u)}(t) = p(t) * h^{(u)}(t) * h_F(t)$, where $*$ denotes convolution. The received signal is written as

$$r_c(t) = \sum_{u=1}^{N_u} \sum_{i=0}^{\infty} \sum_{j=0}^{N_s-1} \sqrt{E^{(u)}} d_i^{(u)} g^{(u)}(t - iT_s - jT_f - \tau^{(u)}) + n(t) \tag{2.3}$$

where N_u is the number of active users in the network, $n(t)$ is the filtered bandpass white Gaussian noise process with mean zero and power spectral density $S_n(f) = \frac{N_0}{2}|H_F(f)|^2$, and $\tau^{(u)}$ is the time offset between user u and the desired user 1.

2.3 TR UWB Systems

2.3.1 Signaling of TR Systems

As briefly discussed in 1.1, a pulse pair is transmitted in each frame. This pulse pair is repeated several times for each symbol. The transmitted signal for a standard TR UWB (STR) system [6] using binary PAM modulation can be written as

$$\begin{aligned} s_s^{(u)}(t) &= \sum_{i=0}^{\infty} \sum_{j=0}^{N_s-1} \sqrt{\frac{E^{(u)}}{2}} \Big[p(t - iT_s - jT_f - c_j^{(u)} T_c) \\ &\quad + d_i^{(u)} p(t - T_d^{(u)} - iT_s - jT_f - c_j^{(u)} T_c) \Big] \end{aligned} \tag{2.4}$$

where $T_d^{(u)}$ is the spacing between the reference and the data pulse. The other parameters are defined in the same way as in (2.2). To prevent the reference pulse from interfering with the data pulse, $T_d^{(u)}$ should be at least as large as the channel delay spread T_{mds}, thus making $T_f \geq 2T_{mds}$. Another binary modulation scheme studied in this chapter is differential TR UWB, with the transmitted signal being

$$s_d^{(u)}(t) = \sum_{i=0}^{\infty} \sum_{j=0}^{N_s-1} \sqrt{E^{(u)}} a_{i,j}^{(u)} p(t - iT_s - jT_f - c_j^{(u)} T_c) \tag{2.5}$$

where $a_{i,j}^{(u)} = a_{i,j-1}^{(u)} d_i^{(u)}$ is the differentially encoded bit for the ith bit $d_i^{(u)}$. The initial state is set to be $a_{0,-1}^{(u)} = 1$. The frame time is chosen such that $T_f \geq T_{mds}$ to prevent intersymbol interference (ISI).

The constraint of the spacing between pulses in TR systems (whether it is STR or DTR) to be larger than the maximum delay spread of the channel limits the data rate for binary TR systems, which can be seen from Fig. 2.1. A multipath channel with several taps is plotted below the transmitted pulses in Fig. 2.1 to show the spacing constraint. In this dissertation, we investigate one technique, M-ary PPM to improve the data rate. Impulse radio using M-ary PPM has been investigated in a number of settings for UWB systems with Rake receivers [27, 28, 29, 30]. The general transmitted signal for user u with M-ary PPM is given by

$$\begin{aligned} s^{(u)}(t) = \sum_{i=0}^{\infty} \sum_{j=0}^{N_s-1} \sqrt{\frac{E^{(u)}}{2}} \Big[& p(t - iT_s - jT_f - c_j^{(u)} T_c) \\ & + p(t - T_d^{(u)} - iT_s - jT_f - c_j^{(u)} T_c - I_i^{(u)} \delta) \Big] \end{aligned} \tag{2.6}$$

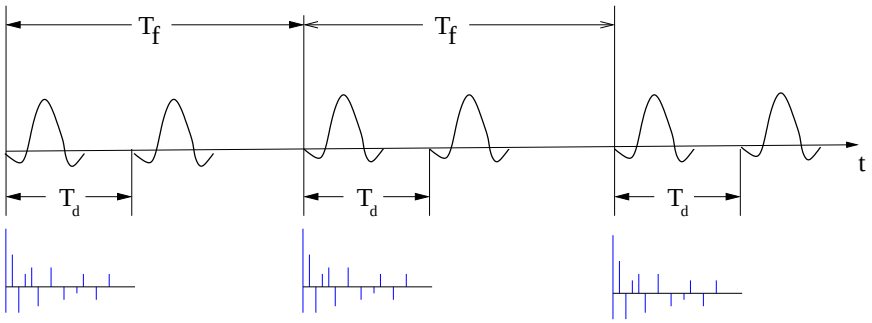

Figure 2.1: Diagram showing the relationship between the separation of data and reference pulses and the channel delay spread.

As in the binary case, the time-hopping sequence $\{c_j^{(u)}\}$ is applied to each user to reduce the probability of collision among users. Each symbol $I_j^{(u)} \in \{0,1,...,M-1\}$ is transmitted N_s times (the repetition factor). The separation between adjacent symbols (the slot length) is δ, which is set to be at least as large as T_{mds}. Thus, there is neither interframe interference (IFI) nor intersymbol interference (ISI) for the M-ary scheme.

2.3.2 Signal Space View: TR

The signaling scheme for STR is shown in Fig. 1.2 and Fig. 2.1, where orthogonality in the time domain is achieved by setting a large spacing between reference signals and data-bearing signals. Consider a single-user environment without time-hopping codes. Fix the spacing to be $T_d^{(1)} = T_d = T_f/2$. The signal space $\mathcal{S}_s$ is defined by the basis functions $\{b_k(t)\}$ given by

$$b_k(t) = p(t - kT_d), \qquad k = 0,1,...,2N_s - 1 \tag{2.7}$$

Then the transmitted signal for user 1 in the form of (2.4) has dimension $2N_s$ for symbol i and is represented by the vector $\sqrt{E^{(1)}/2}\left[1, d_i^{(1)}, 1, d_i^{(1)}, ..., 1, d_i^{(1)}\right]^t$. This signal space view for STR UWB systems is used for comparison with FSR systems.

2.3.3 Received Signal

For binary STR systems, the received signal is

$$\begin{aligned} r_s(t) &= \sum_{u=1}^{N_u}\sum_{i=0}^{\infty}\sum_{j=0}^{N_s-1}\sqrt{\frac{E^{(u)}}{2}}\Big[g^{(u)}(t-iT_s-jT_f-\tau^{(u)}) \\ &\quad +d_i^{(u)}g^{(u)}(t-T_d^{(u)}-iT_s-jT_f-\tau^{(u)})\Big] \\ &\quad +n(t) \end{aligned} \tag{2.8}$$

The parameters and signals in (2.8) are defined in the same way as the received signal for UWB systems in (2.3). When synchronization is established between the desired transmitter and receiver 1, $\tau^{(1)}=0$ and $\tau^{(u)}$ $(u\neq 1)$ is a random variable uniformly distributed on the interval $[0,\ T_f]$[14]. The received signal for binary DTR system is given by

$$r_d(t)=\sum_{u=1}^{N_u}\sum_{i=0}^{\infty}\sum_{j=0}^{N_s-1}\sqrt{E^{(u)}}a_{i,j}^{(u)}g^{(u)}(t-iT_s-jT_f-\tau^{(u)})+n(t) \tag{2.9}$$

For M-ary PPM, the received signal can be written as

$$\begin{aligned} r(t) &= \sum_{u=1}^{N_u}\sum_{i=0}^{\infty}\sum_{j=0}^{N_s-1}\sqrt{\frac{E^{(u)}}{2}}\Big[g^{(u)}(t-iT_s-jT_f-c_j^{(u)}T_c-\tau^{(u)}) \\ &\quad +g^{(u)}(t-T_d^{(u)}-iT_s-jT_f-c_j^{(u)}T_c-I_i^{(u)}\delta-\tau^{(u)})\Big] \\ &\quad +n(t) \end{aligned} \tag{2.10}$$

With M possible transmitted symbols, the frame time T_f must be large enough to accommodate these symbols. Let the time-hopping sequence $c_j^{(u)}$ range from 0 to $N_h^{(u)}$. Then the relationship between T_f and M is

$$T_f \geq \max\{N_h^{(u)} T_c + T_d^{(u)} + M\delta\} \tag{2.11}$$

Since $T_d^{(u)} \geq T_{mds}$ and $\delta \geq T_{mds}$, we have

$$T_f \geq \max\{N_h^{(u)} T_c + (M+1) T_{mds}\} \tag{2.12}$$

The assumption that the frame time T_f is greater than twice the largest delay among M delays results in the following relationship [27]

$$T_f \geq 2MT_{mds} \tag{2.13}$$

2.3.4 Receiver Structure: TR

The receiver structure for TR systems with M-ary PPM is shown in Fig. 2.2. We see that the receiver in Fig. 1.3 for binary TR systems is a special case (with $\delta = 0$) of the general receiver in Fig. 2.2.

For modulation slot m ($0 \leq m \leq M-1$), the reference signal is delayed by $T_d^{(u)} + m\delta$ to align with the signal in the mth slot and correlation is carried out between these two signals. The output of the mth slot is denoted by D_m and the collection of $\{D_m\}_{m=0}^{M-1}$ is used by the receiver to make a decision.

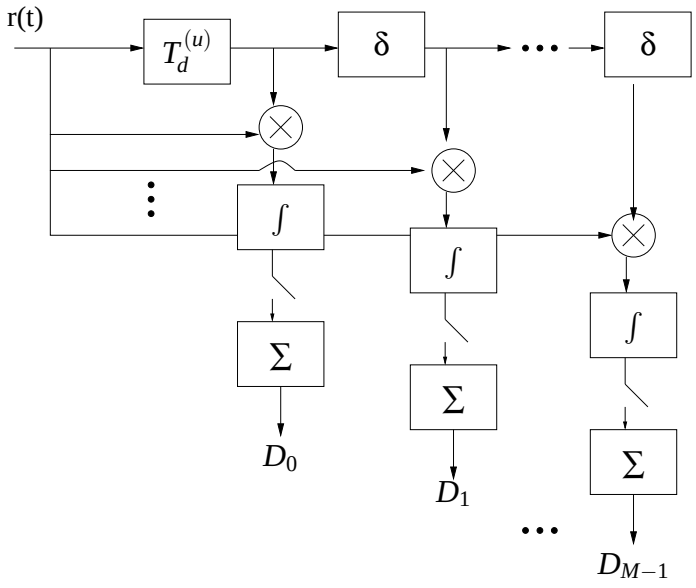

Figure 2.2: The receiver structure of a TR system with M-ary PPM.

2.4 FSR UWB Systems

2.4.1 Signaling of FSR Systems

Slightly frequency-shifted reference (FSR) UWB systems are introduced in [39] to overcome the need for the wideband analog delay line required in TR UWB systems while still maintaining the benefits of TR systems in avoiding channel estimation. Antipodal modulation is used in [39] to carry information bits.

We adopt the notations from [39]. Let $U^{(u)}(t)$ be a pulse train of the uth user with N_s pulses:

$$U^{(u)}(t) = \sum_{j=0}^{N_s-1} p(t - jT_f - c_j^{(u)} T_c) \tag{2.14}$$

where $p(t)$ is the basic transmitted pulse with pulse width T_p and energy $1/N_s$, as in TR systems. Within each frame of length T_f, the pulses are dithered by a user-specific time-hopping code $c_j^{(u)}$. The ith transmitted signal for user u is given by

$$\begin{aligned} & x^{(u)}(i,t) \\ = \; & \left[\sqrt{E_r^{(u)}} + d_i^{(u)}\sqrt{2E_d^{(u)}}\,\mathrm{Rec}(t - iT_s)\cos(2\pi f_0 t)\right] \\ & \times U^{(u)}(t - iT_s) \end{aligned} \tag{2.15}$$

where $E_r^{(u)}$ and $E_d^{(u)}$ are the energy assigned to the reference and data-bearing pulses respectively, with the symbol energy $E_s = E_b = E_r^{(u)} + E_d^{(u)}$. The ith bit $d_i^{(u)}$ takes values independently from $\{\pm 1\}$ with equal probability. The information bit streams for different users are also statistically independent. Each bit is transmitted using N_s pulses which constitutes the pulse train $U^{(u)}(t)$. The function $\mathrm{Rec}(t)$ in (2.15) is a rectangular pulse with

duration $T_s = N_s T_f$ (the symbol time). The frequency offset between the reference pulses and the data-bearing pulses is $f_0 = 1/T_s$. This frequency offset is usually very small compared to the signal bandwidth in UWB communications and has to be chosen to ensure that the reference and the data-bearing pulses are affected by approximately the same channel conditions.

2.4.2 Signal Space View: FSR

The signaling scheme is shown in Fig. 2.3. The top plot in Fig. 2.3 is the transmitted pulses for TR systems where dotted pulses carry information. In this example, six pulse pairs comprise one symbol (bit). These pulses are orthogonal in the time domain as we discussed in Section 2.3.2. The middle plot in Fig. 2.3 shows the same repetition factor $N_s = 6$ of FSR systems as the TR signaling in the top plot. Instead of inserting data-bearing pulses, the six pulses are multiplied by a cosine function with period equal to the symbol interval T_s. The bottom plot is the the output of the multiplication of the two waveforms shown in the middle plot.

As in TR systems, we consider a FSR system in a single-user environment without time-hopping codes. The pulse train is $U^{(1)}(t) = U(t) = \sum_{j=0}^{N_s-1} p(t - jT_f)$. In [39], it is shown that the original pulse train $U(t)$ (the middle plot without the cosine function) and the pulse train multiplied by the cosine function $U(t)\cos(2\pi f_0 t)$ (the bottom plot) are approximately orthogonal given that the repetition factor N_s is large. The orthogonality is achieved in the frequency domain since the two pulse trains ($U(t)$ and $U(t)\cos(2\pi f_0 t)$) are only offset by a cosine term. The information bits are modulated in the pulse train offset by the cosine term: $d_i^{(u)} U(t)\cos(2\pi f_0 t)$. The signal space of binary FSR systems, $\mathcal{S}_f$, thus has two basis

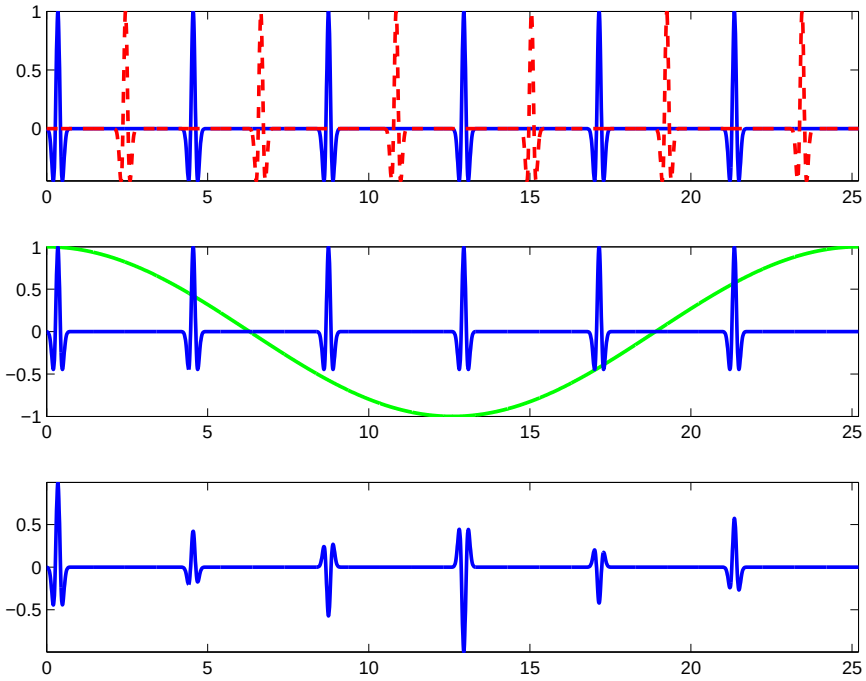

Figure 2.3: Signaling waveforms for FSR systems. Top plot: Signaling of STR UWB systems. Middle plot: The relationship between a pulse train and a cosine function with period equal to the duration of the pulse train. Bottom plot: The production of the pulse train and the cosine function from the middle plot.

functions $b_{f1}(t)$ and $b_{f2}(t)$ given by

$$b_{f1}(t) = U(t) \tag{2.16}$$

$$b_{f2}(t) = U(t)\cos(2\pi f_0 t) \tag{2.17}$$

The signal space view $\mathcal{S}_f$ of FSR systems is different from $\mathcal{S}_s$ of TR systems. The original pulse train $U(t)$ is regarded as a vector (with dimension one) in $\mathcal{S}_f$ while it has dimension N_s in $\mathcal{S}_s$. From the signal space perspective, the signal of one symbol in FSR

signaling has a dimension of two and can be expressed by a vector $\left[\sqrt{E_r^{(1)}}, \quad d_i^{(1)}\sqrt{E_d^{(1)}}\right]^t$.

2.4.3 Received Signal

The received signal at the desired receiver after the receiver front-end filter is

$$r_f(t) = \sum_{u=1}^{N_u}\sum_{i=0}^{\infty} r_x^{(u)}(i,t) + n(t) \tag{2.18}$$

where the signal $r_x^{(u)}(i,t) = x^{(u)}(i,t-\tau^{(u)}) * h^{(u)}(t) * h_F(t)$ is the convolution between the ith transmitted signal, the channel impulse response $h^{(u)}(t)$, and the front-end filter $h_F(t)$, and $n(t)$ is a zero-mean Gaussian random process with power spectral density $S_n(f) = \frac{N_0}{2}|H_F(f)|^2$. As in the TR systems, $H_F(f)$ is the Fourier transform of the impulse response of the front-end filter, $h_F(t)$. The signal $r_x^{(u)}(i,t)$ and the noise $n(t)$ are independent. The element $\tau^{(u)}$ in $x^{(u)}(i,t-\tau^{(u)})$ is the time asynchronism between user u and the desired user 1. When synchronization is established for the desired user, $\tau^{(1)} = 0$ and $\{\tau^{(u)} \neq 0\}$ $(u \neq 1)$ in general (except for a synchronous network). We also assume that $\tau^{(u)}$ is uniformly distributed on the interval $[0,\ T_f]$ $(u \neq 1)$.

2.4.4 Receiver Structure: FSR

Two equivalent FSR receiver structures are shown in Fig. 2.4, where no delay line is deployed [39]. As discussed in Section 2.4.2, the reference signal and the data-bearing signal in FSR systems are orthogonal in the frequency domain. Therefore, analogous to the time-domain alignment of TR systems, frequency-domain alignment of the two signals is done in the top structure of Fig. 2.4 - the received signal is offset by a cosine function

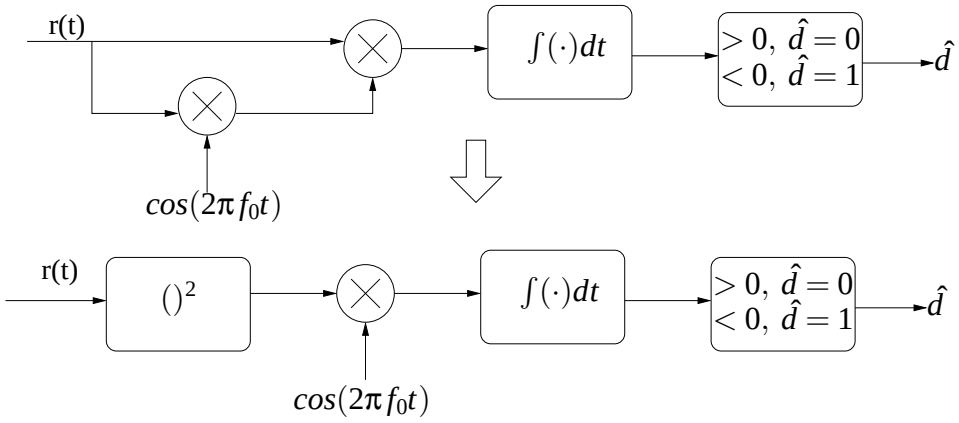

Figure 2.4: A FSR receiver

which aims to ‘align’ the reference signal with the data-bearing signal. A correlation is then computed between the offset received signal and the original signal. The top structure can also be replaced by the bottom structure where the signal processing is the same but requires one fewer mixer (multiplier).

Chapter 3

Performance Analysis: High-Power Users

In this chapter, we analyze the detection performance of TR UWB systems assuming synchronization between the communication parties is established. The environment under consideration is that from Section (2.1). Standard TR (STR) and differential TR (DTR) systems using binary modulation schemes are investigated in the first part of this chapter. Performance of TR UWB systems with M-ary PPM is then analyzed. Users with power levels much higher than the desired user are shown to degrade the performance dramatically. Chip discrimination [23, 24] is applied to suppress the effects from high-power interfering users and restore the system performance. Optimal transmission strategies are discussed along with the numerical results.

3.1 Binary TR Systems

In this section, we replace the spacing of the desired user $T_d^{(1)}$ with T_d for convenience of analysis. The notation $\mathbb{E}\{\cdot\}$ represents the expectation operation and $\Pr\{\cdot\}$ represents the probability of an event.

3.1.1 Decision Statistic

Standard TR

A received signal of STR systems with $d_i^{(1)} = 1$ (also the received signal of M-ary PPM systems with $I_i^{(1)} = 0$) is shown in Fig. 3.1 where the reference signal (dashed) is aligned with the data-bearing signal (solid). Compared to the transmitted pulses shown

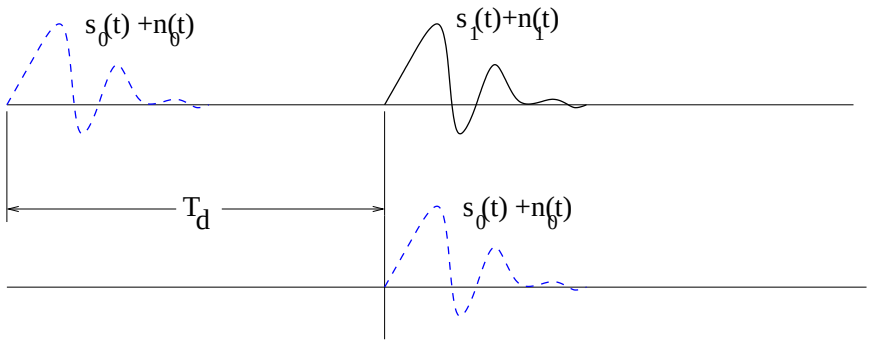

Figure 3.1: A received signal in TR systems

in Fig. 1.2, the signals shown in Fig. 3.1 are dispersed by the channel and bear different shapes. The noise is not shown for clearer illustration. To demodulate the ith bit, the receiver correlates the reference signal and the data-bearing signal within each frame. This

correlation requires a delay line with delay T_d (the receiver structure is shown in Fig. 1.3), with the jth correlation of the ith bit expressed as:

$$d_s(j) = \int_{\Omega_j} r_s(t) r_s(t - T_d) dt \tag{3.1}$$

where Ω_j represents the integration range with $\Omega_j = [iT_s + jT_f + c_j^{(1)} T_c + T_d,\ \ iT_s + jT_f + c_j^{(1)} T_c + T_d + T_I]$. This integration range has a duration T_I. Note that the desired user is user 1 and synchronization is assumed established between user 1 and the receiver. Without loss of generality, we consider the first symbol $i = 0$. The outputs of the N_s correlations are summed and a decision is made on the decision statistic given by

$$\begin{aligned} D_s &= \sum_{j=0}^{N_s-1} d_s(j) \\ &= d_0^{(1)} \frac{E^{(1)}}{2} N_s \varepsilon_1 + n_{s1} + n_{s2} + n_3 + n_e + n_h \end{aligned} \tag{3.2}$$

where

$$\varepsilon_1 = \int_0^{T_I} \left[g^{(1)}(t) \right]^2 dt \tag{3.3}$$

$$n_{sv} := \sqrt{\frac{E^{(1)}}{2}} \sum_{j=0}^{N_s-1} \int_{jT_f}^{jT_f+T_I} g^{(1)}(t) n(t) dt, \ \ v = 1, 2 \tag{3.4}$$

$$n_3 := \sum_{j=0}^{N_s} \int_{jT_f}^{jT_f+T_I} n(t - jT_f) n(t - jT_f - T_d) dt \tag{3.5}$$

The terms $\{n_{sv}\}_{v=1}^{2}$ defined in (3.4) are independent Gaussian random variables due to reference signal $\times$ noise and data-bearing signal $\times$ noise. The notation := represents definition. It is easy to show n_{s1} and n_{s2} have mean zero and variance equal to $E^{(1)} N_s \varepsilon_1 N_0 / 4$.

The term n_3 is a summation of noise $\times$ noise components which are assumed to be Gaussian distributed by invoking the central limit theorem [4, 6, 14, 15] with mean zero and variance $N_s W T_I N_0^2/2$ (W is the bandwidth of the receiver front-end bandpass filter). All noise and interference terms in D_s are independent. For convenience, we express a Gaussian random variable in the way as: $n_{s1} \sim N(0,\ E^{(1)} N_s \varepsilon_1 N_0/4)$. The last two terms in (3.2) are related to multiuser interference, with n_e and n_h capturing effects from equal-power and high-power interfering users, respectively.

As defined in Section 2.1, N_e is the number of equal-power interfering users and N_h is the number of high-power interfering users with $N_e + N_h + 1 = N_u$. When N_e is large enough to validate the Gaussian assumption of n_e [14], we have $n_e \sim N(0,\ N_s \sigma_e^2)$, with σ_e^2 being the interfering power from equal-power interfering users within one frame. Detailed analysis for obtaining the value of σ_e^2 is presented in Chapter 4. In this chapter, we do not delve into the calculation of σ_e^2. Instead, we use an arbitrary value of σ_e^2 to show the effect of equal-power interfering users.

Differential TR

When synchronization is established, a DTR receiver uses a previous frame as a template for the current frame and correlates signals from these two frames. The process is shown in Fig. 3.2 where the dashed signal serves as a template for the solid signal and the solid signal does the same thing for the dash-dotted signal. By summing outputs from N_s correlations, a decision statistic D_d is obtained for DTR receivers as

$$D_d = d_0^{(1)} E^{(1)} N_s \varepsilon_1 + n_d + n_3 + n_e + n_h \tag{3.6}$$

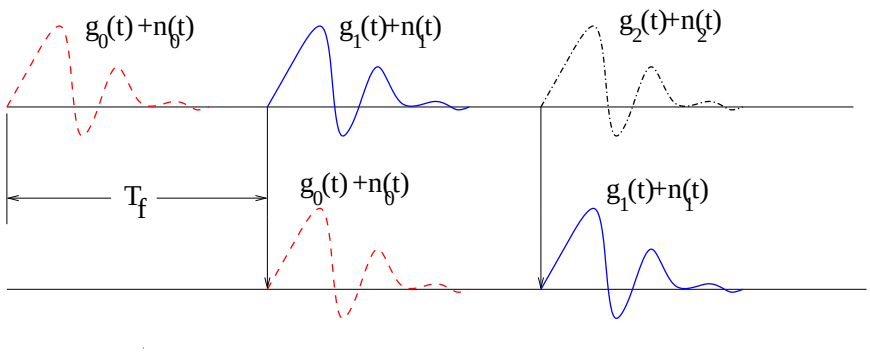

Figure 3.2: Signal processing for DTR

The first term in (3.6) is the useful signal component. The first bit $d_0^{(1)}$ is shown in the first term because $a_{0,j}^{(1)} a_{0,j+1}^{(1)} = d_0^{(1)}$ for $0 \leq j \leq N_s - 1$. The noise term n_3, n_e, and n_h are defined in the same way as the STR decision statistic D_s. The signal $\times$ noise term n_d is different from the summation of n_{s1} and n_{s2} for STR receivers because of the possible correlation in DTR processing. The noise correlation can be seen from Fig. 3.2 where the noise term $n_1(t)$ is correlated with the signal $s_0(t)$ for the first correlation and with $s_2(t)$ for the second correlation. When the channel keeps constant within two consecutive symbols (which is true in most cases), the signals $s_0(t)$ and $s_2(t)$ can be considered as the same. Therefore, the signal $\times$ noise terms in the two consecutive correlations are completed correlated (with correlation coefficient one) except for outputs from the edge. When the correlation outputs are added together to form the decision statistic D_d, correlated noise terms are added coherently in this case. This is reflected in calculating the variance of n_d in Appendix B.

3.1.2 Error Performance: Equal-Power Users

The receiver for a STR UWB system makes a decision based on D_s in (3.2). For binary PAM modulation, the decision rule is

$$D_s \underset{\hat{d}_0^{(1)}=-1}{\overset{\hat{d}_0^{(1)}=1}{\gtrless}} 0 \tag{3.7}$$

where $\hat{d}_0^{(1)}$ is the detected value for $d_0^{(1)}$. Because of the symmetry we can assume the transmitted bit is $d_0^{(1)} = 1$ to obtain the error performance. The random components in D_s are all Gaussian except the term n_h which is caused by high-power interfering users. We first analyze the error performance when $N_h = 0$, then we show the effect of n_h by setting $N_h \neq 0$.

When $N_h = 0$, the decision statistic D_s for STR receivers is Gaussian with mean and variance give by

$$\mu_s = \mathbb{E}\{D_s\} = \frac{E^{(1)}}{2} N_s \mathbb{E}\{\varepsilon_1\} \tag{3.8}$$

$$\sigma_s^2 = \frac{E^{(1)}}{2} N_s \mathbb{E}\{\varepsilon_1\} N_0 + \frac{N_s W T_I N_0^2}{2} + N_s \sigma_e^2 \tag{3.9}$$

The mean μ_s and variance σ_s^2 both contain a term $\mathbb{E}\{\varepsilon_1\}$ which is the average received energy of $g^{(1)}(t)$. The signal $g^{(1)}(t)$ is the response of the pulse $p(t)$ going through the channel. In Appendix A, we provide the derivation for the average received energy $\mathbb{E}\{\varepsilon_1\}$,

which is calculated to be $1/N_s$. Therefore, we can rewrite the mean and variance of D_s as

$$\mu_s = \mathbb{E}\{D_s\} = \frac{E^{(1)}}{2} \tag{3.10}$$

$$\sigma_s^2 = \frac{E^{(1)}}{2}N_0 + \frac{N_s W T_I N_0^2}{2} + N_s\sigma_e^2 \tag{3.11}$$

This result applies to an equal-power user environment with $N_s\sigma_e^2$ being the variance of the Gaussian interference caused by equal-power interfering users. The bit error probability (BEP) of STR UWB systems in such an environment is thus

$$\begin{aligned} P_{s0} &= Q\left(\frac{E^{(1)}/2}{\sigma_s}\right) \\ &= Q\left(\left[2\left(\frac{E^{(1)}}{N_0}\right)^{-1} + 2N_s W T_I\left(\frac{E^{(1)}}{N_0}\right)^{-2} + 4N_s\left(\frac{E^{(1)}}{\sigma_e}\right)^{-2}\right]^{-\frac{1}{2}}\right) \end{aligned} \tag{3.12}$$

We use the subscript '$s0$' to indicate that the error probability shown in (3.12) is obtained for STR receivers when N_h is set to be zero.

Following the same procedure as in STR receivers, we write down the mean and variance of the decision statistic for DTR receivers as

$$\mu_d = \mathbb{E}\{D_d\} = E^{(1)} \tag{3.13}$$

$$\sigma_d^2 = \frac{2N_s - 1}{N_s}E^{(1)}N_0 + \frac{N_s W T_I N_0^2}{2} + N_s\sigma_e^2 \tag{3.14}$$

The term $\frac{2N_s-1}{N_s}E^{(1)}N_0$ is the variance of n_d. The derivation is given in Appendix B. In the derivation of the variance σ_d^2, the correlation between signal $\times$ noise terms and the edge effect are considered. The decision statistic for DTR receivers is also Gaussian. The BEP

of DTR is then given by

$$\begin{aligned} P_{d0} &= Q\left(\frac{E^{(1)}}{\sigma_d}\right) \\ &= Q\left(\left[\frac{2N_s-1}{N_s}\left(\frac{E^{(1)}}{N_0}\right)^{-1}+\frac{1}{2}N_sWT_I\left(\frac{E^{(1)}}{N_0}\right)^{-2}+N_s\left(\frac{E^{(1)}}{\sigma_e}\right)^{-2}\right]^{-\frac{1}{2}}\right) \end{aligned} \tag{3.15}$$

To make fair comparisons between STR and DTR UWB systems, we set the number of pulses in one bit to be N_p for both cases. For STR, $N_s = N_p/2$, while for DTR $N_s = N_p$. The bit energy is the same for both STR and DTR UWB, thus $E_b = E^{(1)}$. Applying N_p and E_b to (3.12) and (3.15) yields

$$P_{s0} = Q\left(\left[2\left(\frac{E_b}{N_0}\right)^{-1}+N_pWT_I\left(\frac{E_b}{N_0}\right)^{-2}+2N_p\left(\frac{E_b}{\sigma_e}\right)^{-2}\right]^{-\frac{1}{2}}\right) \tag{3.16}$$

$$P_{d0} = Q\left(\left[\frac{2N_p-1}{N_p}\left(\frac{E_b}{N_0}\right)^{-1}+\frac{1}{2}N_pWT_I\left(\frac{E_b}{N_0}\right)^{-2}+N_p\left(\frac{E_b}{\sigma_e}\right)^{-2}\right]^{-\frac{1}{2}}\right) \tag{3.17}$$

which are expressions for BEP of STR and DTR UWB respectively when we set the number of high-power users N_h to be zero.

3.1.3 Collision Probabilities

To evaluate BEP when high-power users are present in the network, we first investigate the probability of collision between the desired user and high-power interfering users. The probability of collision is related to the integration time of the receiver, T_I, the frame length

T_f, the number of frames (pulses) in one bit, N_s (N_p), and the number of high-power users N_h.

If designed properly, $c_j^{(u)}$ together with the asynchronization $\tau^{(u)}$ in (2.8), make the positioning of pulses from interfering users uniformly distributed in one frame T_f. Here a uniform distribution within $[0,\ T_f]$ is assumed for $\tau^{(u)}$. Let $p = \frac{2T_I}{T_f}$. For STR UWB, within one frame, the probability that either the desired reference signal, or the desired data signal, or both signals, collides with one high-power user, is given by

$$\mathfrak{p}_s = 2p(1-p) + p^2 \tag{3.18}$$

There are N_h high-power users; pulses from each of them collide independently with user 1 with probability given by $\mathfrak{p}_s$ in (3.18). The probability that at least one high-power user pulse collides with the desired user 1 is

$$\mathfrak{p}_{cs} = \sum_{i=1}^{N_h} \begin{pmatrix} N_h \\ i \end{pmatrix} \mathfrak{p}_s^i (1-\mathfrak{p}_s)^{N_h - i} \tag{3.19}$$

Among N_s frames in one bit, the probability of j frames suffering a collision with at least one high-power user is

$$\mathfrak{p}_{ns,str}(j) = \begin{pmatrix} N_s \\ j \end{pmatrix} \mathfrak{p}_{cs}^j (1-\mathfrak{p}_{cs})^{N_s - j} \tag{3.20}$$

For DTR UWB, the collision probability has a different form and is discussed in the next section.

3.1.4 Error Performance: High-Power Users

In this section, we include the high-power users and show the performance degradation caused by interference from these high-power users even with a small number of them. Note that in [14], the power ratio $\{E^{(u)}/E^{(1)}\}$ between user u and the desired user 1 is assumed to be unity. Equal-power interfering users are assumed to be Gaussian by the central limit theorem when the channel delay spread is large and the number of interfering users is also large. However this assumption is only valid in networks with perfect power control, such as in cellular architectures. In wireless ad-hoc communications, where no power control or very limited power control is available, the power ratios $\{E^{(u)}/E^{(1)}\}$ are no longer unity. In this case performance is overwhelmingly dominated by interfering users' power. The system performance under such situations with imperfect power control thus is mainly determined by the collision probability between the desired user and those high-power users.

The average BEP for STR UWB when high-power users are present is

$$P_{su} = \mathfrak{p}_{ns,str}(0) \times P_{s0} + \frac{1}{2}(1 - \mathfrak{p}_{ns,str}(0)) \tag{3.21}$$

The first term in (3.21) corresponds to the case when no collision occurs between the desired user and high-power users pulses. The second term in (3.21) relates to the situation when at least one such collision occurs. The factor $1/2$ in the second term indicates that a collision between the desired user and high-power users corrupts the decision statistic. In a typical STR UWB system, for example, with $T_I = 25$ ns, $T_f = 2000$ ns, $N_s = 1$, even with only one high-power user, the BEP in (3.21) is no better than 2.5×10^{-3} regardless of

SNR. This is true for DTR systems as well. An example for both STR and DTR systems is shown in Fig. 3.3. Only one high-power user is included in Fig. 3.3. The repetition factor

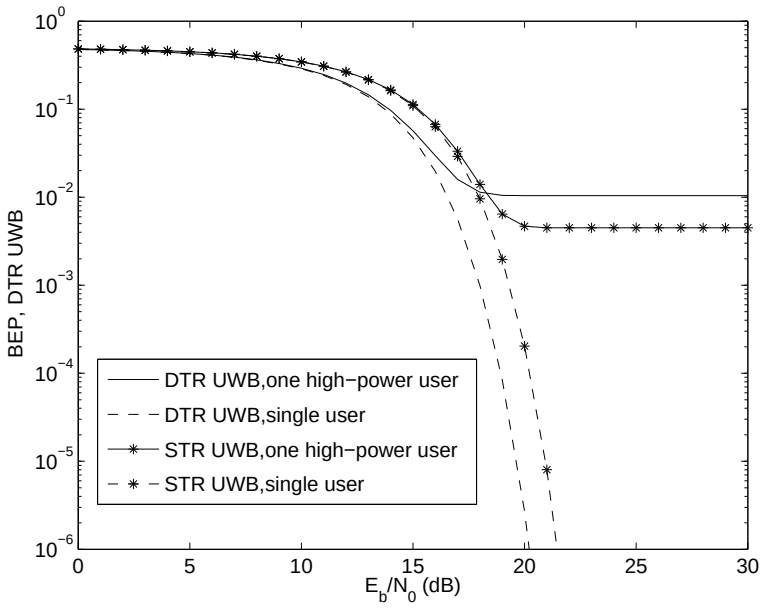

Figure 3.3: BEP of STR and DTR with $N_h = 1$

for STR is $N_s = 3$ and for DTR is $N_s = 6$. It can be seen that BEP is dominated by the collision probability with high-power users. As the number of high-power users N_h increases, BEP is increasingly determined by the collision probability $\mathfrak{p}_{ns,str}(j)$. This degradation of performance motivates our study to improve system performance with imperfect power control.

3.1.5 Chip Discrimination: Binary TR

Chip discrimination has been shown effective in combating the detrimental effects of high-power users in UWB communication networks with AWGN channels [23, 24]. It works by obtaining an estimate of the average received power for the desired signal and then setting a threshold below which correlator outputs are acceptable. If the absolute value of a correlator output is larger than the threshold value, then that correlator output is not added to the bit decision statistic. The final decision statistic is the sum of $(N_s - j)$ correlator outputs where j is the number of correlations being 'removed' after applying the threshold. The effectiveness of chip discrimination is a function of threshold setting. Here we assume an ideal threshold to simplify analysis. The effect of threshold setting for non-multipath channels and matched filter receivers has been investigated in [23].

We add a letter c to subscripts to indicate that chip discrimination is applied. For example, D_{sc} is the decision statistic of STR receivers with chip discrimination, and D_{dc} is that for DTR receivers. If user 1 has j frames suffering collisions with high-power user pulses, the decision statistic of STR UWB, D_{sc}, has $(N_s - j)$ non-zero correlator outputs after applying chip discrimination, with mean and variance

$$\mu_{sc}(j) = \left(\frac{N_s - j}{N_s}\right)\left(\frac{E_b}{2}\right) = \left(\frac{N_p/2 - j}{N_p/2}\right)\left(\frac{E_b}{2}\right) \tag{3.22}$$

$$\begin{aligned}\sigma^2_{sc}(j) &= \left(\frac{N_p/2 - j}{N_p/2}\right)\left(\frac{E_b}{2}\right)N_0 + (N_p/2 - j)\left(\frac{WT_I N_0^2}{2}\right) \\ &\quad + (N_p/2 - j)\sigma_e^2\end{aligned} \tag{3.23}$$

Here the Gaussian assumption holds since the effect of high-power users is removed after applying chip discrimination. Thus the noise term n_h approaches to zero in (3.2). The BEP

with j frames removed is given by

$$P_{sc}(j) = Q\left(\frac{\mu_{sc}(j)}{\sigma_{sc}(j)}\right) \tag{3.24}$$

The overall BEP is obtained by averaging $P_{sc}(j)$ over the probability of j frames being removed and can be written as

$$P_{sc} = \mathbb{E}\{P_{sc}(j)\} = \sum_{j=0}^{N_p/2} P_{sc}(j)\mathfrak{p}_{ns,str}(j) \tag{3.25}$$

For DTR UWB receivers, if j correlator outputs are detected to be out of the limit set by the threshold, the final decision statistic, D_{dc}, consists of $N_p - j$ non-zero correlator outputs with mean $\mu_{dc}(j) = \frac{N_p - j}{N_p} E_b$. The variance of D_{dc} is more complicated than the variance of D_{sc} and is related to the patterns of collisions. For a given number of correlations removed by chip discrimination, the resulting variance is a function of the actual pattern of the correlations removed. The following equation gives the worst case (largest) variance for a given j.

$$\begin{aligned}\sigma_{dc}^2(j) &= \frac{2(N_p - j) - 1}{N_p} E_b N_0 + \frac{(N_p - j) W T_I N_0^2}{2} \\ &\quad + (N_p - j)\sigma_e^2\end{aligned} \tag{3.26}$$

The conditional BEP given j frames being removed is

$$P_{dc}(j) = Q\left(\frac{\mu_{dc}(j)}{\sigma_{dc}(j)}\right) \tag{3.27}$$

However, the probability of j correlations being removed after applying the threshold

Table 3.1: Collision Patterns for DTR

0	1	2	3	4
	↑			
		↑		
			↑	
			↑	↑
↑	↑			
↑				↑

for DTR UWB is not a binomial combination and doesn't have a simple expression as in (3.20). An example is given in Table. 3.1 to show different patterns of collision. The arrows in Table 3.1 indicate the positions of collision and the numbers from 1 to 4 in the first row are the frames for one symbol ($N_s = 4$). The number 0 indicates the frame from the previous symbol. All of the collisions shown by the arrows in Table 3.1 result in two frames being removed after applying chip discrimination. For different values of the repetition factor N_s, collision patterns are different which lead to different expressions for collision probabilities. The authors found it hard to come up with a universal expression for the collision probabilities of DTR systems. Instead, by enumerating every possible collision pattern, the probability of j correlations being removed after chip discrimination, $\mathfrak{p}_{ns,dtr}(j)$, is obtained for the cases when $N_p \in [1,6]$. For $N_p = 6$ and $q = 1-p$, the probability of j correlations being removed from the final decision statistic is given by the following.

$$p_{ns,dtr}(j) = \begin{cases} q^7, & j = 0 \\ 2pq^6, & j = 1 \\ 5pq^6 + 3p^2q^5, & j = 2 \\ 12p^2q^5 + 4p^3q^4, & j = 3 \\ 6p^2q^5 + 18p^3q^4 + 5p^4q^3, & j = 4 \\ 12p^3q^4 + 20p^4q^3 + 6p^5q^2, & j = 5 \\ p^3q^4 + 10p^4q^3 + 15p^5q^2 & \\ \quad + 7p^6q + p^7, & j = 6 \end{cases} \tag{3.28}$$

The overall BEP for DTR UWB with chip discrimination is

$$P_{dc} = \mathbb{E}\{P_{dc}(j)\} = \sum_{j=0}^{N_p} P_{dc}(j)\mathfrak{p}_{ns,dtr}(j) \tag{3.29}$$

The advantage of chip discrimination can be seen by comparing (3.25) (with chip discrimination) and (3.21) (without chip discrimination). Note that $P_{sc}(j) \leq 1/2$ in (3.25) while in (3.21) it is always $1/2$ when $j \neq 0$. Collision with high-power interfering user pulses causes some correlations to be removed, thus resulting in a portion of the energy being lost in this process. But this loss is less significant than the case of keeping those correlations, which would result in a corrupted decision statistic. The consequence is the same for DTR UWB using chip discrimination. The significance of applying chip discrimination to both STR and DTR UWB is numerically demonstrated in Section 3.1.6.

3.1.6 Numerical Results

The channel used in the numerical calculations has a delay spread $T_{mds} = 50$ ns (CM1 channel from [56]). The optimal integration time T_I for the correlator at the receiver is chosen as 25 ns [14] [58]. The receiver has a one-sided bandwidth $W = 4$ GHz. By fixing the number of pulses per bit and changing the frame time T_f, the data rate R_b is changed accordingly. In this section, we first consider the effect of high-power users on performance. Thus the effect of equal-power users is removed by setting $\sigma_e^2 = 0$. We include the effect of equal-power users in the sequel.

To obtain expressions for BEPs in (3.25) and (3.29), the conditional BEPs in (3.24) and (3.27) are needed. Fig. 3.4 shows the conditional BEP for STR and DTR UWB. From Fig. 3.4, we see that when only 1 or 2 pulses remain, the BEP is high for both STR and DTR UWB. This illustrates how the average BEP is determined by the probability of j pulses remaining, when $j = 1, 2$. The expressions for BEP for STR and DTR UWB are obtained by averaging the conditional BEP over $\mathfrak{p}_{ns,str}(j)$ and $\mathfrak{p}_{ns,dtr}(j)$, which are shown in Fig. 3.5 with the number of high-power users $N_h = 6$. Notice that for STR UWB, discarding a single correlation output results in both the reference and data pulses being discarded.

Fig. 3.6 shows the average BEP of STR UWB with and without chip discrimination as a function of the number of high-power users and the data rate. Dashed lines in Fig. 3.6 are BEPs of STR UWB without chip discrimination while solid lines are corresponding BEPs with chip discrimination. Each pair has the same data rate R_b. Here the number of pulses per bit is $N_p = 2N_s = 10$ and $E_b/N_0 = 22$ dB. Note from Fig. 3.6 that without centralized power control, BEPs of STR UWB (dashed lines) are mostly within the interval $[10^{-3}, 0.5]$ when R_b is from 1 Kbps to 100 Kbps. The decrease in data rate R_b decreases the proba-

bility of collision between the desired user and the high-power users, but this offers little improvement in the BEP. With chip discrimination, corresponding BEPs (solid lines) show significant improvement, especially when the data rate $R_b \leq 20$ Kbps. Further decreasing $R_b = 1$ Kbps, we note that the BEP using chip discrimination approaches the performance of single-user STR UWB with $N_s = 5$, which is the best achievable performance in imperfect power control environments for these parameter values.

For fixed R_b and E_b/N_0, the number of frames (pulses) per bit N_s (N_p) determines how energy is distributed within a bit. Fig. 3.7 shows the BEP of STR UWB when $R_b =$ 20 Kbps and $E_b/N_0 = 22$ dB. As in Fig. 3.6, solid lines are BEPs of STR UWB with chip discrimination; dashed lines are corresponding BEPs without chip discrimination. Two important results can be drawn from Fig. 3.7. The first result is that $N_s = 3$ has the best BEP performance. From this result we see that, with a fixed data rate $R_b = 20$ Kbps and $E_b/N_0 = 22$ dB, STR UWB with chip discrimination works best when using $N_s = 3$ frames per bit. As the number of frames per bit N_s increases further, the BEP degrades.

Another important result about Fig. 3.7 is that with $N_s = 1$, the BEP for STR UWB without chip discrimination is the same as that of STR UWB with chip discrimination, but worse than that of STR UWB when $N_s > 1$. To explain why, we note that with $N_s = 1$, a collision with a high-power pulse within one frame results in a BEP $= 1/2$ without chip discrimination. With chip discrimination, the BEP $= 1/2$ when that frame is removed. These results reveal a new aspect of transmission for STR UWB systems in ad-hoc networks without perfect centralized power control. With perfect power control the most efficient strategy for transmission is to concentrate all the bit energy in one frame, $N_s = 1$, and spread the frame time as much as possible to avoid collisions [14]. Here we see that with the presence

of high-power users, $N_s = 1$ does not give the best performance for STR UWB systems.

Chip discrimination also improves the performance of DTR UWB. Fig. 3.8 shows BEPs for DTR UWB with and without chip discrimination where the performance improvement with chip discrimination is clearly evident. Shown in Fig. 3.9 are all BEPs for different values of N_p for $R_b = 20$ Kbps and $E_b/N_0 = 22$ dB. As the number of pulses per bit N_p increases, the BEP performance improves up to $N_p = 4$, beyond which the gain diminishes.

For a single user environment and a multiple access environment with equal-power users, DTR UWB outperforms STR UWB as can be seen from (3.16) and (3.17). When high-power users are present in an ad-hoc network, performance of both STR and DTR UWB degrades. In this case, with chip discrimination, performance of both improves, but not to the same degree. To make a meaningful comparison, $N_p = 6$ is used since this gives satisfactory performance given a fixed data rate. A comparison of STR and DTR UWB is shown in Fig. 3.10. For the same number of pulses per bit $N_p = 6$, when $R_b \leq 20$ Kbps, DTR UWB is better than STR UWB in BEP performance. Unlike the single user case and the equal-power multiple access case, when $R_b > 20$ Kbps, DTR UWB performs slightly worse than STR UWB.

We see from Fig. 3.11 that $N_s = 1$ is optimal for high data rates. However, for data rate less than 167 Kbps in a high-power interfering environment, $N_s > 1$ provides better performance. The effect of including equal-power interfering users with high-power interfering users is shown in Fig. 3.12. Notice that the equal-power users increase the noise floor by shifting the BEP curves upward when E_b/σ_e increases.

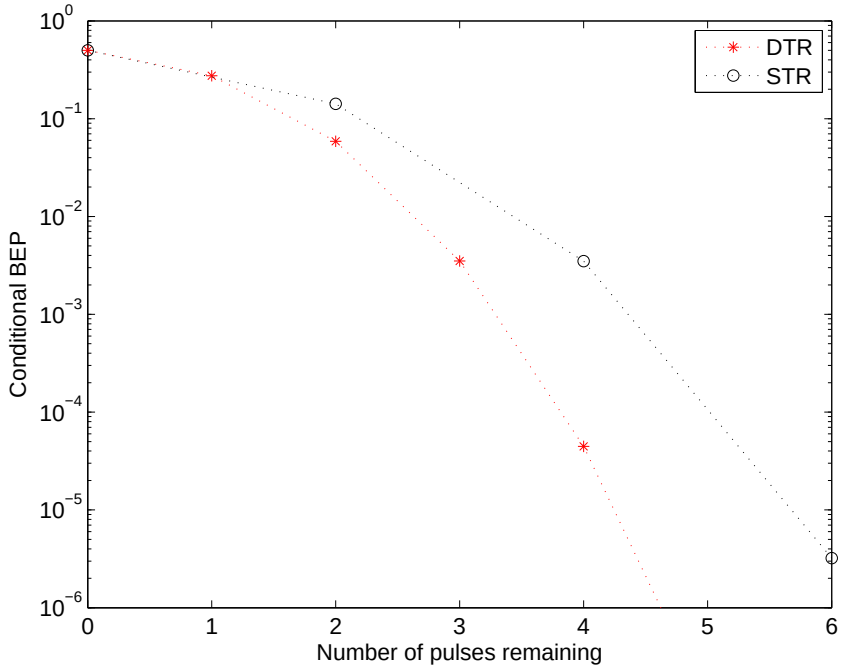

Figure 3.4: The conditional BEP of STR and DTR UWB conditioned on the number of pulses remaining. $E_b/N_0 = 22$ dB, $N_p = 6$, $T_f \geq 2T_{mds}$.

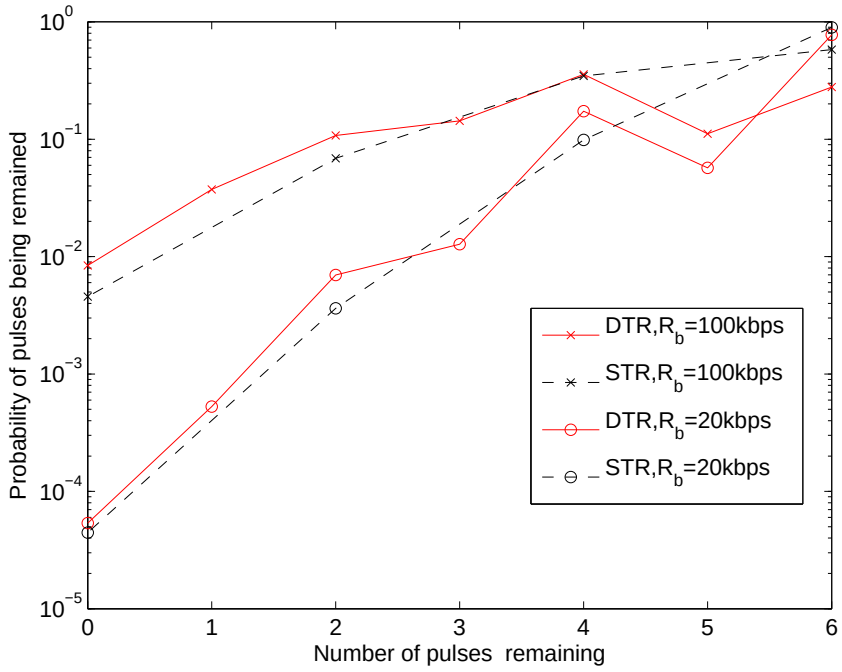

Figure 3.5: The probability of pulses remaining for STR and DTR UWB after chip discrimination. $T_I = 25$ ns, $N_h = 6$, $N_p = 6$.

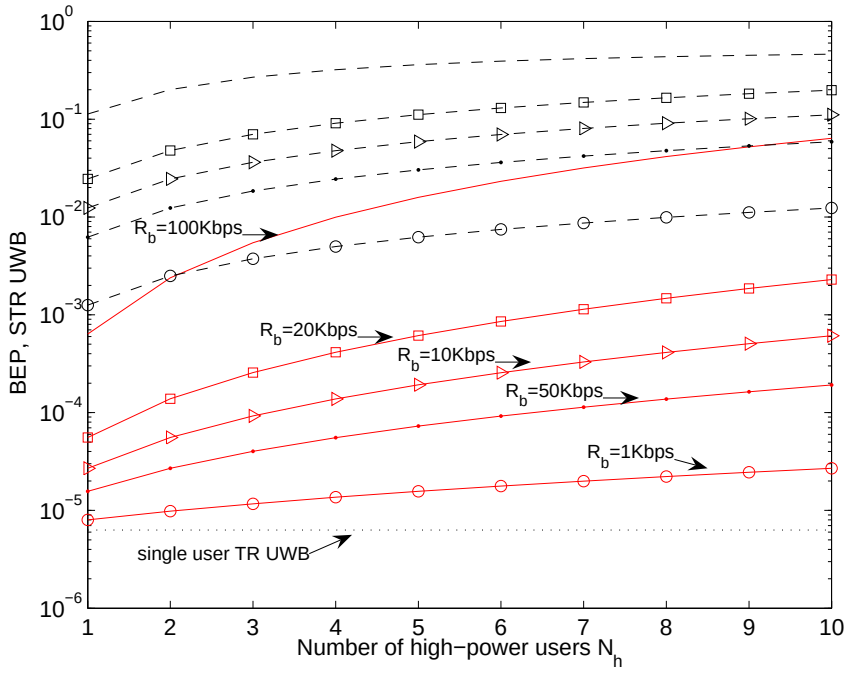

Figure 3.6: The average BEP for STR UWB with (solid) and without (dashed) chip discrimination as a function of the data rate R_b when the number of frames per bit N_s is fixed. $T_I = 25$ ns, $N_s = 5$, $E_b/N_0 = 22$ dB.

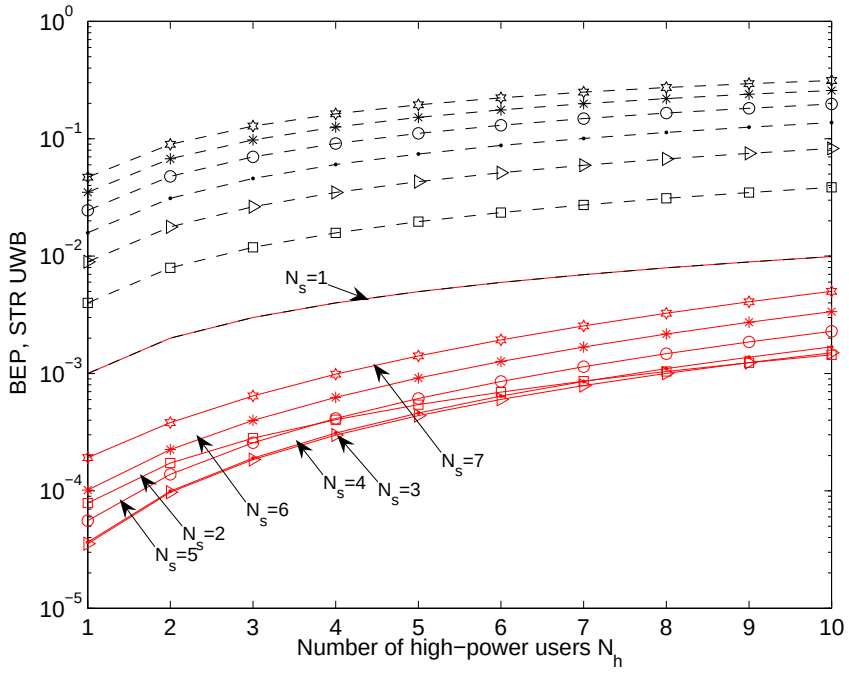

Figure 3.7: The average BEP for STR UWB with (solid) and without (dashed) chip discrimination as a function of the number of frames per bit N_s when the data rate R_b is fixed. $T_I = 25$ ns, $R_b = 20$ Kbps, $E_b/N_0 = 22$ dB.

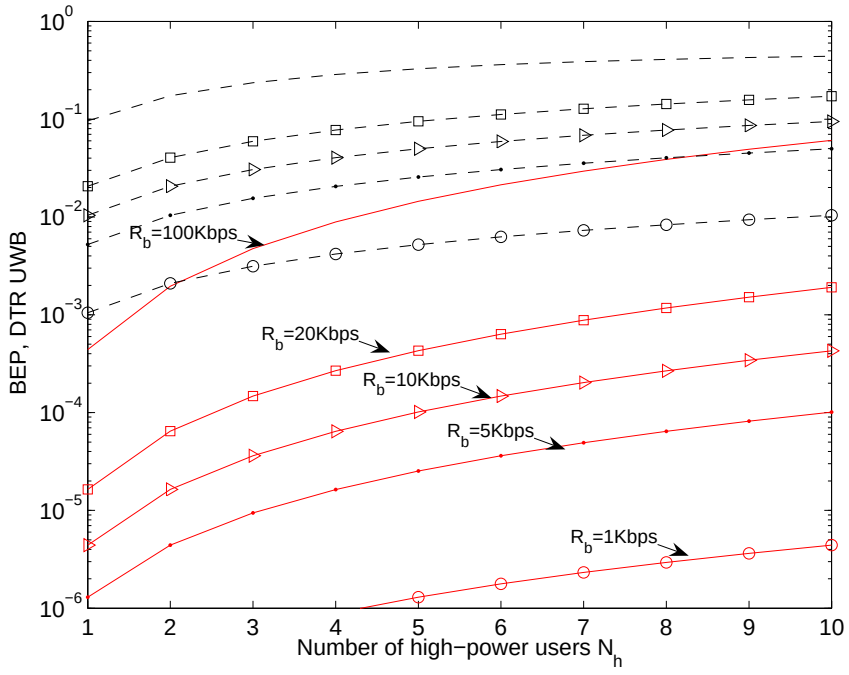

Figure 3.8: The average BEP for DTR UWB with (solid) and without (dashed) chip discrimination as a function of data rate R_b when the number of pulses per bit is fixed. $T_I = 25$ ns, $N_p = 6$, $E_b/N_0 = 22$ dB.

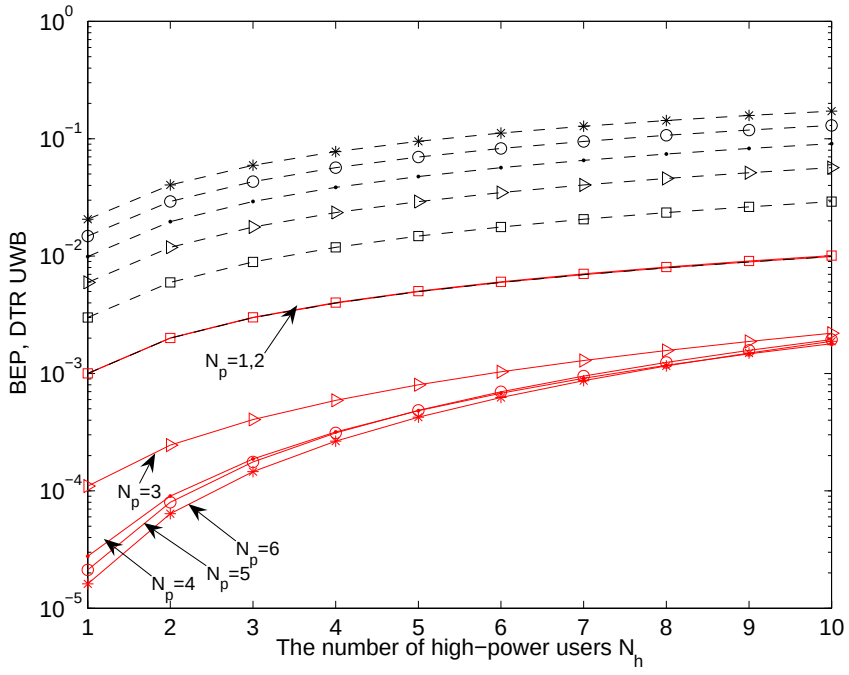

Figure 3.9: The average BEP for DTR UWB with (solid) and without (dashed) chip discrimination as a function of the number of pulses per bit N_p when the data rate R_b is fixed. $T_I = 25$ ns, $R_b = 20$ Kbps, $E_b/N_0 = 22$ dB.

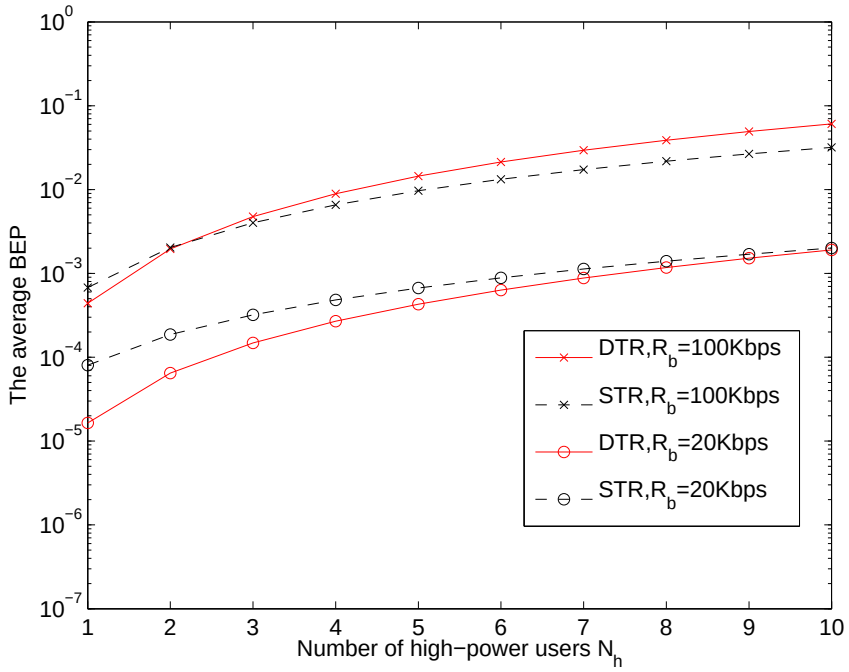

Figure 3.10: Comparison of STR and DTR UWB using chip discrimination. $T_I = 25$ ns, $E_b/N_0 = 22$ dB, $N_p = 6$.

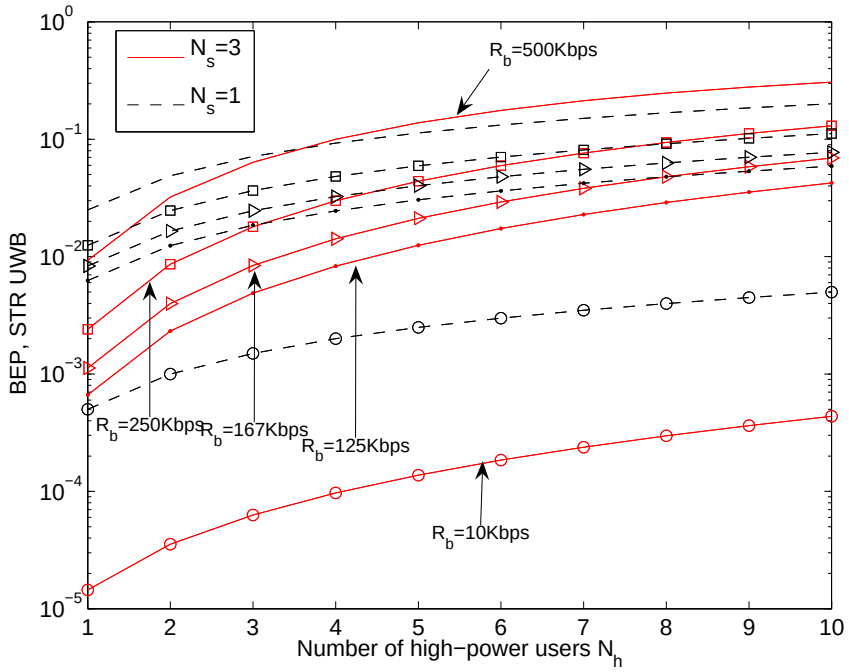

Figure 3.11: The average BEP for STR UWB when $N_s = 1$ and $N_s = 3$. $T_I = 25$ ns, $E_b/N_0 = 22$ dB.

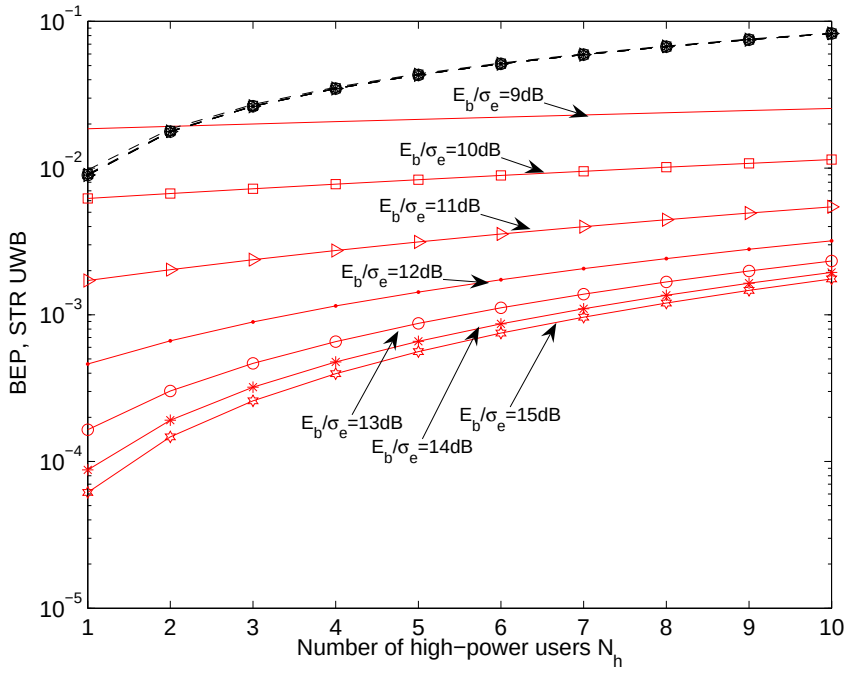

Figure 3.12: The average BEP for STR UWB using chip discrimination (solid lines) with equal-power users as well as high-power users. Dashed lines are BEPs without chip discrimination. $T_I = 25$ ns, $E_b/N_0 = 22$ dB, $N_s = 3$, $R_b = 20$ Kbps.

3.1.7 Conclusion: Binary TR Systems

In this part of the dissertation we investigate the performance of STR and DTR UWB in networks without perfect power control. The dominated factor in determining performance is found to be the collision probability between the desired user pulses and high-power user pulses in the network. To improve the performance of STR and DTR UWB in such networks, chip discrimination is applied. Analysis and numerical calculations both show significant performance improvement when chip discrimination is employed for STR and DTR UWB. One result is that using a single pair of pulses per bit is no longer an optimal way for transmitting information in networks without centralized power control. Instead, the optimal number of pulses per bit N_s is 3 when $R_b = 20$ Kbps and $E_b/N_0 = 22$ dB for STR UWB. For DTR UWB, when the number of pulses per bit N_p increases beyond 4, the performance gain diminishes. Unlike in single user and equal-power user environments, DTR UWB only outperforms STR UWB when the data rate $R_b \leq 20$ Kbps.

3.2 M-ary TR Systems

Our work in the previous section has shown that binary TR UWB communication systems behave differently in ad-hoc networks when compared to an equal-power user environment. To increase the transmission data rate, we propose to use M-ary pulse position modulation (PPM) for TR UWB systems. In this section, the performance of TR UWB systems employing M-ary PPM is investigated in multipath, multiuser environments without centralized power control. Equal-power users are not included in this section in order to highlight the effects of high-power users. Including the interference from equal-power

users would only increase the noise floor since the effects due to equal-power users (MAI) are approximated as Gaussian.

3.2.1 Decision Statistic

For M-ary PPM modulation, within each frame, the receiver correlates the received reference signal with the signal in each of the possible modulation slots, producing M correlation outputs $\{d_{m,j}, 0 \leq m \leq M-1\}$ $(0 \leq j \leq N_s - 1)$. The receiver structure is shown in Fig. 2.2. The signal processing in the receiver is shown in Fig. 3.13 where the dashed signal is the reference signal and the desired modulation slot is slot 0. In the jth frame of

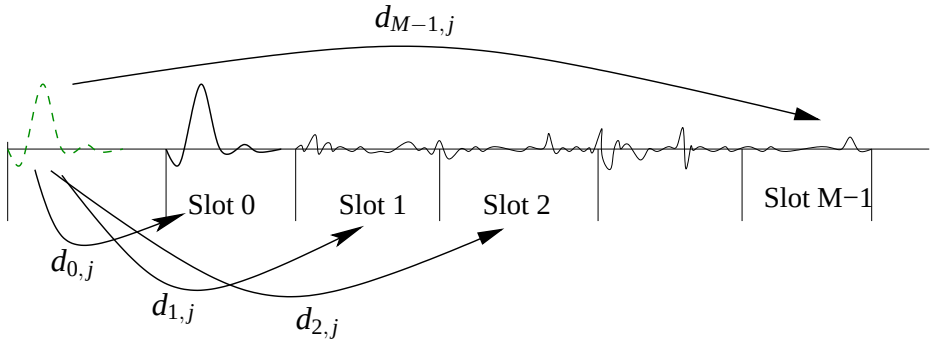

Figure 3.13: Receiver processing of M-ary PPM systems

the ith symbol, the correlation output of the mth slot at the desired receiver is

$$d_{m,j} = \int_{\Omega_{mj}} r(t) r(t - T_d) dt \tag{3.30}$$

where the integration range is $\Omega_{mj} = [iT_s + jT_f + T_d + c_j^{(1)}T_c + m\delta,\ iT_s + jT_f + T_d + c_j^{(1)}T_c + m\delta + T_I]$, and T_I is the integration length. The final output for the mth slot is the sum of N_s outputs

$$D_m = \sum_{j=0}^{N_s-1} d_{m,j} \tag{3.31}$$

The forming of the decision statistic is shown in Fig. 3.14.

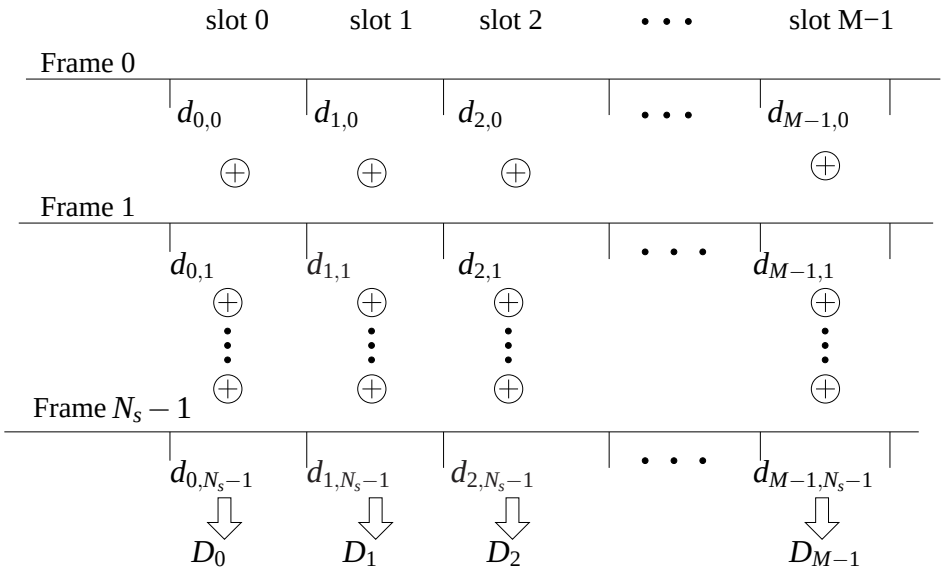

Figure 3.14: Forming decision statistic

Substituting the received signal given by (2.10) into (3.30) and (3.31) yields

$$D_m = \begin{cases} \frac{E^{(1)}}{2} N_s \varepsilon_1 + n_{m1} + n_{m2} + n_{m4} + n_{mh}, & m = 0 \\ n_{m3} + n_{m5} + n_{mh}, & m \neq 0 \end{cases} \tag{3.32}$$

where ε_1 is given in (3.3). The terms $\{n_{mi}\}_{i=1}^{3}$ are due to signal $\times$ noise and are independent

Gaussian random variables. Refer to the corresponding definition of n_{s1} and n_{s2} in (3.4) for binary STR systems. The terms $\{n_{m4},\ n_{m5}\}$ are noise $\times$ noise components and are assumed to be Gaussian distributed with zero mean and variance given by $N_s W T_I N_0^2/2$. The last term n_{mh} captures the high-power interference. All noise terms in D_m are independent. Note again that the equal-power interference is not included as it is approximated as Gaussian and only increases the noise floor when included. We focus on studying the effects of high-power users in this section and the MAI due to equal-power users is investigated in full detail in Chapter 4.

After demodulation, the receiver compares the values of $\{D_m\}_{m=0}^{M-1}$ and chooses the symbol $\hat{m}$ with the largest value. Thus, the desired receiver makes a decision based on

$$\hat{m} = \arg\max_m D_m \tag{3.33}$$

The probability of making a correct decision when symbol 0 is transmitted is then

$$P_c = \Pr\{D_0 > D_1, D_0 > D_2, ..., D_0 > D_{M-1}\} \tag{3.34}$$

To evaluate the performance of TR UWB systems using M-ary PPM, the effects of thermal noise and high-power users need to be studied.

3.2.2 Error Performance: Single User Link

A single user environment is considered ($N_h = 0$) in this section, therefore only thermal noise is present to the TR UWB receiver. Let n_0 denote the total noise of the desired slot,

and $\{n_m\}_{m=1}^{M-1}$ the total noise of other slots.

$$n_0 = n_{01} + n_{02} + n_{04} \tag{3.35}$$

$$n_m = n_{m3} + n_{m5}, \quad m = 1, 2, ..., M-1 \tag{3.36}$$

The variances of n_0 and n_m are calculated to be

$$\sigma_0^2 = \frac{E^{(1)}}{2} N_0 + \frac{N_s W T_I N_0^2}{2} \tag{3.37}$$

$$\sigma_m^2 = \frac{E^{(1)}}{2} \frac{N_0}{2} + \frac{N_s W T_I N_0^2}{2}, \quad m \neq 0 \tag{3.38}$$

In deriving the above results, the expectation $\mathbb{E}\{\varepsilon_1\} = 1/N_s$ is used from Appendix A. The M outputs in (3.32) can be rewritten, using the short notations n_0 and n_m ($m \neq 0$) for the noise terms, as

$$D_m = \begin{cases} \mu_0 + n_0, & m = 0 \\ n_m, & m = 1, 2, ..., M-1 \end{cases} \tag{3.39}$$

where $\mu_0 = \frac{E^{(1)}}{2}$. Since the noise terms $\{n_m\}_{m=0}^{M-1}$ are independent, the probability of a correct decision is evaluated as

$$P_c = \int_{-\infty}^{\infty} \left[\int_{-\infty}^{y} f_1(x) dx \right]^{M-1} f_0(y) dy \tag{3.40}$$

where $f_1(x)$ is the Gaussian probability density function (PDF) of the output of the undesired slot 1 (D_1), with mean 0 and variance σ_1^2, and $f_0(y)$ is the Gaussian PDF of the output of the desired slot (D_0) with mean μ_0 and variance σ_0^2. A simple manipulation of (3.40)

yields

$$P_c = \int_{-\infty}^{\infty} \left[1 - Q\left(\frac{y}{\sigma_1}\right)\right]^{M-1} f_0(y)dy \tag{3.41}$$

The symbol error probability, P_M, is thus

$$P_M = 1 - P_c \tag{3.42}$$

The bit error probability (P_b) for equiprobable orthogonal modulation can be written as [59]

$$P_b = \frac{2^{k-1}}{2^k - 1} P_M \tag{3.43}$$

3.2.3 Error Performance: High-Power Users

Our work in [26] has shown that interference from high-power users dramatically degrades the performance of binary-PAM TR UWB systems. A simple analysis reveals that high-power users have more severe detrimental effects on TR UWB systems with M-ary PPM when $M > 2$.

To illustrate, we use the notation $p = \frac{2T_J}{T_f}$, the fraction of time that an interfering signal occurs within the desired slot during a frame that has effect on the correlation output. The same probability p applies for the reference signal colliding with a high-power interfering user. For N_s successive frames, the probability that the correlation output of the desired slot affected by a signal from N_h high-power users is $\min\{2N_sN_hp,\ 1\}$. Each of the rest of $M-1$ undesired slots has the same collision probability as the desired slot, since the integration time of the correlator is the same for all slots. When a signal from a high-power user (with much higher interfering power level than the desired user) occurs in an

undesired slot $\hat{m} \neq 0$, due to the large correlator output of that slot, the detector of the desired receiver makes an incorrect decision by choosing $\hat{m}$ as the transmitted symbol. The probability of a signal from N_h high-power interferers occurring in any undesired slot is $p_m = \min\{2(M-1)N_s N_h p,\ 1\}$. So the symbol error probability due to high-power users is given by

$$P_{mh} = p_m + (1 - p_m)P_M \tag{3.44}$$

The first term in (3.44) is proportional to M and is not related to E_b/N_0. This can cause a floor in the BEP performance in regions of high E_b/N_0 values, where errors due to collisions with high-power users dominate. This effect becomes more pronounced as M increases.

3.2.4 Chip Discrimination: M-ary TR

To mitigate the detrimental effects of high-power users on the desired user, chip discrimination [23, 24] is applied to TR UWB systems employing M-ary PPM.

The receiver processing with one high-power interfering user occurring in one of the undesired slots is shown in Fig. 3.15. The dashed signal is the reference signal and the dash-dotted signal is the high-power interfering signal. Denote the slot where the high-power user occurs as slot $\tilde{m}$ ($\tilde{m} \neq 0$). If the receiver does not take any measure to suppress the effect from the high-power interfering user, the receiver makes an incorrect decision that $\hat{m} = \tilde{m}$ is the transmitted symbol because symbol $\tilde{m}$ has the largest correlation output. With chip discrimination applied at the receiver, each correlation output $d_{m,j}$ ($0 \leq m \leq M-1$) is compared with a pre-set threshold. If an output is beyond the range of the threshold, that

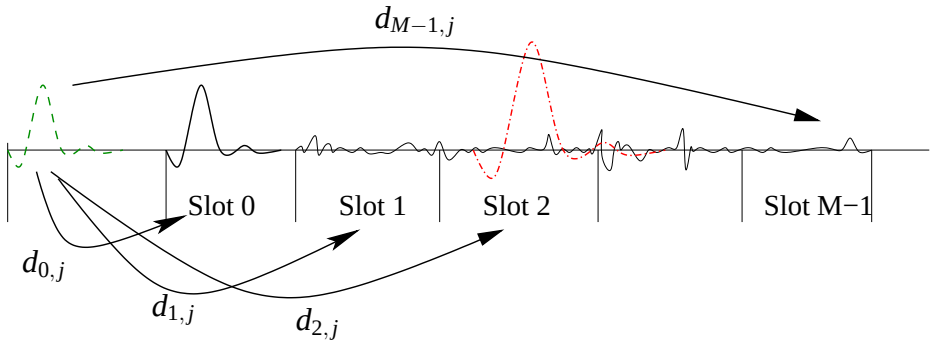

Figure 3.15: Receiver processing of M-ary PPM systems with one high-power user

output is removed. Assume the receiver has an ideal threshold so that correlation outputs corrupted by high-power users are detected and removed. The process is shown in Fig. 3.16 where two outputs affected by high-power users are shown and detected.

Suppose k_0 out of N_s correlation outputs are removed for the desired slot 0. The output D_{0,k_0} has a mean and variance of

$$\begin{aligned} \mu_{0,k_0} &= \frac{N_s - k_0}{N_s}\mu_0 \\ \sigma^2_{0,k_0} &= \frac{N_s - k_0}{N_s}\sigma^2_0 \end{aligned} \tag{3.45}$$

Assuming there are k_m correlation outputs removed by chip discrimination for the mth ($m \neq 0$) undesired slot, the mean of D_{m,k_m} is 0 and the variance is

$$\sigma^2_{m,k_m} = \frac{N_s - k_m}{N_s}\sigma^2_m \tag{3.46}$$

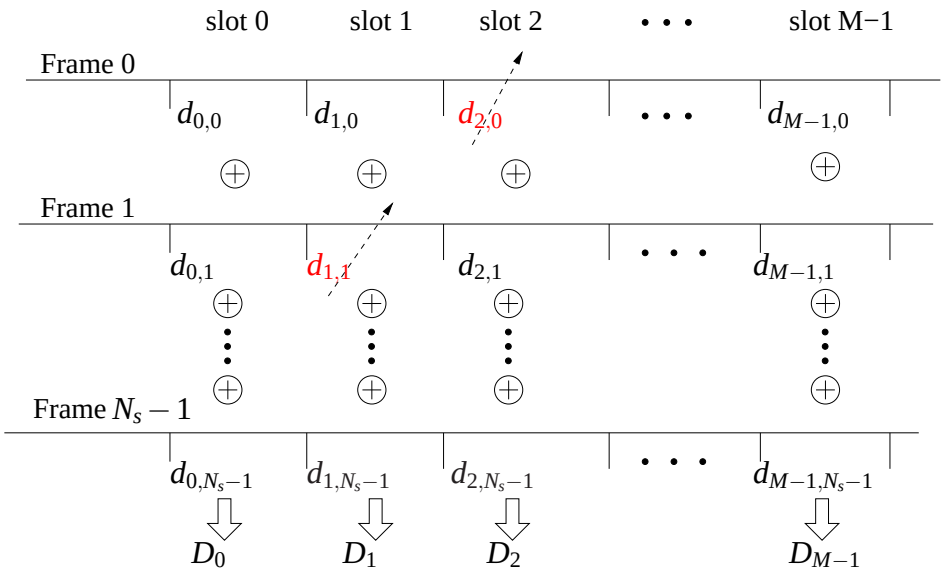

Figure 3.16: Receiver processing of M-ary PPM systems with 2 high-power user

Let $\mathcal{K} = \{k_0, k_1, ..., k_{M-1}\}$ be the sequence of the number of correlation outputs removed by chip discrimination for all slots. This sequence $\mathcal{K}$ is i.i.d. since each slot is affected by interference from high-power users independently with the same probability. Therefore, the probability of a correct decision using chip discrimination has the same form as in (3.41), given by

$$P_{mc} = \mathop{\mathbb{E}}_{k_0}\left\{\int_{-\infty}^{\infty}\left[1-\mathop{\mathbb{E}}_{k_1}\left\{Q\left(\frac{y}{\sigma_{1,k_1}}\right)\right\}\right]^{M-1} f_{0,k_0}(y)dy\right\} \tag{3.47}$$

where $\{f_{0,k_0}(y)\}_{k_0=0}^{N_s}$ is a set of PDFs of Gaussian random variables with mean μ_{0,k_0} and variance σ_{0,k_0}^2 given in (3.45). This probability of a correct decision differs from (3.41) in that it is averaged over the probability mass functions of k_0 and k_1, which are the same.

Denote $P(k)$ as the probability mass function for the i.i.d. sequence $\mathcal{K}$. For a given integration time and frame length, $P(k)$ is unchanged from the binary PAM case in Section 3.1.3 and is given by

$$P(k) = \begin{pmatrix} N_s \\ k \end{pmatrix} \mathfrak{p}_{cs}^{k} (1-\mathfrak{p}_{cs})^{N_s-k} \tag{3.48}$$

where $\mathfrak{p}_{cs}$ is from (3.19). The expression for the probability of the correct decision P_{cd} in (3.47) is difficult to evaluate in general, except for $M = 2$. For $M = 2$, we can use a property of the Q function given by

$$\mathbb{E}\{Q(a+\lambda X)\} = Q\left(\frac{a}{\sqrt{1+\lambda^2}}\right) \tag{3.49}$$

where a and λ are constants and X is a Gaussian RV with mean zero and variance one. Using (3.49) (change of variables in (3.47) is needed), P_{cd} in (3.47) at $M = 2$ can be expressed as

$$P_{mc,2} = 1 - \sum_{k_0=0}^{N_s} \sum_{k_1=0}^{N_s} Q\left(\frac{u_{0,k_0}}{\sqrt{\sigma_{0,k_0}^2 + \sigma_{1,k_1}^2}}\right) P(k_0)P(k_1) \tag{3.50}$$

The symbol error probability is therefore

$$P_2 = 1 - P_{cd,2} \tag{3.51}$$

For $M > 2$, a union bound for the probability of error for M-ary orthogonal modulation is obtained as [59]

$$P_M \leq (M-1)P_2 \tag{3.52}$$

which is proved tight through numerical calculations.

3.2.5 Effect of Duty Cycle on Performance

The probability of correct decision in (3.50) is closely related to the probability mass function $P(k)$ which is determined by $p = 2T_I/T_f$ if N_s and N_h are fixed. Thus for a given value of repetition factor N_s and the number of high-power users N_h in the network, the probability of detection decreases with $P(k)$. Therefore, to maintain given desired levels of BEP and E_b/N_0, there is a maximum p allowed, which translates into a minimum T_f when T_I is fixed. This relates to the low-duty cycle nature of UWB signaling [33]: At the transmitter side, the duty cycle T_p/T_f is low; it also needs to be low at the receiver side, requiring a small value of T_{mds}/T_f. The lower the duty cycle at the receiver side, the smaller the chance of collisions between users. However, given the form of the correct decision $P_{cd,2}$, a closed form of the required p is not obtainable for a given BEP. We resort to numerical calculations to investigate the impact of p (also the impact of T_{mds}/T_f).

3.2.6 Numerical Results

The transmitted pulse is the second derivative of the Gaussian pulse with pulse width 0.7 ns [33]. The CM1 channel model from [56] with the delay spread $T_{mds} = 50$ ns is used. The receiver has a one-sided bandwidth $W = 4$ GHz. The optimal integration time is found to be $T_I = 25$ ns for this channel model. The optimal repetition factor N_s is 3 in Section 3.1.6 for binary-PAM standard TR systems at a rate $R_s = 20$ Kbps. In this section, we first set $N_s = 3$, then the effect of N_s is investigated.

As we discussed in previous sections, the performance of TR UWB systems in the

presence of high-power users is determined by the collision probability $p = 2T_I/T_f$, which fixes the ratio T_{mds}/T_f when T_I is chosen. The plot in Fig. 3.17 shows the effect of this parameter when the number of high-power users is $N_h = 4$. For a given BEP at $P_b = 10^{-4}$, the duty cycle for 4-PPM is found to be less than 5×10^{-3}, resulting in a value of $T_f \geq 10^4$ ns. The symbol rate $R_s = 1/(N_s T_f) \leq 30$ Ksps, which constrains the symbol rate for networks with high-power users. In the following numerical calculations, we use low symbol rates such as $R_s = 20$ Ksps.

The effect of high-power users is demonstrated in Fig. 3.18 (solid lines), which shows the BEP performance of TR UWB systems using M-ary PPM when there are $N_h = 5$ high-power users. The dashed lines are corresponding BEPs in a single user environment. Clearly the detrimental effect of high-power users is seen in Fig. 3.18 by observing that the BEP performance is mainly determined by the probability of collision with high-power users. BEPs increase with M since the receiver 'listens' for a larger fraction of the whole frame time as M increases, resulting in a larger probability of collision and unacceptable performance.

Fig. 3.19 shows the error performance of TR UWB systems with and without chip discrimination for a given symbol rate $R_s = 20$ Ksps. The performance is plotted versus N_h with $E_b/N_0 = 20$ dB. Without chip discrimination, BEPs are no better than 10^{-2}. With chip discrimination, the error performance of TR UWB systems using M-ary PPM is dramatically increased. The BEP performance improves with increasing M, however, the amount of improvement reduces as M increases. With the parameter setting in this figure, increasing M to 32 is optimal. The plots in Fig. 3.20 show the performance of chip discrimination for a given bit rate $R_b = 40$ Kbps. The BEP performance is significantly improved for TR

UWB systems using M-ary PPM compared with the performance without chip discrimination. At $R_b = 40$ Kbps, BEP performance in Fig. 3.20 is better than that in Fig. 3.19 at $R_s = 20$ Ksps. This is because the bit rate in Fig. 3.19 is larger than 40 Kbps when $M > 4$. At a larger bit rate and with the same repetition factor N_s, the frame time for systems in Fig. 3.19 is smaller than that in Fig. 3.20, resulting in a larger probability of collision between the desired user and high-power users.

The effect of the repetition factor N_s on the error performance is illustrated in Fig. 3.21. The modulation order $M = 8$ and the symbol rate $R_s = 20$ Ksps are chosen as an example. For $E_b/N_0 = 20$ dB, the plots in Fig. 3.21 show that $N_s = 5$ gives the best performance. For these parameter values, $N_s = 3$ is optimal for binary-PAM standard TR UWB systems at the same symbol rate with $E_b/N_0 = 22$ dB. The optimal N_s for each M is a function of E_b/N_0 and the collision probability. Setting $N_s = 5$ and picking one value of N_h, (for example, $N_h = 5$), the BEP performance is plotted as a function of E_b/N_0 and M, as in Fig. 3.22. Solid lines are BEPs of TR systems with chip discrimination while dashed lines are those of a single-user environment. The effect of high-power users manifests itself by deviating the BEP performance from the BEP in a single-user environment. The deviation is larger when M increases. The phenomenon of approximately flat error performance with interference from high-power users shown in Fig. 3.18 is not seen in Fig. 3.22. Instead, with the same symbol rate $R_s = 20$ Ksps, chip discrimination with M-ary PPM works robustly against high-power users.

The upper bound for BEP of TR UWB systems using M-ary PPM and chip discrimination is shown in Fig. 3.23. The repetition factor is $N_s = 5$ and there are $N_h = 5$ high-power users. At $R_s = 20$ Ksps, the upper bound is tight at high E_b/N_0 regions shown in Fig. 3.23.

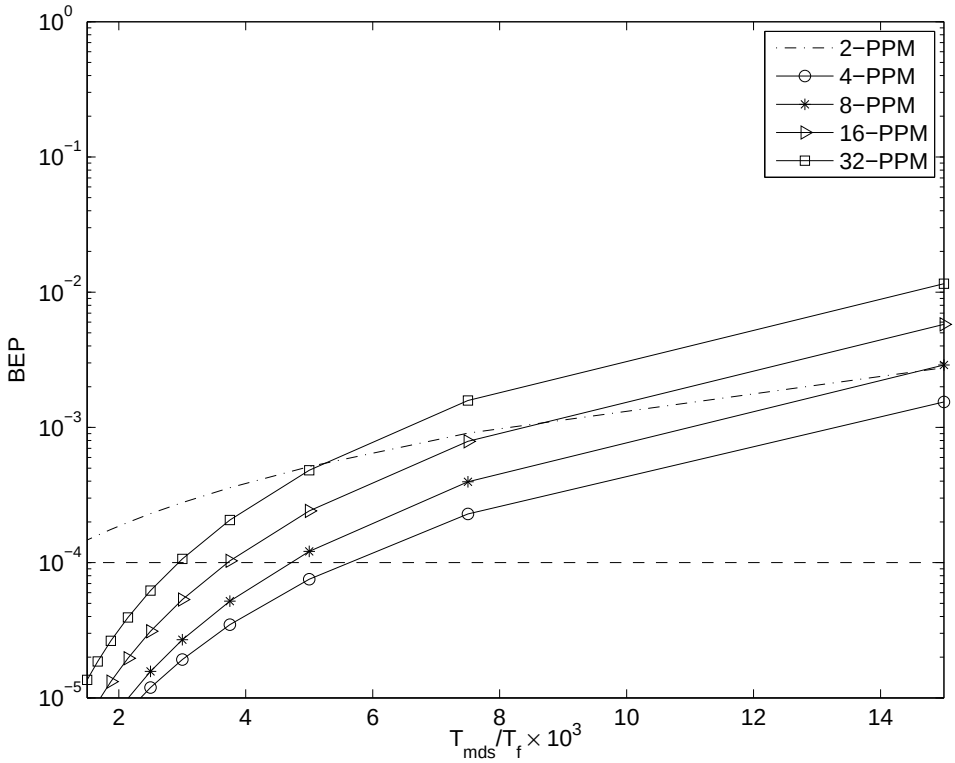

Figure 3.17: BEP of TR UWB as a function of T_{mds}/T_f at $E_b/N_0 = 22$ dB. Other parameters: $N_h = 4$, $T_I = 25$ ns, $T_{mds} = 50$, $N_s = 3$.

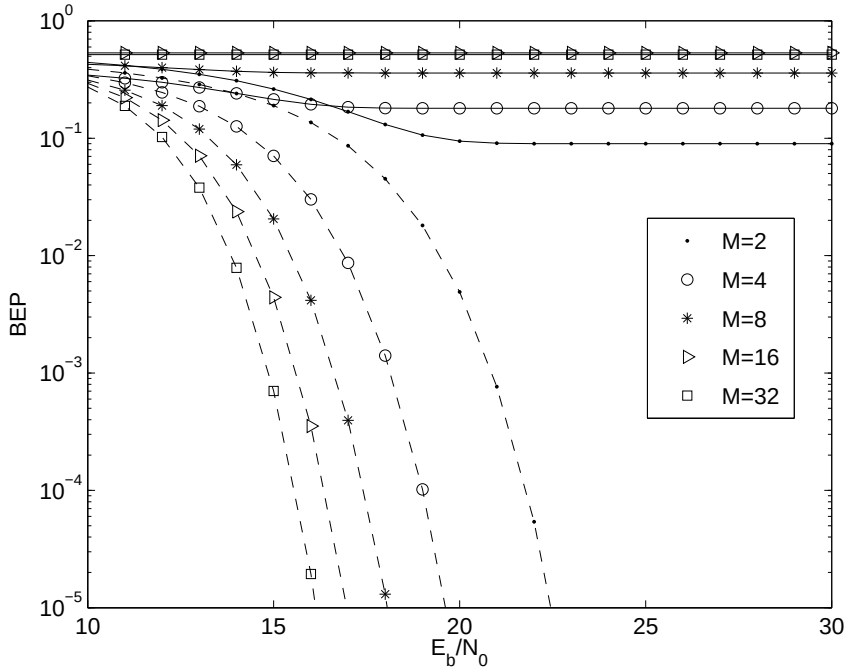

Figure 3.18: BEP for M-ary TR UWB in a single user environment (dashed lines) and with $N_h = 5$ high-power users (solid lines). $T_I = 25$ ns, $N_s = 3$, $R_s = 20$ Ksps.

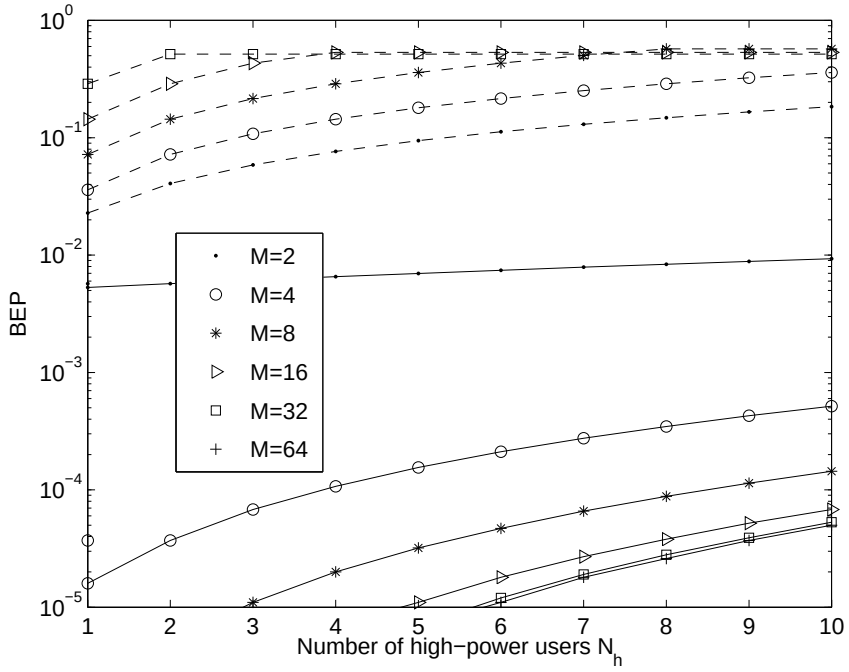

Figure 3.19: BEP for TR UWB in a high-power user environment with (solid lines) and without (dashed lines) chip discrimination at $R_s = 20$ Ksps. $E_b/N_0 = 20$ dB, $T_I = 25$ ns, $N_s = 3$.

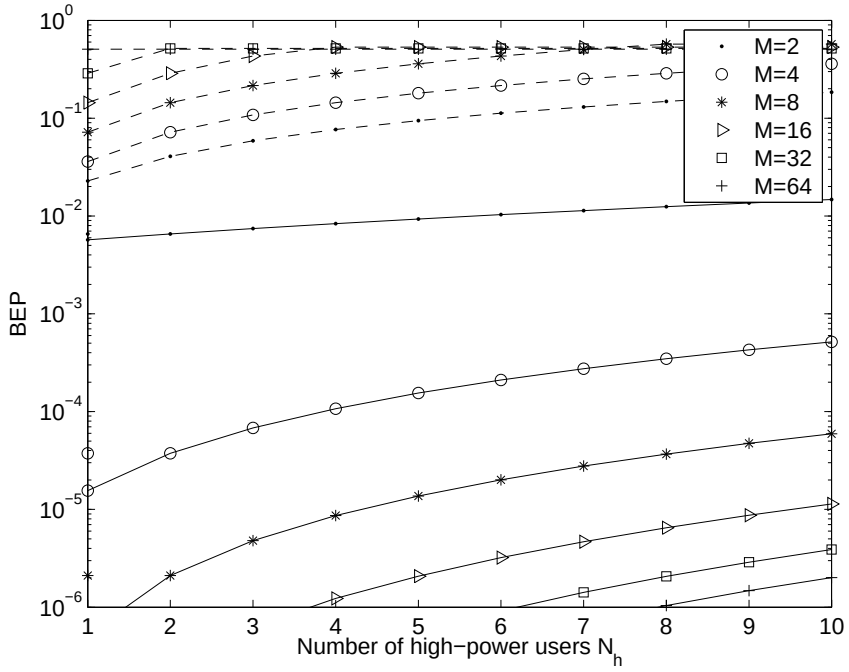

Figure 3.20: BEP for TR UWB in a high-power user environment with (solid lines) and without (dashed lines) chip discrimination at $R_b = 40$ Kbps. $E_b/N_0 = 20$ dB, $T_I = 25$ ns, $N_s = 3$.

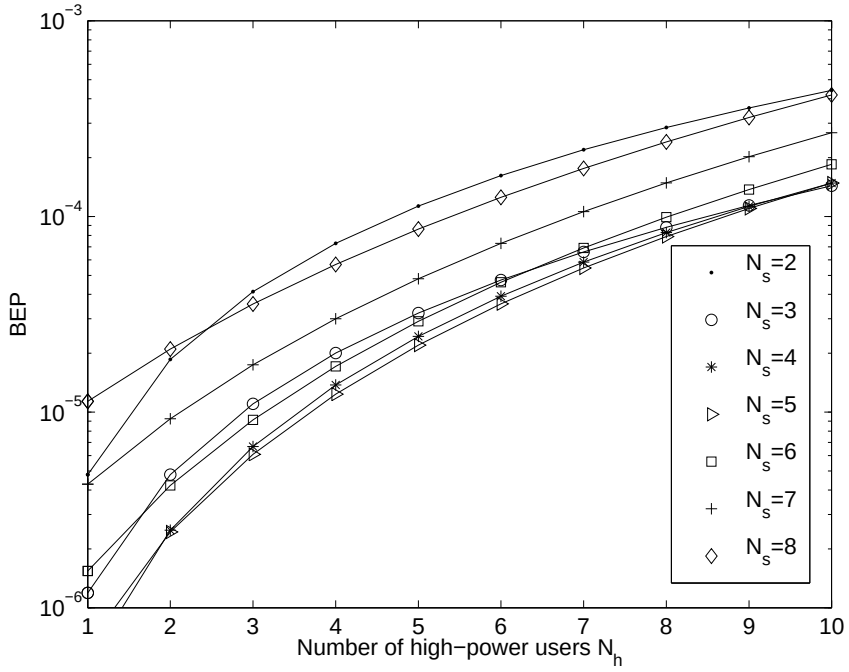

Figure 3.21: BEP of 8-PPM TR UWB in an environment with high-power users. $E_b/N_0 =$ 20 dB, $T_I = 25$ ns, $R_s = 20$ Ksps.

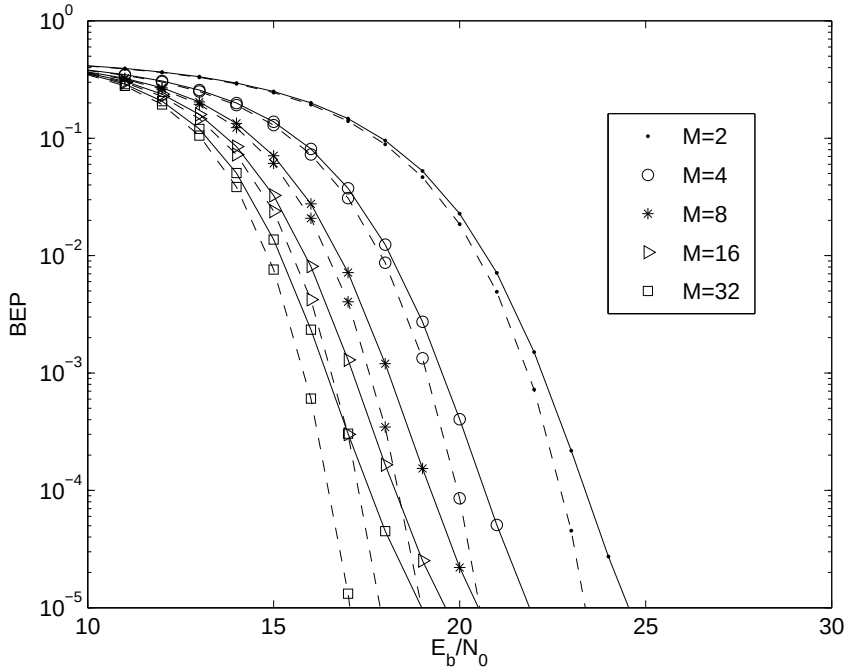

Figure 3.22: BEP of Mary-PPM TR UWB in an single user environment (dashed lines) and with $N_h = 5$ high-power users (solid lines). $N_s = 5$, $T_I = 25$ ns, $R_s = 20$ Ksps.

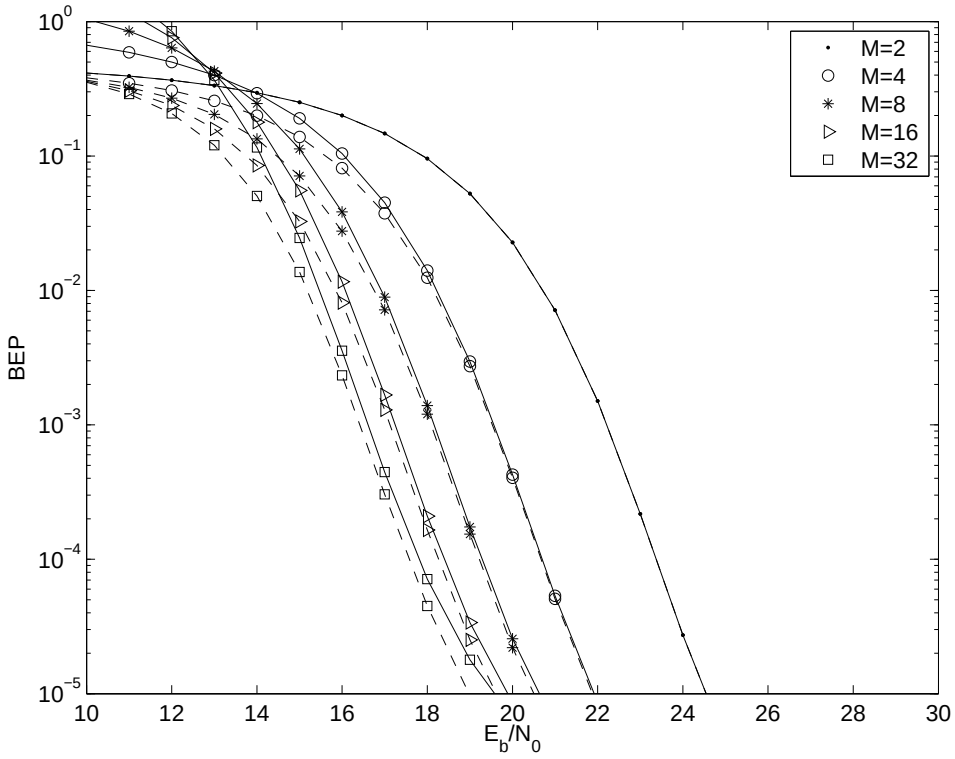

Figure 3.23: The upper bound (solid lines) for BEP and the exact evaluation (dashed lines) of Mary-PPM TR UWB with $N_h = 5$ high-power users. $N_s = 5$, $T_I = 25$ ns, $R_s = 20$ Ksps.

3.2.7 Conclusion: M-ary TR Systems

We have investigated the performance of transmitted reference UWB systems with M-ary pulse position modulation in environments with high-power interfering users. Examples include ad-hoc networks or networks where centralized power control are infeasible. The interference from high-power users is shown to significantly degrade the performance of TR UWB systems using M-ary PPM. Chip discrimination is used to mitigate the detrimental effect of high-power users. Theoretical analysis on the performance of M-ary PPM applied to TR UWB systems is derived. A tight upper bound for the symbol error probability is obtained. Analysis and numerical results show that TR UWB systems with M-ary PPM using chip discrimination is robust against high-power interfering users in wireless networks where centralized power control is infeasible, such as ad-hoc networks. TR systems with chip discrimination are suitable for low data-rate communications.

Chapter 4

Performance Analysis: Equal-Power Users

In Chapter 3 we investigate the performance of binary PAM and M-ary PPM TR systems with a focus on effects of high-power users. In this chapter, we investigate the effects from equal-power users, or the so-called multiple-access interference (MAI), for TR UWB systems with M-ary PPM. A new method for deriving the variance of the Gaussian random variable resulting from MAI is developed using the power delay profile (PDP) of the channel. This makes the theoretical analysis tractable and enables us to predict the system-level performance such as the supported number of users, the achievable data rate, and the required E_b/N_0. The multiple-access performance for slightly frequency-shifted reference (FSR) UWB systems is also investigated in this chapter. Performance comparison is given between FSR and TR systems.

4.1 TR UWB Systems

One contribution of this section is to investigate and address two fundamental issues of communications for TR UWB systems using M-ary PPM: 1) To determine the achievable data rate as a function of system resources. 2) To determine the required E_b/N_0 for the system to achieve a given BEP. The second contribution of this section is to quantify the combined effects of both equal-power and high-power users, including the limit in the data rate in the presence of high-power users, and the optimization of the system performance by finding the optimal operational parameters. A third contribution of this work is the use of the power delay profile (PDP) in deriving the variance of the MAI, which makes the theoretical analysis tractable. This feature in return enables us to theoretically optimize the system parameters as shown in this chapter. We presented this idea in [55].

4.1.1 Decision Statistic

The receiver structure of TR systems employing M-ary PPM is shown in Fig. 2.2. The receiver signal processing is depicted in Fig. 3.13. The decision statistic of the mth modulation slot is formed by summing the correlation outputs from each frame, shown in Fig. 3.14. In this section, we assume there is no high-power users. The decision statistic is given by

$$D_m = \begin{cases} \mu_0 + n_{m1} + n_{m2} + n_{m4} + n_{me}, & m = 0 \\ n_{m3} + n_{m5} + n_{me}, & m = 1,2,\ldots,M-1 \end{cases} \tag{4.1}$$

where the desired slot has a signal component $\mu_0 = \frac{E^{(1)}}{2} N_s \varepsilon_1$. All the noise terms are defined in the same way as in (3.32) except n_{me}, which captures the MAI (equal-power inter-

ference). All noise terms in D_m are independent.

The discussion of the MAI for UWB systems with Rake receivers and for binary TR UWB systems is given in Section 1.2.2. We assume in this dissertation that the number of equal-power users is large enough so that the MAI can be approximated as Gaussian distributed. The decision rule for TR systems with M-ary PPM is given in (3.33) and the probability of making a correct decision is given by (3.34). The performance in a single user environment is discussed in Section 3.2.2. We use the same notations as in Section 3.2.2 for the noise variance in a single user environment: σ_0^2 as the noise variance for the desired slot and σ_m^2 the noise variance for undesired slots with $m = 1, 2, ..., M-1$. Their expressions are given in (3.37) and (3.38), respectively. We now go to the details for the variance of the MAI term n_{me}.

4.1.2 Interference From Equal-Power Users

As in Section 3.1, we replace the spacing of the desired user $T_d^{(1)}$ with T_d for convenience of analysis. To analyze the MAI effect, we first consider the situation where one signal from an equal-power interfering user (with $E^{(1)} = E^{(u)} = E_s$) collides with the desired user's reference signal. The received signal from the first signal pair of the first symbol ($i = 0$) can be written as

$$\begin{aligned} & r(t) = \\ & \sqrt{\frac{E_s}{2}} \Big[g^{(1)}(t - c_0^{(1)} T_c) + g^{(u)}(t - c_0^{(u)} T_c - \tau^{(u)}) \\ & + g^{(1)}(t - c_0^{(1)} T_c - T_d - I_0^{(1)} \delta) + g^{(u)}(t - c_0^{(u)} T_c - T_d^{(u)} - I_0^{(u)} \delta - \tau^{(u)}) \Big] \\ & + n(t) \end{aligned} \tag{4.2}$$

The time offset between reference signals of user 1 and user u is $\tau_u^{'} = (c_0^{(u)} - c_0^{(1)})T_c + \tau^{(u)}$, where $\tau^{(u)}$ is a uniform distribution within the interval $[0,\ T_f]$. The offset between data-bearing signals is $\tau_u^{''} = (c_0^{(u)} - c_0^{(1)})T_c + T_d^{(u)} - T_d + (I_0^{(u)} - I_0^{(1)})\delta + \tau^{(u)}$. If the design of $\{T_d^{(u)}\}_{u=1}^{N_u}$ together with the equiprobable transmitting symbols $I_j^{(u)} \in \{0,1,...,M-1\}$ makes $\tau_u^{''}$ independent of $\tau_u^{'}$, the reference signal and the data-bearing signal are affected by equal-power users independently. Assume the signal from an equal-power interfering user lands in the integration interval of the desired user's receiver correlator. The possible offset $\tau_u^{'}$ is restricted to the interval $[0,\ T_I]$. The jth correlation, $\int_{\Omega_{0j}} r(t)r(t-T_d)dt$, is computed for the desired slot $\Omega_{0j} = [jT_f + T_d + c_j^{(1)}T_c,\ \ jT_f + T_d + c_j^{(1)}T_c + T_I]$. After N_s correlations and the summation of the outputs, the desired slot has an output

$$D_0 = \frac{E_s}{2}N_s\varepsilon_1 + n_{01} + n_{02} + n_{04} + n_{0e} \tag{4.3}$$

where the Gaussian random variable n_{0e} due to multiple-access interference is the summation of N_s independent random variables $\{n_e(j)\}_{j=0}^{N_s-1}$. This random variable $n_e(j)$ is expressed as

$$\begin{aligned} n_e(j) = \quad & n_{em} + n_{en} \\ = \quad & \frac{E_s}{2}\int_{\Omega_{0j}} g^{(1)}(t)g^{(u)}(t-\tau^{(u)})dt \\ & + \sqrt{\frac{E_s}{2}}\int_{\Omega_{0j}} g^{(u)}(t-\tau^{(u)})n(t)dt\Big] \end{aligned} \tag{4.4}$$

where n_{em} results from the collision between the the signal of the interfering user u and the signal of the desired user, and n_{en} corresponds to the noise caused by the cross correlation

between the interfering user u and the thermal noise. In [14], the variance of this Gaussian random variable is given using $g^{(u)}(t)$, its auto-correlations and cross-correlations. To yield a more straightforward mapping between the number of equal-power users N_e and the variance $\sigma_e^2 = \mathrm{Var}\{n_{0e}\}$, we try to obtain an explicit relationship between these parameters. Inspired by the work in [13], we seek a solution by using the power delay profile (PDP) of the channel.

It is easy to show that the MAI term n_{0e} has zero mean. The variance σ_e^2 of n_{0e} contains two parts

$$\sigma_e^2 = N_s\sigma_{em}^2 + N_s\sigma_{en}^2 \tag{4.5}$$

where $\sigma_{em}^2 = \mathbb{E}\{n_{em}^2\}$, $\sigma_{en}^2 = \mathbb{E}\{n_{en}^2\}$, and are given by

$$\sigma_{em}^2 = \mathop{\mathbb{E}}_{h,\tau^{(u)}}\left\{\left(\frac{E_s}{2}\right)^2\left(\int_0^{T_I} g^{(1)}(t)g^{(u)}(t-\tau^{(u)})dt\right)^2\right\} \tag{4.6}$$

$$\sigma_{en}^2 = \mathop{\mathbb{E}}_{h,\tau^{(u)}}\left\{\frac{E_s}{2}\left(\int_0^{T_I} g^{(u)}(t-\tau^{(u)})n(t)dt\right)^2\right\} \tag{4.7}$$

where $\mathbb{E}_{h,\tau^{(u)}}$ denotes expectation with respect to the channel and the random delay $\tau^{(u)}$.

We first calculate the value for σ_{em}^2 by introducing the power delay profile of the channel, $P_h(t)$, which is defined as

$$P_h(t) = \mathbb{E}\left\{\left[h^{(u)}(t)\right]^2\right\} \tag{4.8}$$

The power delay profile for a dense multipath channel typically spans hundreds of nanoseconds for UWB communications. Therefore we assume $P_h(t)$ is approximately constant within the support of the narrow pulse $p(t)$. Substituting the channel model in (2.1) in the

definition of $P_h(t)$, we have

$$P_h(t) = \sum_{l=0}^{L-1} \mathbb{E}\{(\alpha_l^{(u)})^2\}\delta(t-\tau_l^{(u)}) \tag{4.9}$$

The variance of n_{em} (σ_{em}^2) in terms of $P_h(t)$ is calculated by substituting (4.9) into (4.6). With some manipulation, we can write σ_{em}^2 as

$$\begin{aligned}\sigma_{em}^2 &= \frac{E_s^2}{4}\mathop{\mathbb{E}}_{\tau^{(u)}}\left\{\int_0^{T_I}\int_0^{T_I}\mathop{\mathbb{E}}_{h}\{g^{(1)}(t)g^{(1)}(v)\}\right. \\ &\quad \left.\times \mathop{\mathbb{E}}_{h}\{g^{(u)}(t-\tau^{(u)})g^{(u)}(v-\tau^{(u)})\}dtdv\right\}\end{aligned} \tag{4.10}$$

The two parts in (4.10) have the same form and can be obtained as

$$\begin{aligned}\mathop{\mathbb{E}}_{h}\{g^{(1)}(t)g^{(1)}(v)\} &= \sum_{l=0}^{L-1}\sum_{l_1=0}^{L-1}\mathbb{E}\{\alpha_l^{(1)}\alpha_{l_1}^{(1)}\}p(t-\tau_l^{(l)})p(v-\tau_{l_1}^{(1)}) \\ &\overset{(a1)}{\approx} \sum_{l=0}^{L-1}\mathbb{E}\left\{\left(\alpha_l^{(1)}\right)^2\right\}p(t-\tau_l^{(1)})p(v-\tau_l^{(1)}) \\ &= P_h(t) * [p(t)p(v)] \\ &\overset{(a2)}{\approx} \frac{1}{N_s}P_h(t)R_p(t-v)\end{aligned} \tag{4.11}$$

where $R_p(t) = N_s\int_{-T_p}^{T_p} p(v)p(v-t)dv$ is the normalized autocorrelation function of the transmitted pulse $p(t)$. The first approximation (a1) is based on the assumption that the channel has uncorrelated scattering $\mathbb{E}\{\alpha_l^{(1)}\alpha_{l_1}^{(1)}\} = 0$ for $l \neq l_1$. The second approximation (a2) comes from the assumption that the PDP is approximately constant over the narrow support of the autocorrelation function $R_p(t)$. Substituting the approximation (4.11) back

into (4.10), we obtain

$$\sigma_{em}^2 = \left(\frac{E_s}{2N_s}\right)^2 \int_{-T_p}^{T_p} R_p^2(v)dv \underset{\tau^{(u)}}{\mathbb{E}} \left\{ \int_{T_0} P_h(t)P_h(t-\tau^{(u)})dt \right\} \tag{4.12}$$

From (4.12), it is straightforward to obtain the variance σ_{em}^2 as

$$\sigma_{em}^2 = \alpha \left(\frac{E_s}{2N_s}\right)^2 \tag{4.13}$$

where $\alpha = \alpha_c \alpha_p$ and

$$\alpha_c = \frac{1}{T_I} \int_0^{T_I} \int_0^{T_I} P_h(t)P_h(t-\tau)dtd\tau \tag{4.14}$$

$$\alpha_p = \int_{-T_p}^{T_p} R_p^2(t)dt \tag{4.15}$$

$$\tag{4.16}$$

Similarly, the second part of σ_e^2 is obtained as

$$\sigma_{en}^2 = \beta \left(\frac{E_s}{2N_s}\right) \frac{N_0}{2} \tag{4.17}$$

where β is the channel parameter defined as

$$\beta = \frac{1}{T_I} \int_0^{T_I} \int_0^{T_I} P_h(t-\tau)dtd\tau \tag{4.18}$$

To this point, we assume in the analysis that there is one interfering signal waveform within the support of the desired reference signal. This result can extend to collisions with N_e equal-power user waveforms. The collision probability is $p = 2T_I/T_f$. The desired data-

bearing signal is also vulnerable to collisions with the same probability p. When collision occurs to both the desired reference signal and data-bearing signal, the probability is p^2. Therefore, the variance of the Gaussian random variable due to the MAI with N_e equal-power users is

$$\sigma_e^2 = N_s(2N_e p + N_e^2 p^2)(\sigma_{em}^2 + \sigma_{en}^2) \tag{4.19}$$

4.1.3 Error Performance

Since all undesired slots have the same integration time as the desired slot, each undesired slot has the same equal-power-user interference (with variance $\{\sigma_{me}^2\}_{m=1}^{M-1}$) as the desired slot, making $\sigma_{me}^2 = \sigma_e^2$. The mean of the decision statistic D_m in (4.1) is

$$\mathbb{E}\{D_m\} = \begin{cases} \mathbb{E}\{\mu_0\} = \frac{E_s}{2}, & m = 0 \\ 0, & m = 1,2,...,M-1 \end{cases} \tag{4.20}$$

and the variance of the decision statistic D_m is given by

$$\mathbb{E}\{D_m^2\} = \begin{cases} \sigma_0^2 + \sigma_e^2, & m = 0 \\ \sigma_1^2 + \sigma_e^2, & m = 1,2,...,M-1 \end{cases} \tag{4.21}$$

The probability of a correct decision thus has the same form as in (3.41) and is given by

$$P_{ce} = \int_{-\infty}^{\infty} \left[1 - Q\left(\frac{y}{\sqrt{\sigma_1^2 + \sigma_e^2}}\right)\right]^{M-1} g_0(y)dy \tag{4.22}$$

where $g_0(y)$ is the PDF of the Gaussian random variable with mean $\frac{E_s}{2}$ and variance $\sigma_0^2 + \sigma_e^2$.

4.1.4 Union Bound

A union bound for BEP of TR UWB systems in an equal-power environment is

$$\begin{aligned} P_M &\leq (M-1)\Pr\{D_1 > D_0\} \\ &= (M-1)Q\left(\frac{u_0}{\sqrt{\sigma_0^2+\sigma_1^2+2\sigma_e^2}}\right) \end{aligned} \tag{4.23}$$

For a given BEP P_b, taking (3.43) into the bound and denoting the inverse $Q(\cdot)$ function as $Q^{-1}(\cdot)$, we get

$$Q^{-1}\left(\frac{P_b}{2^{k-1}}\right) \geq \frac{kE_b/2}{\sqrt{\sigma_0^2+\sigma_1^2+2\sigma_e^2}} \tag{4.24}$$

To put the most stringent requirement on the system, the inequality sign in (4.24) is dropped and the equality operation is used in the following. Taking (3.37), (3.38) and (4.19) into the equality in (4.24), the number of equal-power users N_e is obtained as

$$N_e(k,T_f) = p^{-1}z \tag{4.25}$$

where $z = \left(\sqrt{1+\xi}-1\right)$, and

$$\xi = \frac{2\left(\eta k^2\gamma^2 - \frac{3}{4}k\gamma - c\right)}{\frac{\alpha}{N_s}k^2\gamma^2 + \beta k\gamma} \tag{4.26}$$

and $\eta = \left[2Q^{-1}\left(\frac{P_b}{2^{k-1}}\right)\right]^{-2}$, $k = \log_2 M$, $\gamma = \frac{E_b}{N_0}$, $c = N_s W T_I$. Note that $N_e(k,T_f)$ is an increasing function of k.

Given a P_b and a modulation order M, the numerator in (4.26) determines the critical value of E_b/N_0 that must be achieved by the system. The problem can be viewed from two

different perspectives: fixing the symbol rate R_s and fixing the bit rate R_b, which lead to different forms for N_e in (4.25). Fixing R_s, the collision probability is $p = \frac{2T_I}{T_f} = 2N_sT_IR_s$, while fixing R_b, $p = \frac{2N_sT_IR_b}{k}$. For both scenarios, the condition (2.11) must hold.

Asymptotically, as $\gamma = E_b/N_0$ approaches infinity, the number of equal-power users that can be supported by the system is obtained from (4.25) and (4.26) by letting $\gamma \to \infty$. The asymptotic N_e is inversely proportional to N_s and M for a given R_s and P_b. Therefore, there is a certain E_b/N_0 level, beyond which N_e is flat. When R_b is fixed for all M, taking $p = \frac{2N_sR_bT_I}{k}$ into (4.25) and letting $\gamma \to \infty$ yields the asymptotic N_e, which increases with M.

The network throughput (N_u users) can be calculated as

$$R_{tot} = N_e(k, T_f)kR_s = \frac{k}{2T_IN_s}z \tag{4.27}$$

when R_s is fixed. The same expression is obtained for the total bit rate of the system when R_b is fixed.

4.1.5 E_b/N_0 and R_b Constraints

We can solve the frame length T_f by substituting $p = 2T_I/T_f$ into (4.25). Suppose the target number of equal-power users is N_{et}. Also taking into account of the constraint in (2.13), we have

$$T_f = \begin{cases} 2T_IN_{et}/z, & N_{et} \leq \frac{1}{T_I}2MT_{mds}z \\ 2MT_{mds}, & \text{otherwise} \end{cases} \tag{4.28}$$

The second expression for T_f arises when the value $2T_I N_{et}/z$ in the first expression of T_f in (4.28) is smaller than $2MT_{mds}$. In this case ($N_{et} \leq \frac{1}{T_I} 2^{k+1} T_{mds} z$), the frame length T_f is given by the modulation constraint. Under this situation, we define the difference

$$\delta_{N_e}(k) = \frac{1}{T_I} 2^{k+1} T_{mds} z - N_{et} \tag{4.29}$$

as the additional number of users that the system can support beyond the value N_{et}. Using the relationship $R_b = kR_s = k/(N_s T_f)$, we have

$$R_b = \min \left\{ \frac{k}{2N_s N_e T_I} z, \;\; \frac{k}{M} \frac{1}{2N_s T_{mds}} \right\} \tag{4.30}$$

Another parameter of interest is E_b/N_0 which, according to (4.25) and (4.26), is given by the roots of the quadratic equation

$$\left(\eta - \eta_1 \frac{\alpha}{N_s} \right) (k\gamma)^2 - \left(\frac{3}{4} + \eta_1 \beta \right) (k\gamma) - c = 0 \tag{4.31}$$

where $\eta_1 = \frac{1}{2} \left[(N_e p + 1)^2 - 1 \right]$. Equation (4.31) has a positive root for $\eta - \eta_1 \frac{\alpha}{N_s} > 0$.

These two variations of (4.25) can be used to address the following two issues of communications:

- To determine the achievable data rate as a function of system resources.
- To determine the required E_b/N_0 for the system to achieve a given BEP.

4.1.6 Numerical Results

In this section, numerical results are presented using the results from previous sections. The transmitted pulse is the second derivative of the Gaussian monocycle with pulse width 0.7 ns [33]. The pulse parameter defined in (4.16) is $\alpha_p = 0.15$. The CM1 channel model from [56] with the channel delay spread $T_{mds} = 50$ ns is used in this section. The receiver has a one-sided bandwidth $W = 4$ GHz. The optimal integration time is found to be $T_I = 25$ ns for this channel model. By generating 100 realizations of the CM1 channel, the power delay profile is obtained and the two parameters associated with it are calculated: $\alpha_c = 0.0108$ and $\beta = 0.1248$.

Error performance for equal-power users

Fig. 4.1 shows a plot of the BEP performance of TR UWB systems in an equal-power user environment from (4.22), (3.42) and (3.43). The number of equal-power users in Fig. 4.1 is $N_e = 1000$. For a fixed symbol rate, increasing the modulation order M increases the bit rate R_b while the BEP performance is also increased as seen in Fig. 4.1. The bit rate R_b for $M = 32$ is five times as that for $M = 2$ while the required E_b/N_0 is decreased by 6.0 dB at $P_b = 10^{-5}$. As the number of equal-power users increases further to 2000, and as M increases from 2 to 32, BEPs in Fig. 4.2 begin to form a floor. This floor level increases with increasing M. We see from Fig. 4.2 that increasing M does not always result in an increase in performance, depending on the available E_b/N_0 and the number of equal-power users in the network.

Union Bound

Using the union bound, a relationship between the number of equal-power users N_e, the bit error probability P_b, the modulation order M, and E_b/N_0 is obtained in (4.25) when the symbol rate is fixed. Fixing $P_b = 10^{-5}$ and the symbol rate $R_s = 20$ Ksps, N_e is plotted as a function of E_b/N_0 and M in Fig. 4.3. Three regions can be identified in Fig. 4.3. System behavior in region 1 is determined by the asymptotical N_e in (4.25). In region 3, the system behaves like a typical orthogonal modulation scheme where at fixed E_b/N_0 higher order modulation has better BEP performance. In region 2, the total interference power is comparable to that of the desired signal. There is no fixed pattern for the number of tolerable equal-power users for different M.

When the bit rate R_b is fixed, the number of equal-power users that can be supported by the system is plotted in Fig. 4.4. As the modulation order M increases, the number of tolerable equal-power users N_e increases at the data rate $R_b = 40$ Kbps. This is because the frame time T_f is increasing when M increases, weakening the effect of equal-power users. A flat region is also seen in Fig. 4.4 as E_b/N_0 is large.

The total system throughput when R_b is fixed is the same as that when R_s is fixed and is plotted in Fig. 4.5.

Discussion of tradeoffs

For a given bit error probability P_b, tradeoffs can be made among system parameters like modulation order M (complexity), E_b/N_0, the number of equal power users N_e, and the total system throughput. For a given environment, there is an optimal integration time T_I. For example, $T_I = 25$ ns was found to be optimal for the CM1 channel used in this section.

If the system operates in region 3 of Fig. 4.3, when N_e is given, with a small E_b/N_0, larger M (higher complexity) is preferred, thus the system having a higher throughput seen from Fig. 4.5.

If the system is in region 1, performance is limited by interference. Tradeoffs can be made between complexity, the number of users N_e, and the throughput. For example, if a large number of users with a low data rate is desired, $M = 2$ is preferred. Tradeoffs in region 2 are E_b/N_0 dependent.

Fundamental Aspects

Two fundamental aspects addressed in Section 4.1.5 are plotted in Fig. 4.6, Fig. 4.7 and Fig. 4.8. Shown in Fig. 4.6 is a plot of the data rate R_b of TR UWB systems using M-ary PPM in the CM1 channel with $N_e = 1000$ equal-power interfering users, operating at the targeted $P_b = 10^{-5}$ and $E_b/N_0 = 20$ dB. Note that $M = 2$ can not be supported under these constraints. For a given M, increasing the repetition factor N_s decreases the data rate as predicted by (4.30). At a given N_s, if R_b is the first term in the min operator of (4.30), the data rate R_b increases with M. If R_b is the second term in (4.30), R_b decreases with M. We see in Fig. 4.6 that at $N_s = 1$ and $M = 256$, the data rate R_b is determined by the second term in (4.30).

Fig. 4.7 shows the actual number of equal-power users that the system can support with the same setting of Fig. 4.6. We can see that for the values $M = 128$, $M = 256$ and $M = 64$ when $N_s > 3$, the data rate R_b is obtained from the second term in (4.30). Thus for these settings, the actual number of supported equal-power users is $N_{et} + \delta_{N_e}(k)$ where the target number of users is $N_{et} = 1000$. For a given M, if the data rate R_b is determined by the

basic constraint of the modulation, the number of supported equal-power users increases with N_s at the given E_b/N_0. This is because the frame time is fixed for a specific M to be $T_f = 2MT_{mds}$ in this situation. At the given E_b/N_0, increasing the repetition factor spreads out the energy further in the time domain, thus reducing the energy per pulse. This results in a smaller variance due to MAI. Therefore, more equal-power users can be supported.

Fig. 4.8 shows the required E_b/N_0 to achieve $R_b = 60$ Kbps and $P_b = 10^{-5}$ in the CM1 channel with $N_e = 1000$ equal-power users. Note that for $M = 2$, only at $N_s = 1$ and $E_b/N_0 = 30.5$ dB can the system support $N_e = 1000$ users and achieve $P_b = 10^{-5}$. From Fig. 4.8, we also see that for $N_s > 5$, the system with $M = 4$ cannot achieve the target. At a fixed N_s, the required E_b/N_0 is smaller as M increases. For a given M, the required E_b/N_0 increases with increasing repetition factor N_s.

From Fig. 4.6 and Fig. 4.8, we see that $N_s = 1$ yields the largest possible data rate and requires the smallest E_b/N_0 for all M to achieve the same target. This is in agreement with the analysis in [14] where $N_s = 1$ is considered the optimal repetition factor in terms of BEP performance. Here we show from two different perspectives that when there are only equal-power users in the network (namely a network with perfect power control), concentrating the transmitted energy as much as possible is optimal with respect to the system parameters such as bit error rate, data rate, and E_b/N_0.

Combined Effects of High-Power and Equal-Power Users

For $E_b/N_0 = 20$ dB, Fig. 4.9 shows the BEP performance as a function of the repetition factor N_s. The symbol data rate is $R_s = 20$ Ksps for all values of M and $N_e = 2000$ equal-power users are present. With $N_h = 4$ high-power users, we see the BEP for each value

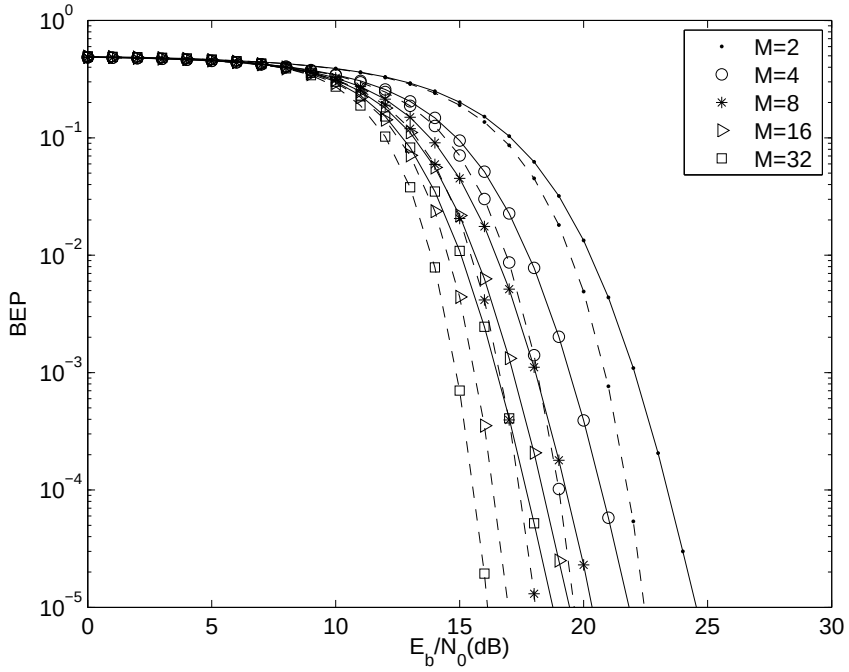

Figure 4.1: BEP for TR UWB in an equal-power user environment (solid lines) and single-user environment (dashed lines). The number of equal-power users is $N_e = 1000$. $T_I = 25$ ns, $N_s = 3$, $R_s = 20$ Ksps.

of M (except $M = 2$) decreases first with N_s and then increases. For $M = 2$, the system is in the noise-limited region instead of interference-limited region. For $M \geq 4$, there is a repetition factor N_s which yields the best BEP performance. Larger values of M yields larger optimal values of N_s, better BEP performance, and higher bit rates. The optimal repetition factor $N_s \geq 1$ shows a new transmission strategy for TR UWB systems in the presence of high-power users.

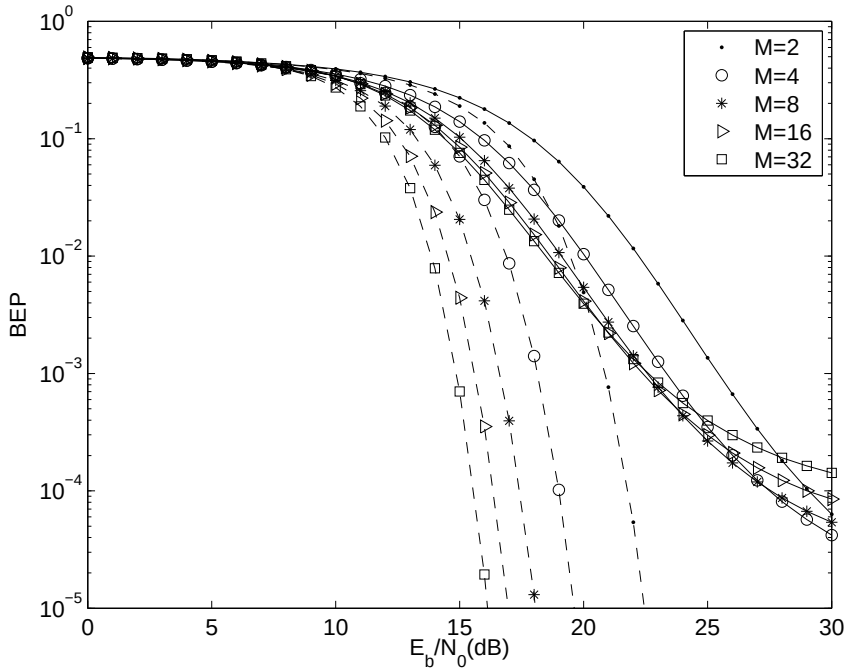

Figure 4.2: BEP for TR UWB in an equal-power user environment (solid lines) and single-user environment (dashed lines). The number of equal-power users is $N_e = 2000$. $T_I = 25$ ns, $N_s = 3$, $R_s = 20$ Ksps.

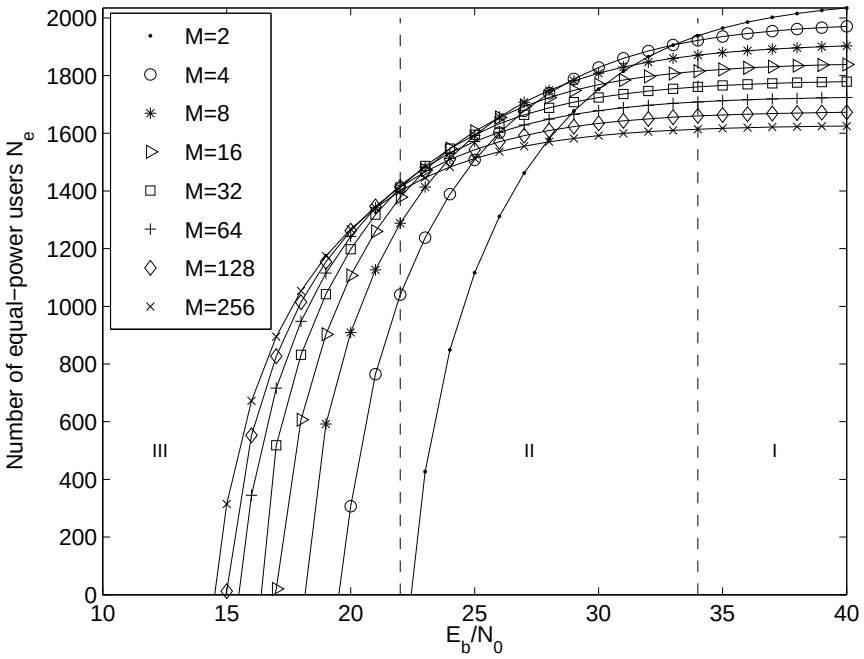

Figure 4.3: Number of equal-power users versus E_b/N_0 of TR UWB at $R_s = 20$ Ksps in an equal-power user environment. $P_b = 10^{-5}$, $T_I = 25$ ns, $N_s = 3$.

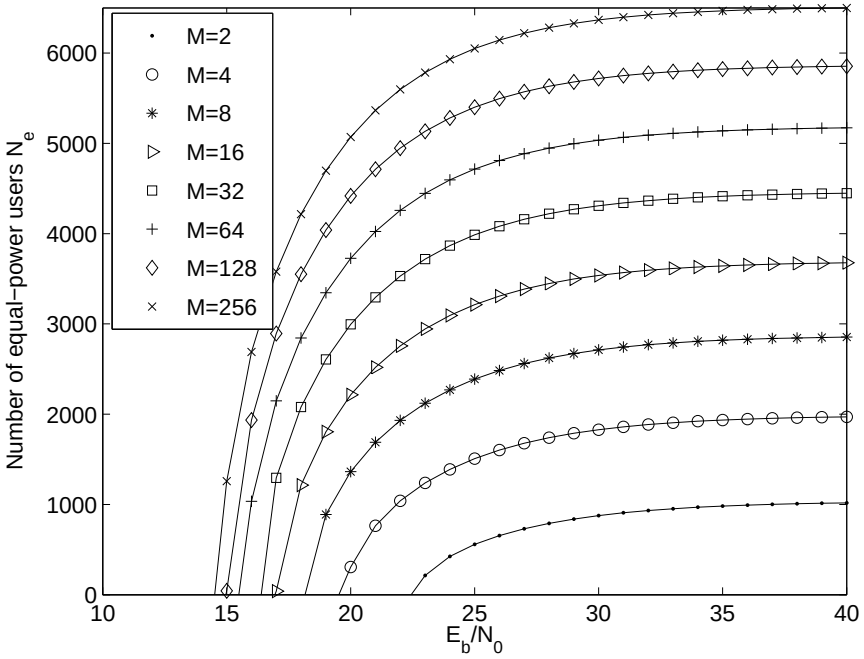

Figure 4.4: Number of equal-power users versus E_b/N_0 of TR UWB at $R_b = 40$ Kbps in an equal-power user environment. $P_b = 10^{-5}$, $T_I = 25$ ns, $N_s = 3$.

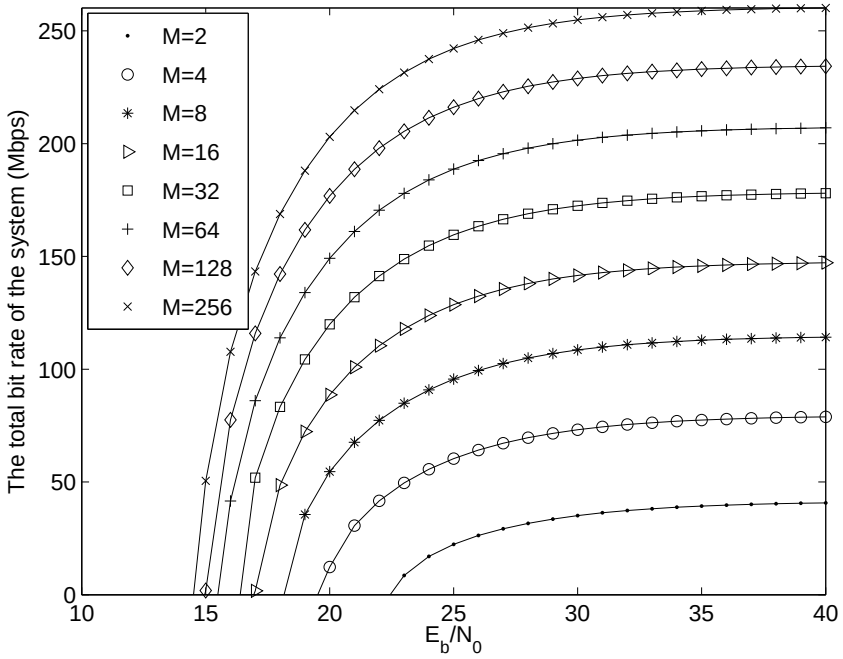

Figure 4.5: The system throughput of TR UWB in an equal-power user environment. $P_b = 10^{-5}$, $T_I = 25$ ns, $N_s = 3$, $R_s = 20$ Ksps.

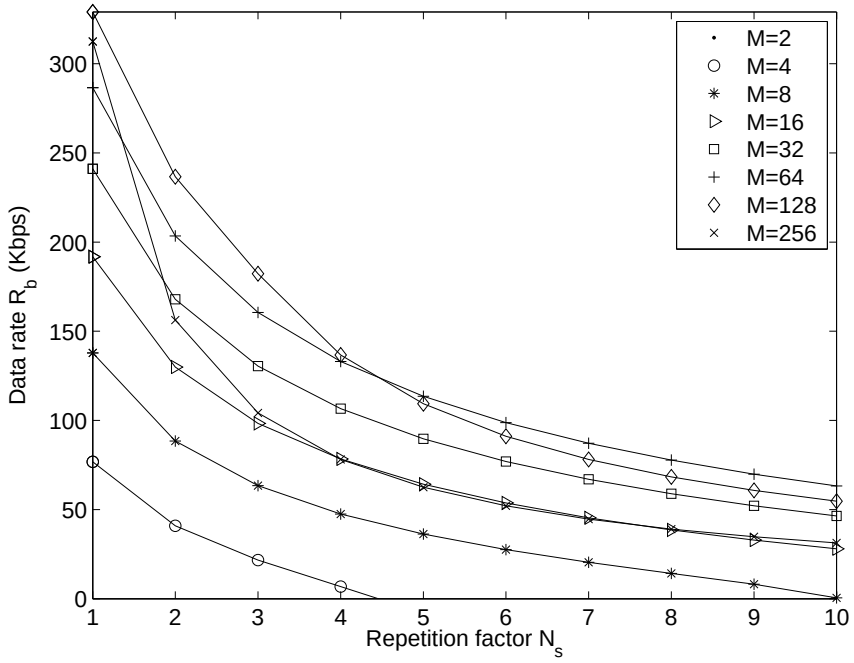

Figure 4.6: The possible data rate R_b at $E_b/N_0 = 20$ dB of TR UWB in an equal-power user environment. Other parameters: $P_b = 10^{-5}$, $N_e = 1000$, $T_I = 25$ ns.

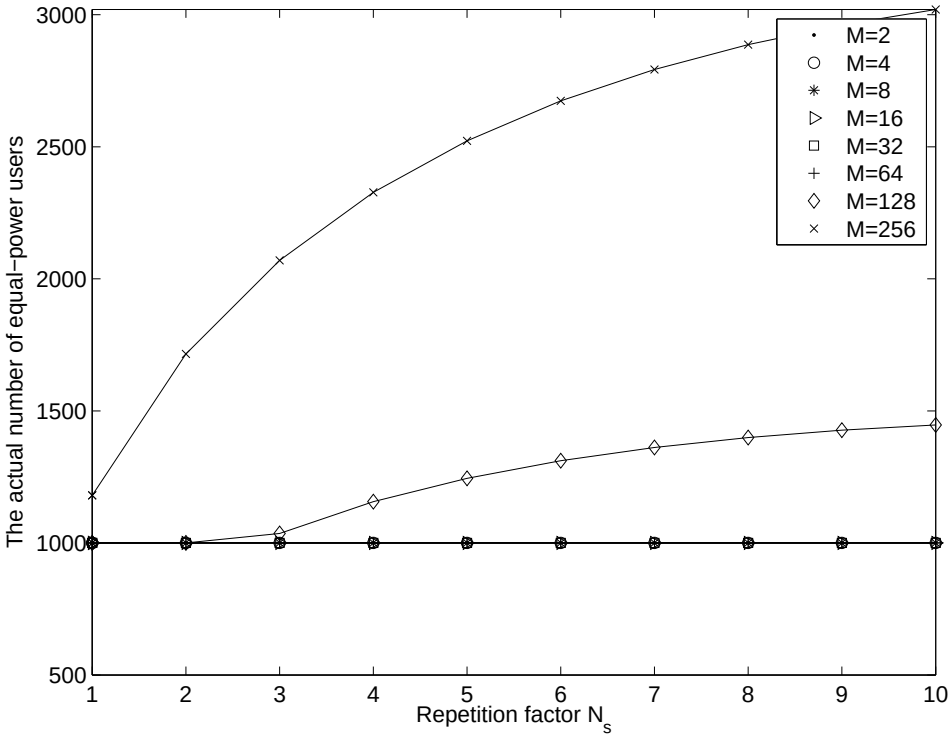

Figure 4.7: The actual number of equal-power users at $E_b/N_0 = 20$ dB of TR UWB. Other parameters: $P_b = 10^{-5}$, $N_{et} = 1000$, $T_I = 25$ ns.

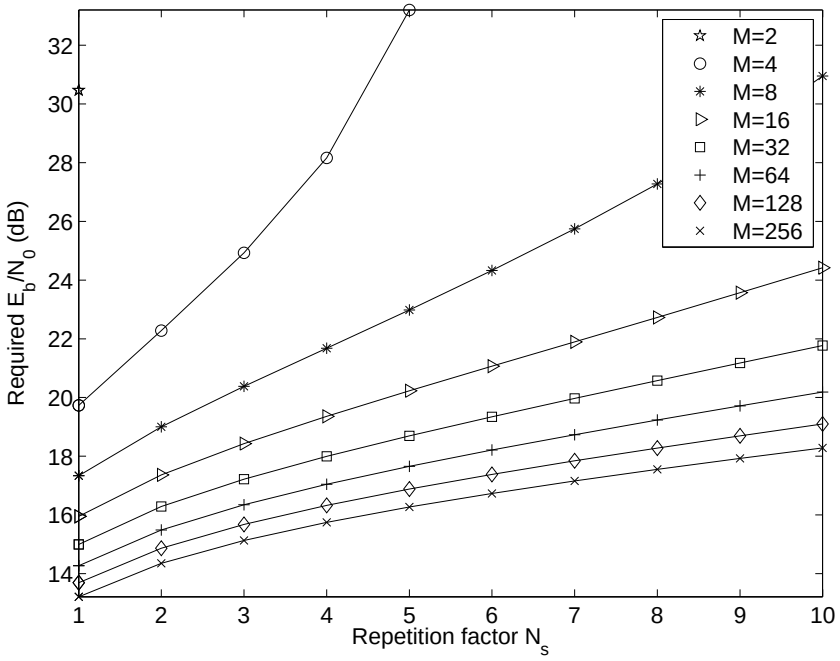

Figure 4.8: The required E_b/N_0 of TR UWB in an equal-power user environment. Other parameters: $P_b = 10^{-5}$, $N_e = 1000$, $T_I = 25$ ns, $R_b = 60$ Kbps.

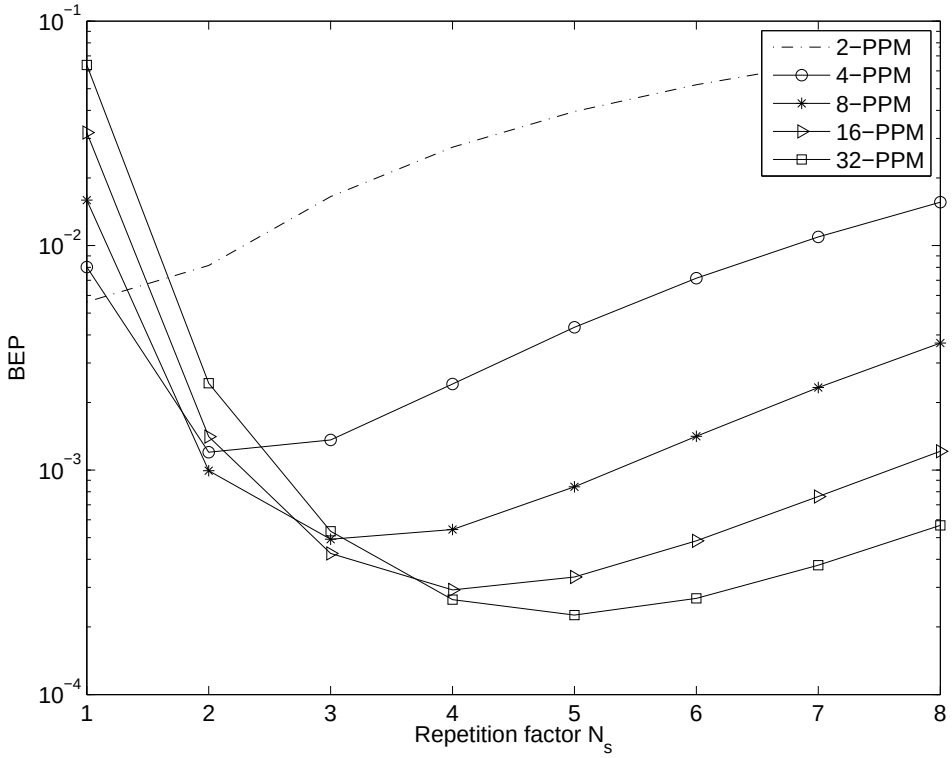

Figure 4.9: BEP for TR UWB as a function of M and N_s in an environment with $N_h = 4$ high-power and $N_e = 2000$ equal-power users. $E_b/N_0 = 20$ dB, $T_I = 25$ ns, $R_s = 20$ Ksps.

4.1.7 Conclusion: TR Systems

In networks without power control, the performance of TR UWB systems employing M-ary PPM is evaluated. The PDP of the channel is used in obtaining the variance of the Gaussian random variable due to multiple-access interference. A union bound is used to obtain the number of supported equal-power users. Two fundamental communication aspects are investigated. Combined effects of both high- and equal-power users are quantified. Using the analytical techniques developed for TR UWB systems with M-ary PPM, tradeoffs are evaluated with respect to the system parameters, E_b/N_0, the number of equal-power users, the BEP level, and complexity.

4.2 FSR UWB Systems

Slightly frequency-shifted reference (FSR) systems are proposed in [39] to overcome the need for the wideband analog delay line, while still maintaining the benefits of TR systems in avoiding channel estimation. In this section, we investigate the multiple-access (MA) performance of FSR UWB systems. One contribution of this work is the development of an analytical technique for evaluating the performance of FSR UWB systems with multiple users. Both AWGN channel and multipath channel conditions are considered in the theoretical analysis. Due to the receiver structure of FSR UWB systems, the multiple-access interference (MAI) is much more severe than the MAI in TR UWB systems. When the MAI dominates, the number of supported users is analyzed for a given BEP level. The relative multiple-access performance of TR and FSR systems is derived under an AWGN channel. To investigate the effects of the MAI in a multipath channel, the power delay

profile (PDP) of the channel is incorporated to obtain a tractable analytical expression, the same analytic technique used in TR UWB systems. For numerical calculations, we obtain PDPs from channel realizations of the IEEE 802.15.3a [56] and IEEE 802.15.4a [57] UWB channel models.

4.2.1 Decision Statistic

The signaling and receiving of FSR systems is discussed in Section 2.4 where a receiver structure is also presented in Fig. 2.4. As assumed, user 1 is the desired user and synchronization is established for user 1. The FSR UWB receiver for user 1 squares the received signal and then multiplies it with a cosine signal with frequency $f_0 = 1/T_s$ before the integration operation [39]. Sampling the integration output of each frame and summing the N_s outputs gives the decision statistic. For notational simplicity, we consider the first symbol ($i = 0$) of user 1. The decision statistic is given by

$$r_0 = \sum_{j=0}^{N_s-1} \int_{\Omega_j} \sqrt{2}\cos(2\pi f_0 t) r_f^2(t) dt \tag{4.32}$$

where $\Omega_j = [jT_f + c_j^{(1)} T_c,\ jT_f + c_j^{(1)} T_c + T_I]$, T_I is the integration duration, and the received signal $r_f(t)$ is given in (2.18). Decomposing the right side of (4.32), we obtain the desired signal part in (4.32) as

$$r_d = \sum_{j=0}^{N_s-1} \int_{\Omega_j} \sqrt{2}\cos(2\pi f_0 t) \left[r_x^{(1)}(0,t) \right]^2 dt \tag{4.33}$$

where $r_x^{(1)}(0,t)$ is the received signal of symbol 0 from user 1. Define the overall interference signal $I(t)$ by the following

$$I(t) = \sum_{u=2}^{N_u} r_x^{(u)}(0, t - \tau^{(u)}) \tag{4.34}$$

where $\tau^{(u)}$ in $r_x^{(u)}(0, t-\tau^{(u)})$ is the time asynchronism between user u and user 1. By assumption, $\tau^{(1)} = 0$ and $\{\tau^{(u)} \neq 0\}$ $(u \neq 1)$. Using $I(t)$ to decompose r_0, the MAI in the jth integration of r_0 is given by

$$r_I(j) = r_I(j,1) + r_I(j,2) \tag{4.35}$$

where

$$r_I(j,1) = 2\int_{\Omega_j} \sqrt{2}\cos(2\pi f_0 t) r_x^{(1)}(0,t) I(t) dt \tag{4.36}$$

$$r_I(j,2) = \int_{\Omega_j} \sqrt{2}\cos(2\pi f_0 t) I^2(t) dt \tag{4.37}$$

The thermal noise related term from the jth integration of r_0 has three components given by

$$\begin{aligned} n(j) = & \; 2\int_{\Omega_j} \sqrt{2}\cos(2\pi f_0 t) r_x^{(1)}(0,t) n(t) dt \\ & + 2\int_{\Omega_j} \sqrt{2}\cos(2\pi f_0 t) I(t) n(t) dt \\ & + \int_{\Omega_j} \sqrt{2}\cos(2\pi f_0 t) n^2(t) dt \end{aligned} \tag{4.38}$$

We can rewrite the decision statistic r_0 in (4.32) as

$$r_0 = r_d + \sum_{j=0}^{N_s-1} [r_I(j) + n(j)] \tag{4.39}$$

In the evaluation of the performance of FSR UWB systems, the MAI term $\sum_j r_I(j)$ can be modeled as Gaussian when the number of interfering users is large, evoking the central limit theorem. We investigate FSR UWB system performance assuming that the energy allocation are the same for all users $E_r^{(u)} = E_d^{(u)} = E_s/2$.

4.2.2 MAI in an AWGN channel

In an AWGN channel with synchronization of the desired user established, and setting the integration time $T_I = T_p$, the receiver collects all of the energy of the desired user. The received waveform (without thermal noise) for user u is

$$r_x^{(u)}(i,t) = x^{(u)}(i, t - \tau^{(u)}) \tag{4.40}$$

The useful signal component r_d in (4.39) is easily calculated as

$$r_d = d_0^{(1)} E_s \tag{4.41}$$

The MAI term $r_I(j)$ has two parts given by (4.36) and (4.37). The first part (4.36) has an equivalent in TR UWB systems except for the low-frequency cosine term. The second part in (4.37) has no corresponding term in TR UWB systems. Note that the MAI power is larger in FSR than that in TR UWB systems because of the squared interference signal in

(4.37). We first calculate the interference power in (4.37). It can be shown that the mean of $r_I(j,2)$ is 0. Let the bold $\boldsymbol{x}$ denote the vector consisting of the variables $\{x^{(2)}, x^{(3)}, \ldots\}$. The variance of $r_I(j,2)$ is given by

$$\sigma_I^2(j,2) = \mathbb{E}\left\{r_I^2(j,2|\boldsymbol{d}_0, \boldsymbol{\tau}_j\right\} \tag{4.42}$$

where

$$\begin{aligned} & r_I^2(j,2|\boldsymbol{d}_0, \boldsymbol{\tau}_j) \\ \approx\ & \frac{E_s^2}{N_s^2} \sum_{u_1=2}^{N_u} \sum_{u_2=2}^{N_u} \sum_{u_3=2}^{N_u} \sum_{u_4=2}^{N_u} \\ & R_p(\tau_j^{(u_1)}, \tau_j^{(u_2)}) R_p(\tau_j^{(u_3)}, \tau_j^{(u_4)}) \\ & \times A(j,u_1,u_2) A(j,u_3,u_4) \cos^2(2\pi f_0 j T_f) \end{aligned} \tag{4.43}$$

The definitions for terms in (4.43) are

$$R_p(v_1,v_2) = N_s \int_0^{T_p} p(t-v_1) p(t-v_2) dt \tag{4.44}$$

$$\begin{aligned} A(j,u_1,u_2) &= \left(\sqrt{\frac{1}{2}} + b_0^{(u_1)} \cos(2\pi f_0 j T_f)\right) \\ &\times \left(\sqrt{\frac{1}{2}} + b_0^{(u_2)} \cos(2\pi f_0 j T_f)\right) \end{aligned} \tag{4.45}$$

The new random variable $\tau_j^{(u)} = \tau^{(u)} + (c_j^{(u)} - c_j^{(1)}) T_c$ in (4.43) is independent in each frame. In approximating the variance of $r_I(j,2)$, we use the fact that N_s is large which makes the cosine function almost constant during each frame. To facilitate further calculation, we

make the following denotations

$$E_p(\tau) = R_p(\tau,\tau) \tag{4.46}$$

$$R_p(\tau) = R_p(0,\tau) \tag{4.47}$$

Note that $R_p(\tau)$ is the normalized autocorrelation function of the pulse $p(t)$. We first take the expectation of $r_I^2(j,2|\boldsymbol{d}_0,\boldsymbol{\tau}_j)$ with respect to $\boldsymbol{\tau}_j$, then with respect to $\boldsymbol{d}_0$, and then sum the results to obtain

$$\begin{aligned}
\sigma_I^2(2) &= \sum_{j=0}^{N_s-1} \sigma_I^2(j,2) \\
&= \frac{25}{8}\frac{E_s^2}{N_s}(N_e p_1)\overline{E_p^2(\tau_j^{(i)})} \\
&\quad + \frac{13}{8}\frac{E_s^2}{N_s}(N_e p_1)^2\left(\overline{E_p(\tau_j^{(i)})}\right)^2 \\
&\quad + \frac{13}{4}\frac{E_s^2}{N_s}(N_e p_1)^2\overline{R_p^2(\tau_j^{(i)},\tau_j^{(k)})}_{(i\neq k)}
\end{aligned} \tag{4.48}$$

where $p_1 = \frac{2T_p}{T_f}$, $N_e = N_u - 1$, and $\overline{x}$ is the expectation of x, $\overline{x} = \mathbb{E}\{x\}$. The last term in $\sigma_I^2(2)$ is much smaller than the second term due to the nature of functions in the expectation operations. Similarly, we obtain the variance of $r_I(j,1)$ in (4.36) and sum over N_s frames yielding

$$\sigma_I^2(1) = \frac{13}{2}\frac{E_s^2}{N_s}(N_e p_1)\overline{R_p^2(\tau_j^{(i)})} \tag{4.49}$$

The variance of the MAI (the interference power) is given by

$$\sigma_I^2 = \sigma_I^2(1) + \sigma_I^2(2) \tag{4.50}$$

The variance of the thermal noise component is calculated to be

$$\begin{aligned}\sigma_n^2 &= \mathrm{Var}\{\sum_{j=0}^{N_s-1} n(j)\} \\ &= \frac{5}{2}E_s N_0 [1+(N_e p_1)\alpha_n] \\ &\quad + W N_s T_p N_0^2 \end{aligned} \tag{4.51}$$

and

$$\alpha_n = \overline{E_p(\tau)} \tag{4.52}$$

The BEP for FSR systems with $N_e = N_u - 1$ interfering users can be written as

$$P_{b,FSR} = Q\left(\frac{E_s}{\sqrt{\sigma_n^2+\sigma_I^2}}\right) \tag{4.53}$$

To compare the BEP performance to TR systems with the same data rate and symbol energy, we use superscript 't' to denote the repetition factor and the frame length for TR systems: N_s^t and T_f^t. To keep the same data rate between these two systems, we have: $N_s^t = N_s/2$ and $T_f^t = 2T_f$. The BEP for TR systems can be obtained by substituting N_s^t and T_f^t into (4.22).

A parameter which is of interest in evaluating BEP is the peak pulse-energy-to-noise

ratio ε/N_0. For FSR and TR UWB, the relationship between E_s/N_0 and ε/N_0 is

$$\frac{E_{s,fsr}}{N_0} = \frac{N_f}{3/2+\sqrt{2}}\frac{\varepsilon}{N_0} \tag{4.54}$$

$$\frac{E_{s,tr}}{N_0} = 2N_{f,tr}\frac{\varepsilon}{N_0} \tag{4.55}$$

When ε/N_0 is the same for both systems, we see that FSR systems have a E_s/N_0 4.65dB smaller than TR UWB systems, which translates into a BEP degradation of FSR systems compared with TR systems.

In (4.53), when the MAI dominates, the number of interfering users that can be supported is obtained for a given BEP level P_b and is given by

$$N_{e,fsr} = \frac{1}{p_1}\left(\sqrt{\left(\frac{25\alpha_{se}+52\alpha_r}{26\alpha_{es}}\right)^2+\frac{8N_f}{13\vartheta^2\alpha_{es}}} - \frac{25\alpha_{se}+52\alpha_r}{26\alpha_{es}}\right) \tag{4.56}$$

$$\tag{4.57}$$

where $\vartheta = Q^{-1}(P_b)$ (the inverse Q function), $\alpha_{se} = \overline{E_p^2(\tau)}$, $\alpha_{es} = \left(\overline{E_p(\tau)}\right)^2$, and $\alpha_r = \overline{R_p^2(\tau)}$. The last term in (4.48) is dropped in the above calculation of supported users because it is very small compared with the second term in (4.48) for narrow pulses such as the second derivative of the Gaussian pulse. The corresponding number of supported users can be found by analyzing the union bound (4.23)

$$N_{e,tr} = \frac{1}{p_1}\left(\sqrt{4+2\frac{N_f}{\vartheta^2\alpha_r}}-2\right) \tag{4.58}$$

The relative multiple-access performance of these two systems can be evaluated by taking the ratio of $N_{e,tr}$ and $N_{e,fsr}$ at the same data rate and E_s/N_0, obtaining

$$\kappa = \frac{N_{e,tr}}{N_{e,fsr}} \tag{4.59}$$

4.2.3 MAI in Multipath Channels

Using the PDP of the channel and assuming that $P_h(t)$ is constant within the short duration of the pulse $p(t)$, the desired signal part and the variances of the interference and noise components in (4.39) are calculated below. First, the desired signal component is

$$r_{d,mp} = \alpha_s d_0^{(1)} E_s \tag{4.60}$$

where

$$\alpha_s = \int_0^{T_I} P_h(t)\cos(2\pi f_0 t)dt \tag{4.61}$$

We see that the energy collection is determined by the integration time T_I and the frequency offset f_0. The variance of the thermal noise related random variable is the sum of variance of $n(j)$ in (4.38). We give this result as

$$\sigma_{n,mp}^2 = \sigma_{f1}^2 + \sigma_{f2}^2 \tag{4.62}$$

where

$$\sigma_{f1}^2 = \sigma_{11}^2 + \sigma_{12}^2 \tag{4.63}$$

$$\sigma_{f2}^2 = WN_f T_I N_0^2 \tag{4.64}$$

The expressions for σ_{11}^2 and σ_{12}^2 are

$$\sigma_{11}^2 = 2E_s N_0 + \alpha_{n11} \cdot \frac{1}{2} E_s N_0 \tag{4.65}$$

$$\sigma_{12}^2 = N_e p \times [\alpha_{n12} \cdot 2E_s N_0 + \alpha_{n13} \cdot \frac{1}{2} E_s N_0] \tag{4.66}$$

where the probability p is defined before as $p = \frac{2T_I}{T_f}$ and

$$\alpha_{n11} = \int_0^{T_I} P_h(t) \cos(4\pi f_0 t) dt \tag{4.67}$$

$$\alpha_{n12} = \frac{1}{T_I} \int_0^{T_I} \int_0^{T_I} P_h(t-\tau) dt d\tau \tag{4.68}$$

$$\alpha_{n13} = \frac{1}{T_I} \int_0^{T_I} \int_0^{T_I} P_h(t-\tau) \cos(4\pi f_0 t) dt d\tau \tag{4.69}$$

Here we also assume that T_I is chosen so that $\int_0^{T_I} P_h(t) dt = 1$ as in the TR case.

The first MAI term $r_I(j,1)$ in (4.36) results from the interfering signal correlated with the signal of the desired user. The variance of $r_I(j,1)$ summed over N_s frames is given by

$$\sigma_{I,mp}^2(1) = (N_e p) \frac{E_s^2}{N_s} \alpha_p \times (\frac{9}{2} \alpha_{m11} + 2\alpha_{m12}) \tag{4.70}$$

where α_p is defined in deriving MAI variance for TR systems as $\alpha_p = \int_{-T_p}^{T_p} R_p^2(t)dt$ and

$$\alpha_{m11} = \frac{1}{T_I}\int_0^{T_I}\int_0^{T_I} P_h(t)P_h(t-\tau)dtd\tau \tag{4.71}$$

$$\alpha_{m12} = \frac{1}{T_I}\int_0^{T_I}\int_0^{T_I} P_h(t)P_h(t-\tau) \times \cos(4\pi f_0 t)dtd\tau \tag{4.72}$$

The other MAI term $r_I(j,2)$ in (4.37) results from squaring of the MA interfering signal which does not appear in TR UWB systems. The variance of (4.37) summed over N_s frames is approximated as

$$\begin{aligned}\sigma^2_{I,mp}(2) \approx\ & (N_e p)\frac{E_s^2}{N_s}\alpha_p\left(\frac{17}{4}\alpha_{m21} + 2\alpha_{m22}\right) \\ & +(N_e p)\frac{E_s^2}{N_s}\left(\frac{25}{8}\alpha_{m23} + \frac{9}{8}\alpha_{m24}\right) \\ & +(N_e p)^2\frac{E_s^2}{N_s}\left(\frac{13}{8}\alpha_{m25} + \frac{5}{8}\alpha_{m26}\right)\end{aligned} \tag{4.73}$$

where

$$\begin{aligned}
\alpha_{m21} &= \frac{1}{T_I}\int_0^{T_I}\int_0^{T_I} P_h^2(t-\tau)dtd\tau \\
\alpha_{m22} &= \frac{1}{T_I}\int_0^{T_I}\int_0^{T_I} P_h^2(t-\tau)\cos(4\pi f_0 t)dtd\tau \\
\alpha_{m23} &= \frac{1}{T_I}\int_0^{T_I}\left[\int_0^{T_I} P_h(t-\tau)\cos(2\pi f_0 t)dt\right]^2 d\tau \\
\alpha_{m24} &= \frac{1}{T_I}\int_0^{T_I}\left[\int_0^{T_I} P_h(t-\tau)\sin(2\pi f_0 t)dt\right]^2 d\tau \\
\alpha_{m25} &= \left[\frac{1}{T_I}\int_0^{T_I}\int_0^{T_I} P_h(t-\tau)\cos(2\pi f_0 t)dtd\tau\right]^2 \\
\alpha_{m26} &= \left[\frac{1}{T_I}\int_0^{T_I}\int_0^{T_I} P_h(t-\tau)\sin(2\pi f_0 t)dtd\tau\right]^2
\end{aligned}$$

The MAI variance of FSR systems in multipath environments is given by

$$\sigma_{I,mp}^2 = \sigma_{I,mp}^2(1) + \sigma_{I,mp}^2(2) \tag{4.74}$$

The BEP for FSR UWB systems in a multipath channel is then given by

$$P_{fsr,mp} = Q\left(\frac{\alpha_s E_s}{\sqrt{\sigma_{I,mp}^2 + \sigma_{n,mp}^2}}\right) \tag{4.75}$$

4.2.4 Numerical Results

In this section, we evaluate the MA performance of FSR UWB systems relative to TR UWB systems. The second derivative of the Gaussian pulse is used with the pulse width $T_p = 0.7$ and the pulse parameter $\tau_m = 0.2877$ [54]. In an AWGN channel, the optimal

integration time is $T_I = T_p$.

Fig. 4.10 shows the ratio κ between the number of supported users of TR and FSR UWB systems at a data rate $R_s = 50$ Kbps. We see that at the desired BEP level of $P_b = 10^{-4}$, the ratio κ decreases with increasing repetition factor N_s. Within the interested range of N_s, TR UWB systems can support more users than FSR UWB systems seen from Fig. 4.10. For example, with $N_s = 20$, a TR UWB system with the parameter setting as in Fig. 4.10 supports five times as many users as a FSR UWB system.

In Fig. 4.11, the MA performance is plotted versus E_b/N_0 given different numbers of supported users. The solid line and the dashed line are the single-link BEP for FSR and TR UWB systems. Here we set $N_{e,tr} = 5.5N_{fsr}$ to investigate the MA performance. These two systems perform almost the same at $P_b = 10^{-4}$ with TR UWB supporting a factor of 5.5 more users than FSR UWB systems, which is expected from Fig. 4.10 at $N_s = 20$.

To illustrate the performance of the FSR UWB system in a multipath channel, we use the CM1 channel [56] and the office NLOS channel (CM4) [57]. The channel models are used to generate corresponding PDPs, which are employed by our analytical technique. The MA performance is shown in Fig. 4.12 and Fig. 4.13. Also shown in Fig. 4.12 and Fig. 4.13 is the performance of TR UWB systems in the same environment. The integration time for the CM1 channel is $T_I = 25$ ns while the integration time for the CM4 channel [57] is $T_I = 75$ ns. These integration intervals are chosen such that nearly all of the desired signal energy is collected (up to 99%). The larger delay spread in the CM4 channel and corresponding increased integration time interval results in a reduced data rate to maintain the same performance.

We see that TR UWB systems support more users than FSR UWB at the same data

rate and E_b/N_0. The disadvantage of FSR UWB systems comes directly from the square operation in the receiver.

4.2.5 Conclusion: FSR Systems

Multiple-access performance of FSR UWB communications systems is presented in this section. Expressions are derived giving the performance of FSR UWB systems in AWGN and multipath channels and numerical results are presented. One result is that the simplicity of FSR UWB systems comes with a considerable reduction in the number of supported users when compared with TR UWB systems.

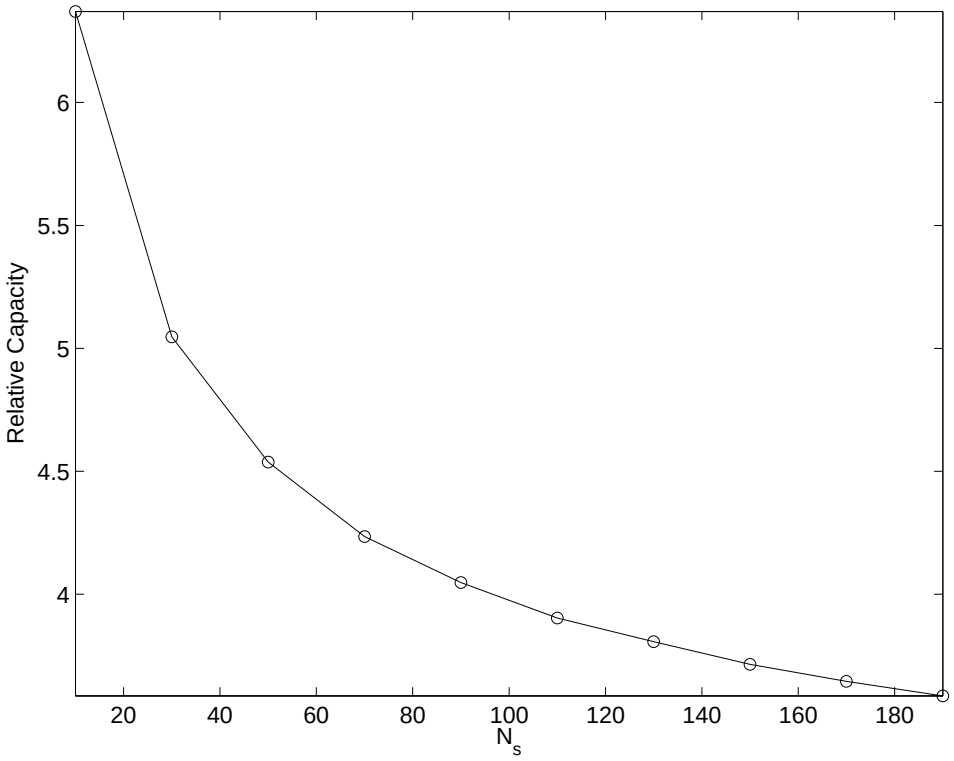

Figure 4.10: The ratio κ between the supported users for FSR and TR UWB in an AWGN channel. $N_s^t = N_s/2$, $T_I = T_p = 0.7$ ns, $R_b = 50$ Kbps, $P_b = 10^{-4}$.

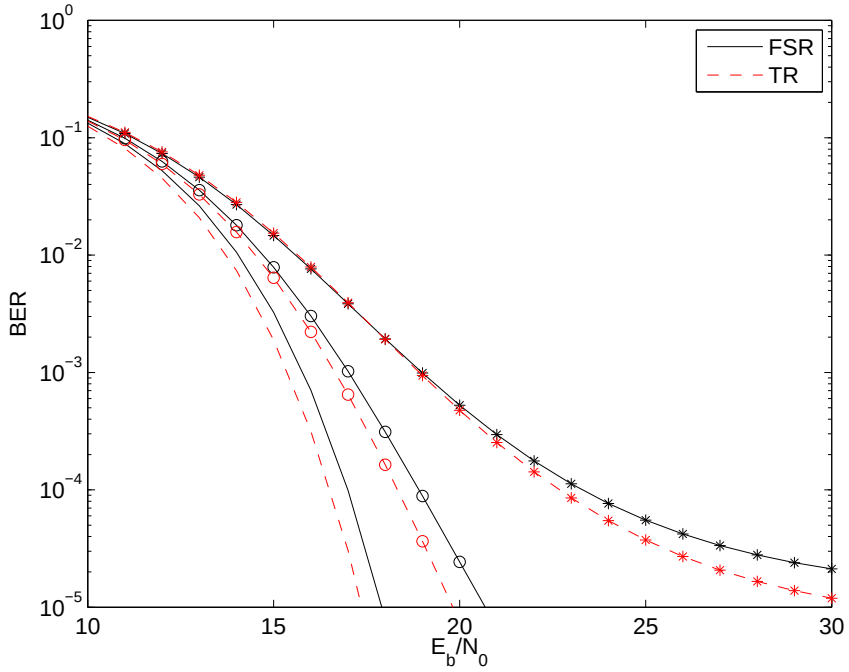

Figure 4.11: BEP for FSR and TR UWB with $N_{e,fsr} = 0, 169, 339$ (solid line, circled line, and stared line respectively) and the corresponding $N_{e,tr} = 5.5N_{e,fsr}$. $N_s^t = N_s/2$, $T_I = 0.7$ ns, $N_s = 20$, $R_b = 50$ Kbps, $W = 4$ GHz.

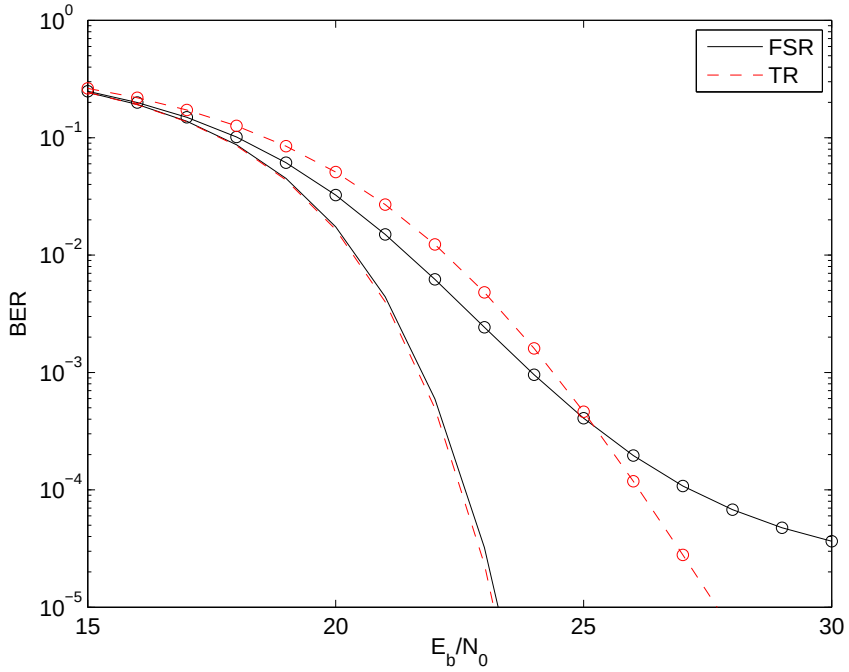

Figure 4.12: BEP for FSR and TR UWB with $N_{e,fsr} = 0,40$ (solid line, circled line) and the corresponding $N_{e,tr} = 30N_{e,fsr}$. The multipath channel is CM1 from 802.15.3a. $N_s^t = N_s/2$, $T_I = 25$ ns, $N_s = 20$, $R_b = 20$ Kbps, $W = 4$ GHz.

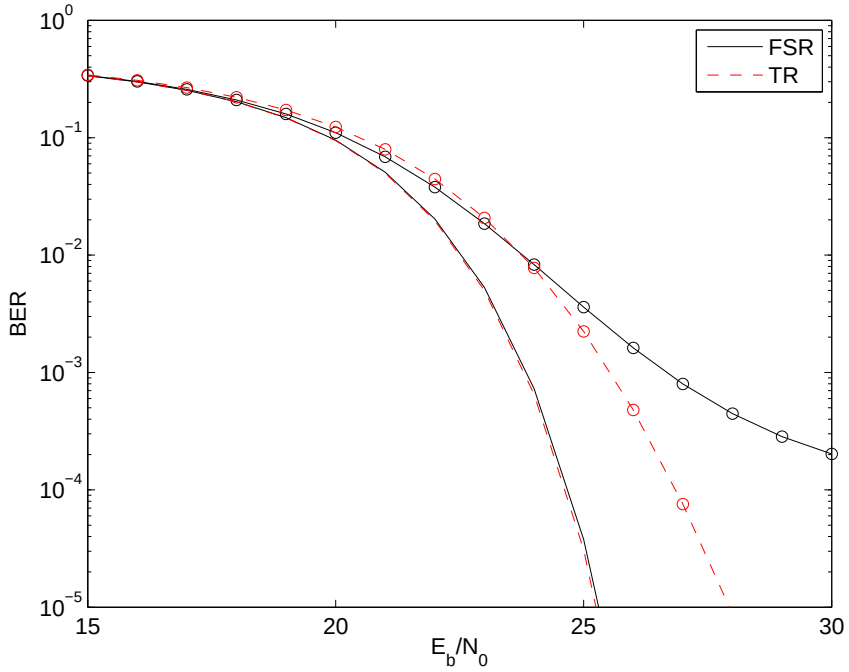

Figure 4.13: BEP for FSR and TR UWB with $N_{e,fsr} = 0,40$ (solid line, circled line) and the corresponding $N_{e,tr} = 30N_{e,fsr}$. The multipath channel is CM4 from 802.15.4a. $N_s^t = N_s/2$, $T_I = 70$ ns, $N_s = 20$, $R_b = 10$ Kbps, $W = 4$ GHz.

Chapter 5

Near-Far Resistant Synchronization

In this chapter, symbol-level synchronization is studied for UWB systems in the presence of the near-far problem. Power control is not assumed in the network contrast to the current literature. The near-far problem dramatically degrades the performance of synchronization for UWB communications. We propose an easy-to-implement procedure to suppress the interfering waveforms from high-power users without requiring their spreading codes. Following the suppression process, we propose a new dimension-based method to determine the code phase (acquisition) for the desired user. Detailed issues related to the suppression and dimension detection technique are presented. Simulation results are provided to show the superior performance of the near-far resistant synchronization procedure proposed in this chapter when compared to the best alternative from the literature.

5.1 ML Synchronization

Direct Sequence (DS) UWB systems are considered in this chapter. By assuming low cross-correlation levels among all spreading codes, the synchronization problem of DS-UWB systems is decomposed into parallel estimation problems for each user by applying the ML criterion [49]. The received signal for UWB systems with N_u users is given by (2.3). The objective of the synchronization function at the receiver is to estimate $\boldsymbol{\tau} = [\tau^{(1)}, \tau^{(2)}, \ldots, \tau^{(N_u)}]$ at the symbol level (coarse acquisition).

As shown in [49], if all the spreading codes $\{\mathbf{d}^{(u)}\}_{u=1}^{N_u}$ have sufficiently low cross-correlation levels, the ML estimate of the delay $\boldsymbol{\tau}$ can be decomposed to a single-user estimator as if users were not interfering with each other. Therefore the spreading code of user 1 is applied to the received signal to extract the timing information for user 1. For ease of illustration, we drop the superscript for user 1 for some parameters in the following analysis. Denote the block length of the code for all users to be M. The optimal receive symbol-waveform estimate for user 1 can be found to be [49]

$$\hat{g}(t;\tilde{\tau}) = \frac{1}{M}\sum_{i=0}^{M-1} d_i^{(1)} r(t + iT_s + \tilde{\tau}) \tag{5.1}$$

where $\tilde{\tau}$ is the trial value of $\tau^{(1)}$. The optimal delay estimate is given by [49]

$$\hat{\tau} = \underset{\tilde{\tau}\in[0,\, MT_s]}{\arg\max} \int_0^{T_s} [\hat{g}(t;\tilde{\tau})]^2\, dt \tag{5.2}$$

The form of the symbol-waveform estimate at trial position $\tilde{\tau}$ in (5.1) is like the de-spreading process in CDMA systems where chips are multiplied by the corresponding codes. Here,

starting from the trial position $\tilde{\tau}$, the received symbol segments are multiplied by the corresponding codes and folded back to form a symbol-waveform estimate. Fig. 5.1 and Fig. 5.2 show the difference between the modulation schemes of conventional CDMA systems and the UWB systems considered in this chapter, which also reflect different de-spreading processes at the receiver.

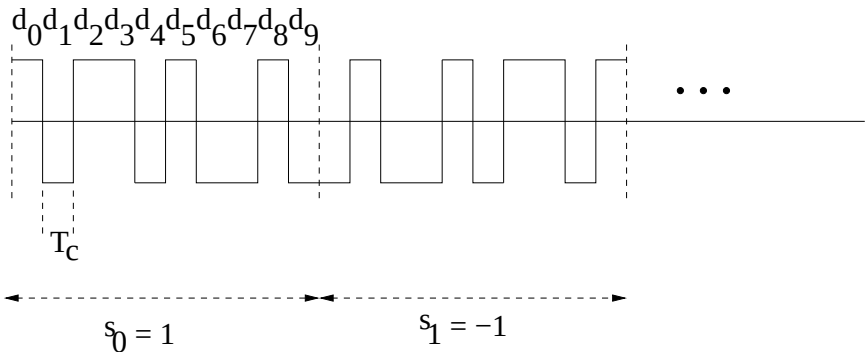

Figure 5.1: The relationship between chips and symbols for CDMA systems: One symbol is divided into multiple chips.

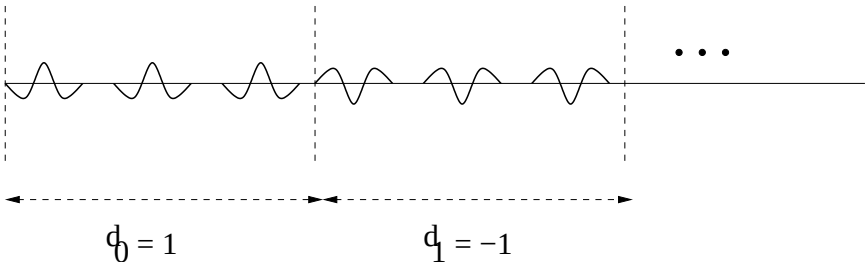

Figure 5.2: Each symbol in UWB systems has multiple pulses. Each symbol is multiplied by the corresponding code value.

In Fig. 5.1, one symbol s_i ($i = 0, 1$ in this figure) is divided into $M = 10$ chips. The symbol is multiplied by the code waveforms (square waveforms in this example) at the transmitter. At the receiver, the same code waveforms are used to de-spread the received signal for each symbol. The UWB signal shown in Fig. 5.2 has $N_s = 3$ pulses for each symbol. The pulses of each symbol are multiplied (or modulated) by the corresponding code. At the receiver, the entire symbol waveform is multiplied by the corresponding code value as indicated by (5.1).

The detection process shown by (5.2) is an energy detection: Energies of the symbol-waveform estimates from different trial positions are compared and the delay corresponding to the largest energy is selected as the estimate of the delay $\tau^{(1)}$. In this chapter, we focus on the coarse acquisition stage where the symbol-level timing, or the code phase information, is targeted. For notational convenience, we call the procedure given by (5.1) and (5.2) the ML energy detection (ML-ED) since the values of energy from different trial positions are compared.

Fig. 5.3 shows the symbol-waveform estimate with the ML processing without suppression when there is one equal-power interfering user. Fig. 5.3 (a) is the symbol waveform estimate at the correct code phase. We see the signals for all frames in a symbol are restored and appear in the correct positions corresponding to the time-hopping codes. Fig. 5.3 (b) shows the symbol waveform estimate at an incorrect code phase. The estimate is basically noise, which is expected. Viewed from the signal space perspective, the maximal-likelihood energy-detection method (expressed by (5.1) and (5.2)) projects the received signal into the signal space of the desired user. Since the codes have low cross-correlation values, the leakage of the interfering signals into the desired signal space is

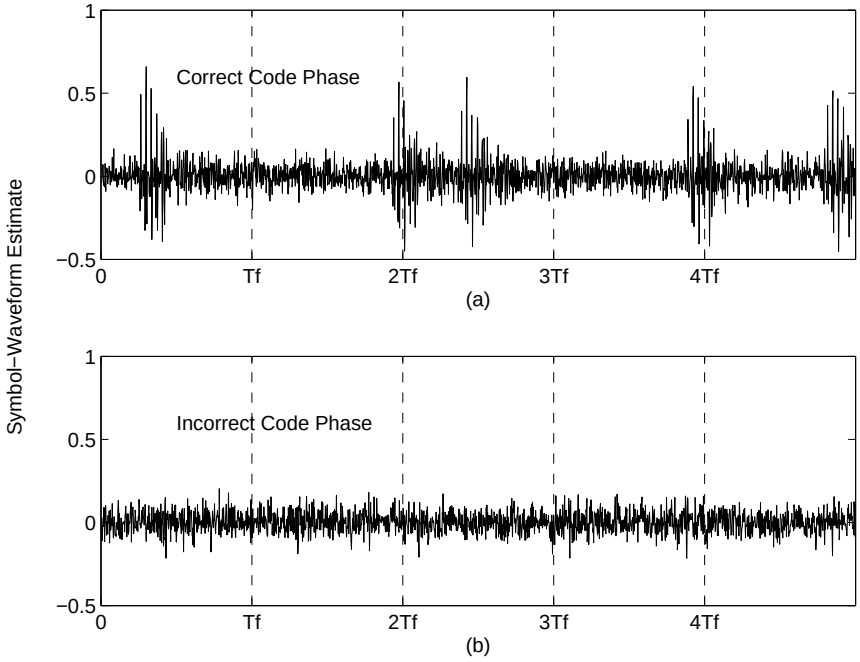

Figure 5.3: Symbol-waveform estimate using the ML processing without suppression for for user 1 in the presence of one equal-power interfering user, $N_e = 1$, $N_h = 0$. Parameters: $N_s = 5$, $E_b^{(1)}/N_0 = 5$ dB, $T_f = 40$ ns. The interfering user has a delay of 20 ns relative to the desired user. Time hopping codes for the desired user and the interfering user are uniformly distributed within $[0,\ 38]$ ($T_c = 1$ ns), and are recorded as $[10, 37, 15, 35, 32]$ and $[30, 9, 22, 13, 35]$ respectively in generating the waveforms in this figure. The channel model is taken from the CM1 realizations in [56].

negligible. The decision process (given in (5.2)) based on the energy of the symbol estimates at different trial positions (different code phases) is not affected by the interfering users. This is seen from Fig. 5.3 where the energy of the symbol estimate in (b) is less than that of (a). This ML-ED procedure (given in (5.1) and (5.2)) works for a multiple-access environment where interfering users have power levels similar to or lower than the desired user. Ideally, if the cross correlation of codes $\{\mathbf{d}^{(u)}\}$ is zero (orthogonal), the ML criterion

always yields a high probability of acquisition.

Note, however, that there are practical situations that can destroy the low leakage level from interfering signals. One important example is when power levels are not regulated. In this case, we find that the synchronization function fails, due to the relatively large leakage of high-power interfering signals into the desired signal space. The symbol-waveform

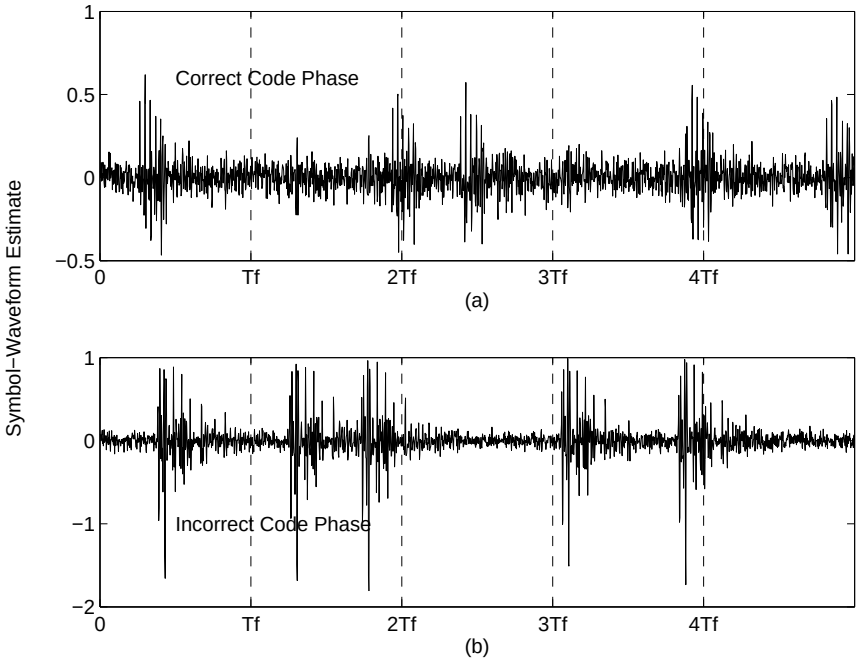

Figure 5.4: Symbol-waveform estimate using the ML processing without suppression for user 1 in the presence of one high-power interfering user, $N_h = 1$, $N_e = 0$. Parameters: $N_s = 5$, $E_b^{(1)}/N_0 = 5$ dB, $T_f = 40$ ns. The high-power user has a power level 20 dB larger than the desired user and has a delay of 20 ns relative to the desired user. Time hopping codes for the desired user and the interfering user are uniformly distributed within $[0,\ 38]$ ($T_c = 1$ ns), and are recorded as $[10, 37, 15, 35, 32]$ and $[30, 9, 22, 13, 35]$ respectively in generating the waveforms in this figure. The channel model is taken from the CM1 realizations in [56].

estimate at an incorrect code phase is not pure noise in Fig. 5.4 (b) as it is in Fig. 5.3 (b). The signals from the high-power interfering user are not sufficiently suppressed in the de-spreading process and the leakage is clearly shown in Fig. 5.4 (b). The energy of the symbol-waveform estimate at the incorrect code phase in Fig 5.4 (b) is larger than that from the correct code phase in Fig. 5.4 (a). Therefore, the decision process based on (5.2) fails.

5.2 Suppressing High-Power Users

In the previous section, we have shown that in networks where power levels can vary widely, additional effort is needed in order to establish synchronization. In the context of multiuser detection (MUD), global optimization can be achieved by jointly estimating the parameters for all users given that the timing information and the code waveforms for all users are known at the receiver [60]. To retrieve the timing information for CDMA systems in the presence of the MAI, the authors in [50, 51, 52, 53] considered either equal-power environments or employed procedures which involved matrix operations.

In contrast, we propose in this section a much simpler procedure that allows synchronization in the presence of high-power interfering users, requiring only knowledge of the desired user's code. The technique exploits the disparate power levels between high-power interfering users and the desired user.

Using the decomposition of the users $N_u = N_e + N_h + 1$ (explained in Section 2.1), the

received signal can be rewritten for analysis purposes as:

$$\begin{aligned} r(t) &= \sum_{i=0}^{M-1} \left\{ d_i^{(1)} \sqrt{E^{(1)}} g^{(1)} \left(t - iT_s - \tau^{(1)} \right) \right. \\ &\quad + \sum_{u_1=2}^{N_e+1} d_i^{(u_1)} \sqrt{E^{(u_1)}} g^{(u_1)} \left(t - iT_s - \tau^{(u_1)} \right) \\ &\quad \left. + \sum_{u_2=N_e+2}^{N_e+N_h+1} d_i^{(u_2)} \sqrt{E^{(u_2)}} g^{(u_2)} \left(t - iT_s - \tau^{(u_2)} \right) \right\} \\ &\quad + n(t) \end{aligned} \tag{5.3}$$

Note that in (5.3) only the coarse symbol-level signal is shown. The frame-level signal structure is included within the symbol waveform since we are focusing on symbol-level signal processing at this point.

Suppose the high-power interfering signals are present in the observed waveform. Since the energy levels $\{E^{(u_2)}\}_{u_2=N_e+2}^{N_e+N_h+1}$ (from high-power interfering users) are much higher than the other users, it is easy to verify that the cross correlation between the ith symbol and the i'th symbol ($i < i' < M$) is determined by

$$\begin{aligned} r_h(\tilde{\tau}; i, i') &= \sum_{u_2=N_e+2}^{N_e+N_h+1} \sum_{u_3=N_e+2}^{N_e+N_h+1} \int_0^{T_s} d_i^{(u_2)} d_{i'}^{(u_3)} \sqrt{E^{(u_2)} E^{(u_3)}} \\ &\quad \times g^{(u_2)}(t + iT_s + \tilde{\tau}) g^{(u_3)}(t + i'T_s + \tilde{\tau}) dt \end{aligned} \tag{5.4}$$

Assume once the interfering user is active, its signal transmission lasts for at least M symbols. This is a practical assumption since the synchronization itself requires at least one block of M symbols. The channels for different users are assumed to be statistically inde-

pendent from each other. The channel for each user is also assumed independent from burst to burst but remains constant within the observation interval of the M symbols. Thus, the symbol waveforms for one user in different symbol intervals are approximately the same except for the possible sign difference as seen in Fig. 5.5, where the first symbol waveform of the high-power interfering user bears the same form as the second symbol waveform and has the same sign. Also note that in Fig. 5.5 the desired signals (the signals within the two dashed lines) are buried under the interfering signals (indicated by the dash dotted lines). Noise is not shown for clearer illustration.

Using this fact that in the presence of high-power users the sign of the cross correlation between different symbols is determined by the waveforms of the dominant high-power users, the signal waveforms from high-power users can be canceled by the following procedure.

Suppose the sign of $r_h(\tilde{\tau}; i, i')$ is positive as shown in Fig. 5.5. In the despreading process (5.1), each symbol waveform is multiplied by the corresponding spreading code of the desired user and is folded back into the first symbol interval to form the symbol-waveform estimate $g(t; \tilde{\tau})$. Since the desired user's spreading code is known by the receiver, the code $d_{i'}^{(1)}$ ($i < i' < M$) can be tested to determine if the condition $d_i^{(1)} d_{i'}^{(1)} = -1$ holds. This is to test to see if the subsequent symbol has a different sign as $d_i^{(1)}$. If yes, these two symbols are marked as a pair. When these two symbol waveforms are added after the corresponding spreading codes are multiplied, the interfering signals are canceled out and the desired symbol waveforms are coherently combined if the code phase is correct. In the same manner, if $r_h(\tilde{\tau}; i, i') < 0$ and the symbol $d_{i'}^{(1)}$ has the same sign as $d_i^{(1)}$, then the two corresponding received waveforms are also retained when forming the symbol-

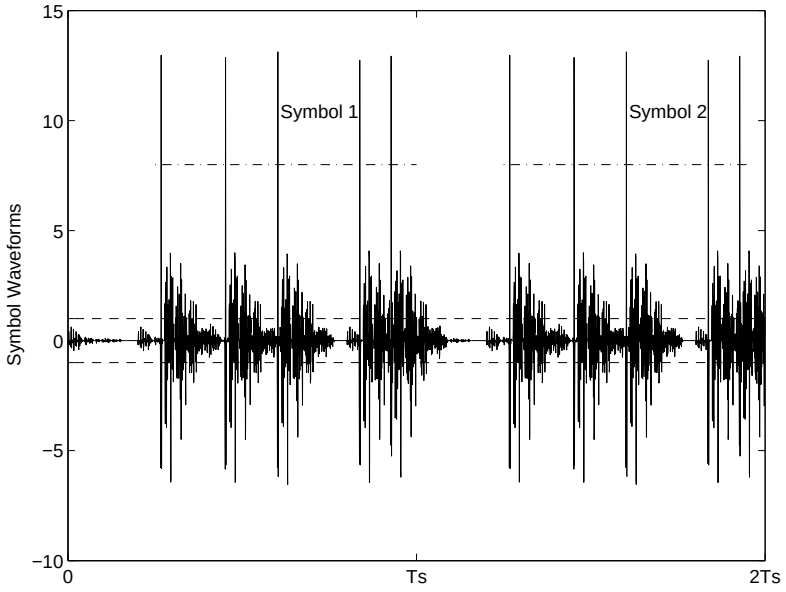

Figure 5.5: Waveforms of duration two symbols at the receiver when one high-power user is present $N_h = 1$. Parameters: $N_s = 5$, $E_b^{(1)}/N_0 = 5$ dB. The high-power user (large bursts) has a power level 20 dB larger than the desired user (small bursts). Time hopping codes for the desired user is set to be all zero and is uniformly generated for the high-power user from integers $[0, 38]$ with $T_c = 1$ ns. Channel model is taken from the CM1 realizations in [56].

waveform estimate. Note that once a symbol is marked as a member of a pair, it can not be used again in another pair. Fig. 5.6 illustrates this process by showing five successive symbols. The first two symbol waveforms are retained in the folding process to form the symbol-waveform estimate. The third symbol waveform together with the fifth symbol-waveform are also retained because the desired user's symbols have the same signs and the interfering symbols have different signs. Depending on whether the fourth symbol can form a pair according to the rules defined above, determines the acceptance of the fourth

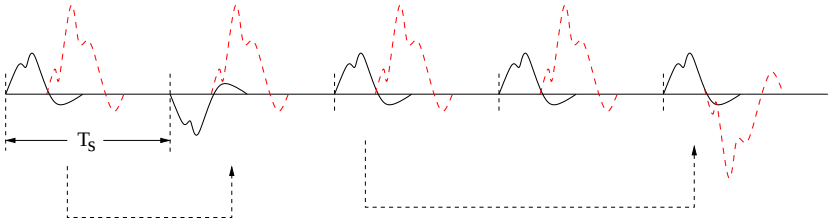

Figure 5.6: The suppression process showing bursts from the desired user (solid) and high-power users (dashed). Dashed arrow lines indicate pairs selected to result in cancellation of the high-power interfering waveforms when combined.

symbol waveform.

Mathematically, we can describe the above process as follows. The condition upon which the ith and the i'th symbol form a pair is

$$\begin{aligned} C(\tilde{\tau};i) &= C(\tilde{\tau};i') \\ &= \begin{cases} 1, & r_h(\tilde{\tau};i,i') > 0 \text{ and } d_i^{(1)} d_{i'}^{(1)} = -1 \\ 1, & r_h(\tilde{\tau};i,i') < 0 \text{ and } d_i^{(1)} d_{i'}^{(1)} = 1 \end{cases} \\ C(\tilde{\tau};i) &= 0, \text{ otherwise} \end{aligned} \tag{5.5}$$

where $0 \le i < M$ and $i < i' < M$. Denote the symbol-waveform estimate using the suppression process as $\hat{g}_s(t;\tilde{\tau})$ to differentiate it from (5.1) which gives the symbol-waveform estimate without the suppression process. The suppressed symbol waveform can be written as

$$\hat{g}_s(t;\tilde{\tau}) = \frac{1}{M} \sum_{i=0}^{M-1} C(\tilde{\tau};i) d_i^{(1)} r(t + iT_s + \tilde{\tau}) \tag{5.6}$$

Note in (5.6), for each symbol i, if a subsequent symbol i' can be found to satisfy $\mathcal{C}(\tilde{\tau}; i) = 1$, the two symbols are included in the summation and the symbol i' is marked as used by setting $\mathcal{C}(\tilde{\tau}; i') = 1$, indicating that it is no longer available for inclusion in a subsequent pair, thus ensuring that each symbol is either used once or discarded. One consequence of this process is that symbols received earlier are more likely to be paired than symbols received later. This is a result of a reduced pool of symbols available for pairing as the process evolves.

The selection process described above effectively cancels out or suppresses the signal waveforms of the high-power users. Fig. 5.7 shows examples of symbol-waveform estimates using two schemes: Figures (a) and (b) are the maximal likelihood symbol-waveform estimates which do not include our suppression procedure (as in [49]), and Figures (c) and (d) include our suppression procedure. In both schemes, the symbol-waveform estimates at two code phases are shown, one being the estimate at the correct code phase and the other being an estimate at an incorrect code phase. Ideally, the symbol-waveform estimate at the incorrect code phase should only include noise and no signal bursts.

We see from Fig. 5.7 (b) that without our suppression procedure, the symbol-waveform estimate from the incorrect code phase has signals present in every dimension. This is because the signals from high-power users can not be sufficiently suppressed by the de-spreading processing shown by (5.1). Since no measures are taken to suppress the high-power interfering waveforms, the ML-ED acquisition based on (5.2) fails since the energy of the symbol-waveform estimate from the incorrect code phase (Fig. 5.7 (b)) is very likely to be larger than that from the correct code phase (Fig. 5.7 (a)).

The symbol-waveform estimates in Fig. 5.7 (c) and (d) show the two symbol-waveform

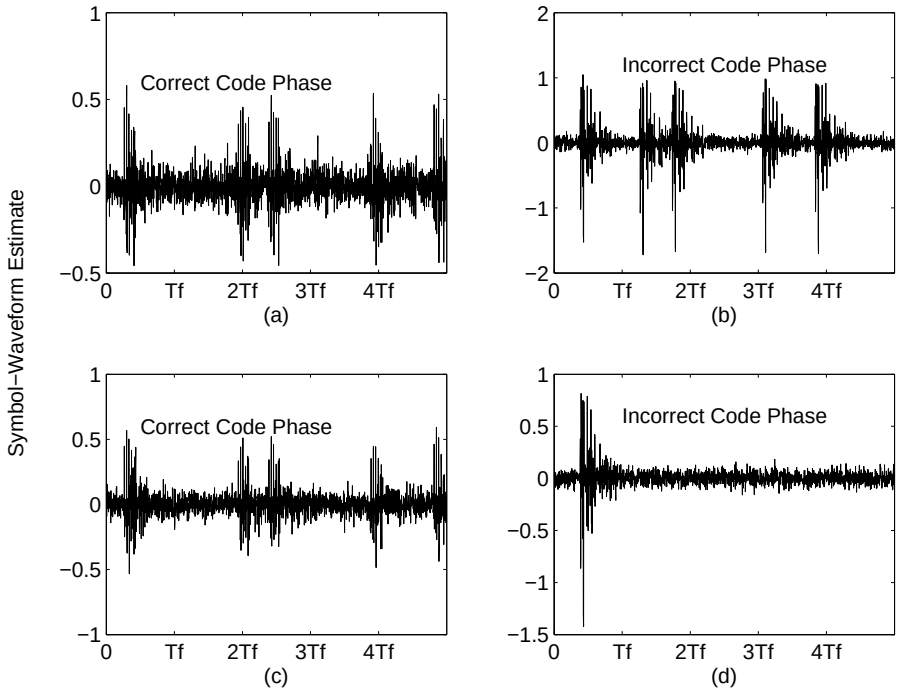

Figure 5.7: The symbol-waveform estimates for user 1 at two code phases. For (a), (b) Symbol-waveform estimate based on (5.1). For (c), (d) Symbol-waveform estimate based on (5.6). The code used is the $M = 31$ Gold code. There is one high-power interfering user signal present. Parameters: $N_s = 5$, $E_b^{(1)}/N_0 = 5$ dB, $T_f = 40$ ns. The high-power user has a power level 20 dB larger than the desired user and has a delay of 20 ns relative to the desired user. Time hopping codes for the desired user and the interfering user are uniformly distributed between $[0,\ 38]$ ($T_c = 1$ ns), and are recorded as $[10, 37, 15, 35, 32]$ and $[30, 9, 22, 13, 35]$ respectively in generating the waveforms in this figure. The channel model is taken from the CM1 realizations in [56].

estimates after applying our suppression procedure. We see the symbol-waveform estimate (d) from the undesired code phase is much cleaner (in the sense that less signal components are present) than the corresponding waveform shown in (b). The code phase offset of (a) and (b) is the same as that of (c) and (d) in Fig. 5.7. But due to what we call the edge

effect, which is unavoidable, the interfering signals can not be fully canceled as shown in Fig. 5.7 (d). This is expected because only when the trial position $\tilde{\tau}$ lines up perfectly with the dominant signal from the high-power user can the signals from the high-power user be fully canceled.

Fig. 5.8 shows the edge effect where the symbol segments from high-power interfering users are represented by square waves for easy illustration. The starting search position of the algorithm happens to be at the edge of the high-power interfering waveform. The symbols (a) and (b) in Fig. 5.8 are included if the desired user has corresponding successive codes of the same sign. But as shown in Fig. 5.8, the small shaded areas in symbols (a) and (b) are combined instead of canceled. The existence of the edge effect suggests

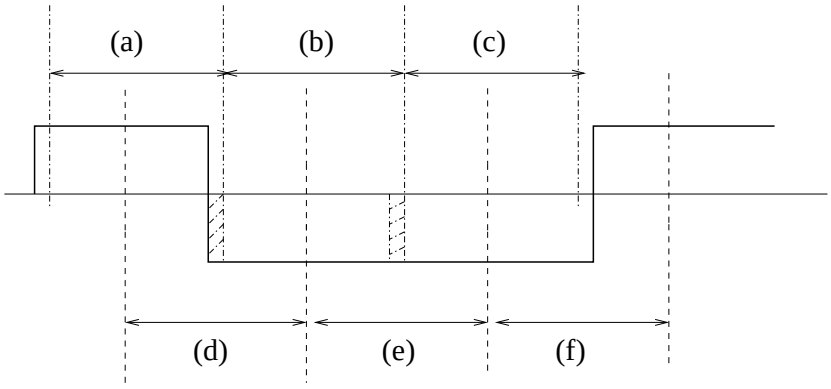

Figure 5.8: The edge effect in suppressing the waveforms from the high-power users.

that the ML-ED acquisition procedure based on (5.2) from [49] is not reliable since it is mainly comparing the energy of symbol-waveform estimates from different code phases. The symbol energy from the incorrect code phase can exceed the symbol energy from the

correct code phase as seen in Fig. 5.7 (c) and (d). But as we observed, the signal dimension from the incorrect code phase is smaller than that from the correct code phase. This observation motivates the search for the correct code phase based on the signal dimension of the suppressed symbol-waveform estimate.

5.3 Dimension-Based Code Phase Detection

To determine the signal dimension of $\hat{g}_s(t;\tilde{\tau})$ in the absence of the channel estimate, subspace-based theory such as given in [61] can be applied. This, however, requires computationally intensive singular value decomposition (SVD). To avoid this, our technique is based on a simpler energy-based dimension detection. In the following, we first analyze the components of the frame energy and then propose two different methods to set up the threshold for the dimension detection.

The system parameter N_s is assumed to be known by the receiver. The maximum signal dimension of $\hat{g}_s(t;\tilde{\tau})$ is thus N_s, which ideally should be reached only when the signal is aligned at the correct code phase. The energy of the jth frame of $\hat{g}_s(t,;\tilde{\tau})$ is

$$\varepsilon_j(\tilde{\tau}) = \int_{jT_f}^{(j+1)T_f} [\hat{g}_s(t;\tilde{\tau})]^2\, dt \tag{5.7}$$

To obtain the frame energy $\varepsilon_j(\tilde{\tau})$, we first substitute (5.3) into (5.6) to obtain the frame-waveform estimate as

$$\hat{g}_s(t;\tilde{\tau};j) = y_0(t;\tilde{\tau}) + y_e(t;\tilde{\tau}) + y_h(t;\tilde{\tau}) + n_s(t) \tag{5.8}$$

where the desired-user waveform, the interfering waveforms of users with power levels similar to or lower than the desired user, the high-power interfering waveforms, and the thermal noise are obtained respectively as

$$y_0(t;\tilde{\tau}) = \gamma(\tilde{\tau})R_1(i_1)\sqrt{E^{(1)}}g(t+\tilde{\tau}-\tau^{(1)}) \tag{5.9}$$

$$y_e(t;\tilde{\tau}) = \gamma(\tilde{\tau})\sum_{u_1=2}^{N_e+1} R_{u_1}(i_{u_1})\sqrt{E^{(u_1)}} \times g^{(u_1)}(t+\tilde{\tau}-\tau^{(u_1)}) \tag{5.10}$$

$$y_h(t;\tilde{\tau}) = \sum_{u_2=N_e+2}^{N_e+N_h+1} R_{u_2}(i_{u_2})\sqrt{E^{(u_2)}} \times g_r^{(u_2)}(t+\tilde{\tau}-\tau^{(u_2)};\mathcal{C}) \tag{5.11}$$

$$n_j(t) = \frac{1}{M}\sum_{i=0}^{M-1} n(t+iT_s+jT_f) \tag{5.12}$$

and $\gamma(\tilde{\tau}) = \frac{1}{M}\sum_{i=0}^{M}\mathcal{C}(\tilde{\tau};i)$ is the fraction of symbols that remain after applying our suppression technique. The function $R_1(i_1)$ is the normalized, cyclic auto-correlation function of the spreading code for user 1 with offset i_1. The function $R_{u_1}(i_{u_1})$ is the normalized, cyclic cross-correlation function of the spreading codes for user 1 and user u_1 with offset i_{u_1}. The offset is obtained from $i_u = \lceil(\tilde{\tau}-\tau^{(u)})/T_s\rceil$, $u = 1,2,...N_u$. The waveform $g_r^{(u_2)}(t+\tilde{\tau}-\tau^{(u_2)};\mathcal{C})$ in (5.11) is the random residual signal after the suppression process which has fewer signal components ($\leq N_s$) as seen in Fig. 5.7 (d). The residual waveform $g_r^{(u_2)}(\cdot)$ depends on the spreading codes, the suppression process indicated by $\mathcal{C}$, and the relative offset between $\tilde{\tau}$ and $\tau^{(u_2)}$. Note that when the function $\mathcal{C}(\tilde{\tau};i)$ is used in other signals, we omit the function's arguments to simplify notations, as seen in the residual waveform $g_r^{(u_2)}(t+\tilde{\tau}-\tau^{(u_2)};\mathcal{C})$. We can then substitute (5.8) into (5.7) to obtain the frame

energy

$$\begin{aligned}\varepsilon_j(\tilde{\tau}) &= \gamma^2(\tilde{\tau})\left(R_1^2(i_1)\varepsilon_1+\sum_{u_1=2}^{N_e+1}R_{u_1}^2(i_{u_1})\varepsilon_{u_1}\right)\\ &\quad+\sum_{u_2=N_e+2}^{N_e+N_h+1}R_{u_2}^2(i_{u_2})\varepsilon_{u_2}(\mathcal{C})\\ &\quad+2R_c(\tilde{\tau};\mathcal{C})+n_j \qquad (5.13)\end{aligned}$$

where

$$\varepsilon_u = \int_0^{T_f}\left[g^{(u)}(t)\right]^2 dt,\ \ u=1,2,...,N_e \qquad (5.14)$$

and

$$\begin{aligned}R_c(\tilde{\tau};\mathcal{C}) &= \int_0^{T_f}[y_0(t;\tilde{\tau})y_e(t;\tilde{\tau}) \qquad (5.15)\\ &\quad+y_0(t;\tilde{\tau})y_h(t;\tilde{\tau}) \qquad (5.16)\\ &\quad+y_e(t;\tilde{\tau})y_h(t;\tilde{\tau})]\,dt \qquad (5.17)\end{aligned}$$

is the cross correlation between signals of all users. The lower dimension of the residual waveform due to the edge effect results in residual energy $\varepsilon_{u_2}(\mathcal{C})$ zero in most frames of the symbol-waveform estimate. The cross-correlation term $R_c(\tilde{\tau};\mathcal{C})$ is random and depends on the spreading codes and the delays $\boldsymbol{\tau}$. The thermal noise related term n_j has mean equal to

$\frac{1}{2M}T_f N_0$ and its variance is easily calculated to be

$$\begin{aligned}\sigma_n^2(\tilde{\tau}) &= \frac{2N_0}{M}R_1^2(i_1)\gamma^2(\tilde{\tau})\varepsilon_1 \\ &\quad + \frac{2N_0}{M}\gamma^2(\tilde{\tau})\sum_{u_1=2}^{N_e+1}R_{u_1}^2(i_{u_1})\varepsilon_{u_1} \\ &\quad + \frac{2N_0}{M}\sum_{u_2=N_e+2}^{N_e+N_h+1}R_{u_2}^2(i_{u_2})\varepsilon_{u_2}(\mathcal{C}) \end{aligned} \tag{5.18}$$

To determine whether a signal is present in the jth frame based on the frame energy $\varepsilon_j(\tilde{\tau})$ requires a threshold. The terms related to the residual waveform in (5.13) can be ignored in the threshold setting since the goal is to identify signals from the desired user. The random variable $R_c(\tilde{\tau};\mathcal{C})$ has zero mean because the mean of $R_1(i_1)R_{u_1}(i_{u_1})$ is zero for most codes with unrelated random offset i_1 and i_{u_1}. Disregarding the residual waveform, the mean of the frame energy is therefore

$$\begin{aligned} m(\tilde{\tau}) &= \mathop{\mathbb{E}}_{n}\{\varepsilon_j(\tilde{\tau})\} \\ &= \gamma^2(\tilde{\tau})\left(R_1^2(i_1)\varepsilon_1 + \sum_{u_1=2}^{N_e+1}R_{u_1}^2(i_{u_1})\varepsilon_{u_1}\right) \\ &\quad + \frac{1}{M}T_f\frac{N_0}{2} \end{aligned} \tag{5.19}$$

where $\mathbb{E}_n\{\cdot\}$ represents the expectation operation with respect to the thermal noise. The corresponding variance is the variance of n_j in (5.18) without the residual term. We do not consider the variance of $R_c(\tilde{\tau};\mathcal{C})$ in setting the threshold since the cross correlation between users is small compared to the square of the signals in (5.18).

Given the mean and variance of $\varepsilon_j(\tilde{\tau})$, we can adopt the Neyman-Pearson test to set the

threshold [62]. Let the probability of false alarm be constrained by

$$\Pr\{\varepsilon_j(\tilde{\tau}) \geq \eta_t, \text{ for } \tilde{\tau} \notin (\tau^{(1)} - T_s,\ \tau^{(1)} + T_s)\} \leq f_a \tag{5.20}$$

where $\Pr\{\cdot\}$ represents the probability of an event, η_t is the threshold, and f_a is the maximum false alarm rate. Substituting (5.18) and (5.19) into (5.20), we can solve for the threshold η_t as

$$\begin{aligned} \eta_t \quad \geq \quad & \gamma^2(\tilde{\tau}) R_1^2(i_1)\varepsilon_1 + m_e + c \\ & + Q^{-1}(f_a)\gamma(\tilde{\tau})\sqrt{(2N_0 R_1^2(i_1)\varepsilon_1 + 2N_0 m_e)/M}\,, \\ & \text{for} \quad i_1 \neq 0 \end{aligned} \tag{5.21}$$

where we denote $c = \frac{1}{2M} T_f N_0$, $m_e = \sum_{u_1=2}^{N_e+1} R_{u_1}^2(i_{u_1})\varepsilon_{u_1}$ and $Q^{-1}(\cdot)$ as the inverse function of the Q function.

The Neyman-Pearson test maximizes the detection probability while ensuring the false alarm rate is within a given range. We see from (5.21) that this test requires the knowledge of every parameter of the system. In the absence of knowledge of system parameters (such as the number of interfering users N_e), we can set the threshold based on the only known term in (5.21), namely $c = \frac{1}{2M} T_f N_0$. Using c, the threshold can be set as $\eta_c = \alpha c$, where α can be chosen by the algorithm.

Once the threshold is set, the frame energy $\varepsilon_j(\tilde{\tau})$ is then compared to the threshold to determine whether or not a signal is present in the frame. The symbol waveform with the highest dimension is determined as the symbol-waveform estimate and the corresponding

$\tilde{\tau}$ is taken as the estimate of $\tau^{(1)}$

$$\hat{\tau} = \arg\max_{\tilde{\tau}} \sum_{j=0}^{N_s-1} I(\varepsilon_j(\tilde{\tau}) \geq \eta_t) \tag{5.22}$$

where $I(\cdot)$ is the identity function which takes the value one when the inside argument is true and zero otherwise. The threshold η_t is chosen as an example in (5.22).

5.3.1 Threshold Setting

The setting of the threshold η_t in (5.21) depends on three main factors: the value of $\gamma(\tilde{\tau})$, $R_1(i_1)$, and the instantaneous value of ε_u ($u = 1,2,...N_e+1$). To guarantee the false alarm rate f_a, the values of $\gamma(\tilde{\tau})$ and $R_1(i_1)$ can be set to their largest possible values. For $\gamma(\tilde{\tau})$, the largest value is one. The largest value for $R_1(i_1)$ ($i_1 \neq 0$) depends on the spreading codes. For example, $R_1(i_1) = 9/31$ ($i_1 \neq 0$) for the Gold code with a length $M = 31$ [63], which is the code used in the simulations in this paper. To see the effect of the channel, we use the channel model from [56]. The energy ε_u can be calculated as

$$\varepsilon_u = \frac{X_u^2}{N_s} \tag{5.23}$$

where X_u is the log-normal shadowing experienced by user u. Note that the multipath channel model from [56] has the total energy contained in the multipath components normalized to be one and the log-normal term X_u captures the total multipath energy. From (5.23), we see the instantaneous value of ε_u depends on the channel and can be very small when the channel is in a deep fade. We show the effect of $\rho = X_1^2$ in the simulations by varying the value of ρ.

5.3.2 The Middle Effect

One key element in suppressing the waveforms from high-power interfering users is to determine the sign in (5.4) of the cross correlation between two symbol segments of the received signal. The random trial value $\tilde{\tau}$ may result in a less favorable statistic upon which the sign of the cross correlation is determined. This phenomenon is shown in Fig. 5.8 where the edge effect is also shown. The symbol segments in Fig. 5.8 (d) and (e) have cross correlation nearly zero because the trial position is approximately at the center of the waveform from high-power interfering users. We call this the middle effect, as opposed to the edge effect discussed before. The middle effect is characterized by signs of cross correlations being mainly determined by noise. In this case, a symbol waveform with a dominant dimension is unlikely to be detected. For coarse code phase estimation, the uncertainty due to the middle effect can be easily resolved by using a new starting search position with an offset value equal to a fraction of one symbol interval. Several steps suffice to guarantee a symbol-waveform estimate with a dominant dimension.

5.3.3 Algorithm Description

All delays are referenced to the desired user, resulting in $\tau^{(1)} = 0$ and $\tau^{(u)}$ uniformly distributed on the interval $[0,\ MT_s]$ for $u \neq 1$. Like the ML-ED algorithm from [49], our algorithm uses N successive blocks of the length-M codes for each user. Suppose the receiver starts searching at the time instant τ^0 which is set to be a random number between 0 and MT_s. The trial position $\tilde{\tau}$ is then stepped through $[\tau^0,\ \tau^0 + MT_s)$ with a step size T_s. Ideally the symbol with the highest dimension should be detected when $|\tilde{\tau} - mMT_s| \leq T_s$ with $m = \{0, 1, 2\}$. There are three possible correct code phases because of the uniformly

distributed starting point $\tau^0 \in [0,\ MT_s]$. If no symbol waveform with a dominant dimension is detected after searching through $[\tau^0,\ \tau^0 + MT_s)$, then an offset starting position discussed in Section 5.3.2 are employed. Suppose the number of offsets is V. At the vth offset, the search range is $vT_s/V + [\tau^0, \tau^0 + MT_s)$, $v = 1, ..., V$. If a decision is made at the vth offset, the searching terminates. If no decision is made after V offsets, then an error occurs. In our simulations, we set a large number $\hat{\tau} = 2.5MT_s$ to indicate an error. This yields the largest possible error of $0.5MT_s$. When errors occur, the receiver can either vary the value of the threshold or request a retransmission.

A summary of the algorithm is given as follows.

1. Set up a threshold as $\eta_c = \alpha c$ or η_t from (5.21).
2. Start searching at a random instant τ^0.
3. Clear the values of $\mathcal{C}(\tau^0; i) = 0$ for all symbols $0 \leq i \leq MN - 1$.
4. For the ith symbol ($0 \leq i \leq MN - 1$), search a subsequent symbol i' according to the rule given in (5.5).
5. If a subsequent symbol i' is paired with the ith symbol, mark $\mathcal{C}(\tau^0; i) = 1$ and $\mathcal{C}(\tau^0; i') = 1$.
6. Form the symbol waveform estimate $\hat{g}_s(t; \tau^0)$ according to (5.6).
7. Detect the dimension of $\hat{g}_s(t; \tau^0)$ and store the value of the dimension for the trial position τ^0.
8. Return to step 2 with a trial position $\tau^0 + mT_s$ where $1 \leq m \leq M - 1$.

9. Compare the values of the dimension for all M trial positions within the range $\left[\tau^0,\ \tau^0 + MT_s\right)$.

10. If a maximum dimension is found, terminate the search process. If no dominant dimension exists, the algorithm selects an offset starting instant. The offset is T_s/V. The new start instant is given by $\tau^0 + (v/V)T_s$ in the vth offset, $1 \leq v \leq V$. Return to step 2 with the new start instant until $v = V$.

11. If a decision is made, the search process is terminated. If no decision is made after $v = V$, the receiver can either vary the value of the threshold or request a retransmission. In the case of varying the threshold (either vary α of η_c or vary ρ of η_t), return to step 1 with the new threshold value. In the case of retransmission, return to step 2 with a new random start instant.

5.4 Simulations

In this section we demonstrate the performance of our suppression and dimension-detection synchronization technique in the presence of high-power interference. We compare the performance of our suppression and dimension detection technique to the maximal-likelihood energy detection algorithm from [49].

The transmitted pulse shape is the second derivative of the Gaussian monocycle with pulse width 1.0 ns. The channel model is CM1 taken from [56]. One hundred channel realizations are generated. The entire set of one hundred realizations is used for the desired user's signal while interfering users' signals use channel realizations independently from the desired user and from all other interfering users. Note that shadowing is included in the channel model. All users have $N_s = 5$ and $T_f = 40$ ns. Balanced Gold codes with a length of

$M = 31$ are used. As in [49], $N = 10$ successive blocks of the $M = 31$ balanced Gold codes are transmitted for each user. In all the simulations, a maximum of eight starting offset values are allowed, $V = 8$. If the synchronization algorithm can not reach an estimation for the delay using the first set of pilot symbols, one retransmission can be attempted. The second failure results in an unsuccessful acquisition.

Shown in Fig. 5.9 are plots of average acquisition probability versus E_b/N_0 using our algorithm as well as the maximal-likelihood energy detection from the current literature.The threshold $\eta_c = \alpha c$ is used in Fig. 5.9. The acquisition probability in a single-user environment is plotted as a benchmark. There are several issues that are illustrated in this figure. First, in the presence of a high-power interfering user's signal, synchronization using our suppression and dimension detection technique, shown by the stared, crossed, triangular, and squared lines respectively, performs significantly better than the maximal-likelihood energy detection technique from [49] shown by the circled line. Note that without our suppression technique, the maximal-likelihood energy detection completely breaks down in this case. Successful acquisition is only possible when the high-power interfering signal experiences a deep fading channel while the desired user's signal has a relatively good channel, which is approximately 0.15 for the CM1 channel model since the deep fading probability is approximately 0.2.

Second, the effects of the parameter settings for our suppression and dimension-detection technique are shown in Fig. 5.9. The stared line shows the average acquisition probability of using η_c with a fixed $\alpha = 2.0$. The effect of decreasing the threshold by using a smaller value of $\alpha = 1.5$ when decisions can not be made using $\alpha = 2.0$ is shown by the crossed line. At low to moderate E_b/N_0, varying the threshold between $\eta_c = 2.0c$ and $\eta_c = 1.5c$

significantly increases the acquisition probability by approximately 25 percent comparing to a fixed $\eta_c = 2.0c$ case.

Retransmission (the top triangular line) also improves the acquisition probability although the improvement is not as significant as varying the value of α at low E_b/N_0. This is because the relatively high level of the threshold prevents some signals from being detected even when the channel is not in a deep fade. In this case, lowering the threshold is more effective. The combination of varying the threshold with retransmission further increases the acquisition probability at low E_b/N_0.

Third, an acquisition strategy can be obtained from the curves in Fig. 5.9. At high E_b/N_0, varying the threshold and retransmission separately yields the same performance as the combination of the two techniques. This observation motivates the following acquisition procedure: In cases when the receiver has relatively less knowledge of the interfering environment (e.g. the value of N_e is unknown), the threshold is set to be $\eta_c = \alpha c$. Also in this situation, without loss of acquisition performance, the receiver can vary the value of α when errors occur to save the power and delay incurred by retransmission.

The performance of the Neyman-Pearson threshold setting η_t (5.21) is shown in Fig. 5.10. The overall acquisition probability using η_t is better than both the ML-ED technique without suppression [49] (given by (5.1) and (5.2)) and the case when using η_c. The effects of parameter settings when using η_t are different from the situations where η_c is used. When the fading coefficient $\rho = X_1^2$ varies, it is chosen from $\{1.0,\ 0.5\}$. Varying the threshold (crossed line) is not as efficient as retransmission (top triangular line) seen from Fig. 5.10, which is opposite to the observations in Fig. 5.9. This can be explained by the optimal threshold setting of the Neyman-Pearson test which implies that uncertainties occur mainly

due to the deep fading of the channel, instead of the settings of the threshold. Varying the threshold can not combat the deep fading of the channel which implies that in this case, retransmission is the only viable option.

The effects of varying the threshold and retransmission from Fig. 5.10 are also observed in Fig. 5.11. The line marked by five stars in Fig. 5.11 is the acquisition probability with the knowledge of the instantaneous channel gain $\rho = X_1^2$. From this figure we see that retransmission with $\rho = 1.0$ outperforms the scheme with knowledge of the instantaneous channel gain $\rho = X_1^2$, indicating that retransmission is the way to combat deep fading of the channel. The knowledge of channel gain together with retransmission (squared line) yields better performance than $\rho = 1.0$ with retransmission at high E_b/N_0.

5.5 Conclusions

In this chapter, we investigate the near-far resistant acquisition issue of DS-UWB systems. Using our simpler suppression technique we reduce the dimension of the high-power interfering waveforms without complex matrix operations. Only the spreading code of the desired user is required. A new dimension-based detection is proposed to detect the dimension of the suppressed received signal. Simulation results validate the techniques proposed in this chapter and show significant performance improvement in the presence of high-power interfering users when compared with ML-ED procedures.

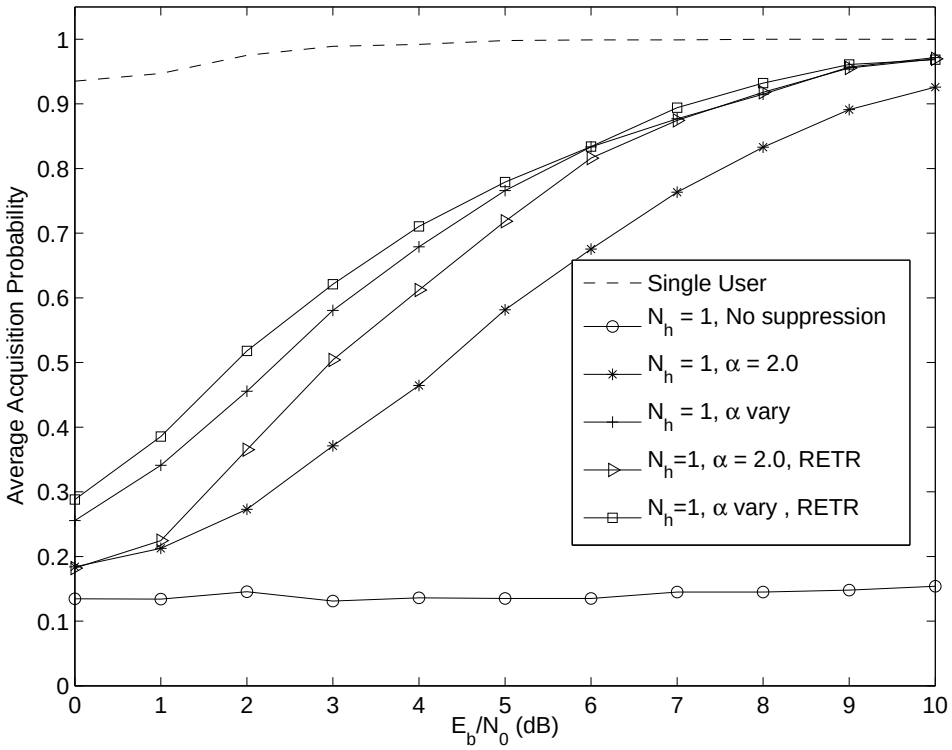

Figure 5.9: Comparison of acquisition probability using the threshold $\eta_c = \alpha c$ with $N_e = 0$. The varying values of α are $\{2.0, 1.5\}$. The legend 'RETR' represents 'with Retransmission'.

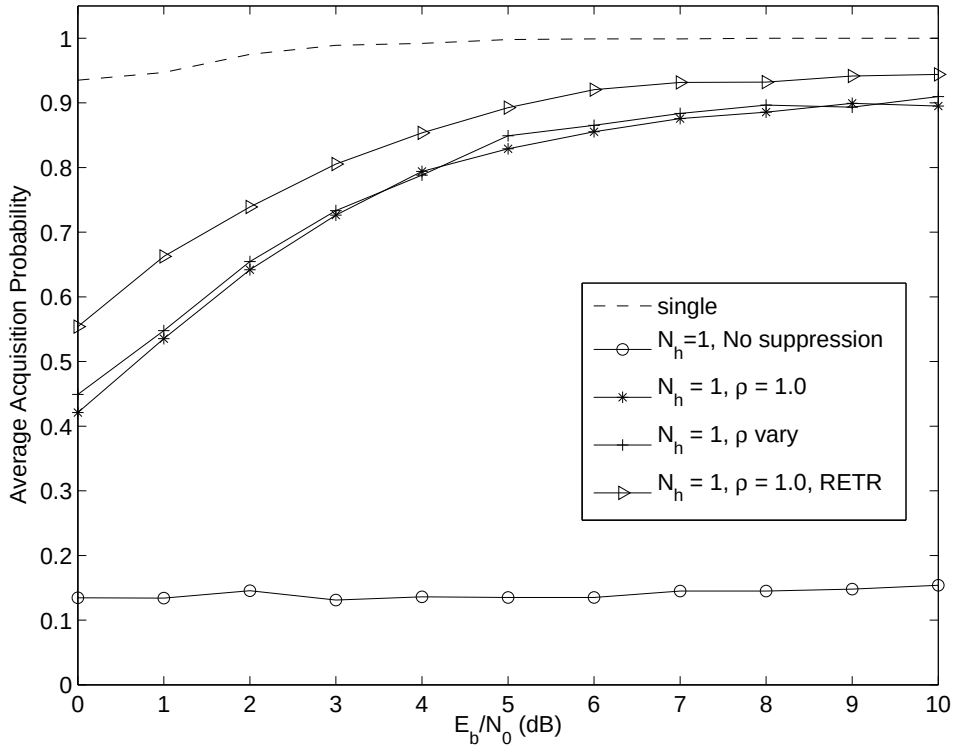

Figure 5.10: Comparison of acquisition probability using the threshold η_t with $N_e = 0$. When varying the fading coefficient, $\rho = X_1^2 \in \{1.0,\ 0.5\}$. The false alarm rate is $f_a = 0.02$. The legend 'RETR' represents 'with Retransmission'.

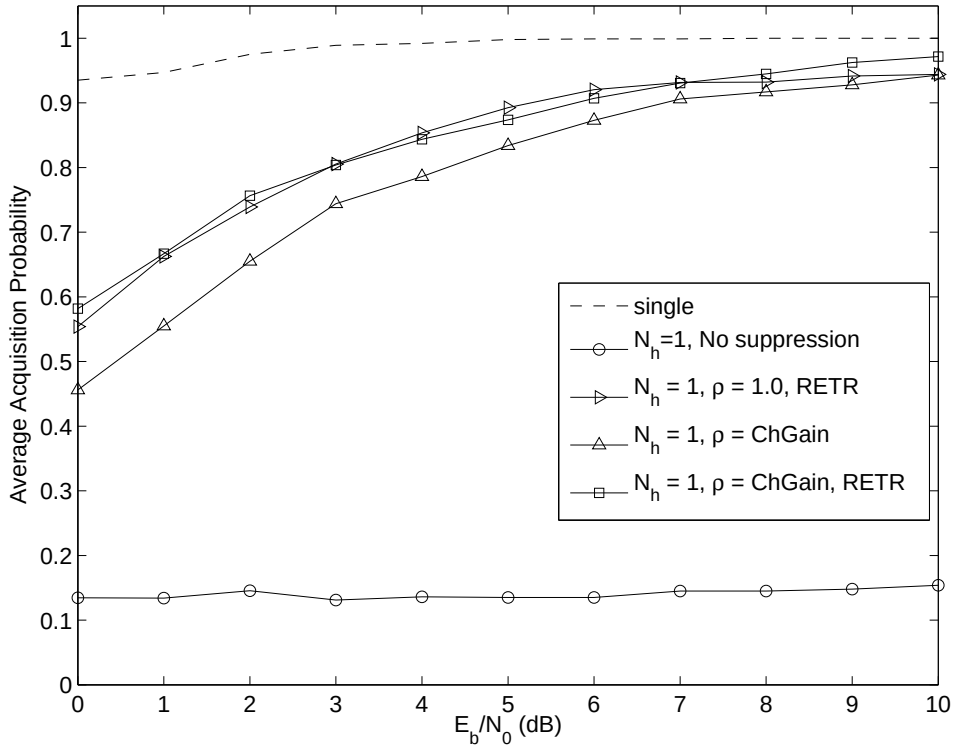

Figure 5.11: Comparison of acquisition probability using different scenarios and η_t with $N_e = 0$. The false alarm rate is $f_a = 0.02$. The legend 'ChGain' represents the instantaneous channel gain.

Chapter 6

Conclusion

This chapter presents a summary of the investigations in this dissertation, followed by some ideas for future work.

6.1 Summary of Dissertation

The investigations of this dissertation can be categorized into two groups: detection performance of TR UWB systems (Chapter 3 - Chapter 4) and synchronization of conventional UWB systems (Chapter 5).

In contrast to the current literatue on UWB systems, surveyed in Chapter 1, this dissertation focuses on UWB networks that do not have centralized power control. More specifically, we assume the network includes interfering users from two sets: equal-power and high-power, as introduced in Chapter 2.

By including a small number of high-power users in the network, the multiple access analysis for TR UWB systems in this dissertation has a different focus from the literature

[13, 14, 15]. Even a small number of high-power users degrades the system performance dramatically as analyzed in Chapter 3. No increase in SNR can improve the system performance, indicating the system completely in the interference-limited region. Chip discrimination which is proposed in [23, 24] is applied to suppress the effects of high-power interfering users. Note that we assume synchronization is established in this part of analysis.

TR UWB systems using binary PAM modulation is investigated in the first part of Chapter 3. Collision probabilities are discussed and presented in a closed form for standard TR (STR) systems. Such closed form expressions do not exist for differential TR (DTR) systems. However, an example of enumeration of collision probabilities is presented for DTR systems. Chip discrimination is shown in Chapter 3 to effectively restore the performance of binary-PAM TR systems. An important observation from this study is that the optimal transmission strategy depends on the system parameters such as E_b/N_0 and the data rate, which is different from the case with only equal-power interfering users [14] where concentrating all energy in one frame is found optimal.

In the second part of Chapter 3 TR systems using M-ary PPM are investigated. Higher order modulation is motivated by the need to improve data rates for TR systems which typically have a large spacing between pulses in a frame to avoid interframe interference. Another reason to investigate higher order modulation is that chip discrimination works with satisfactory performance when the data rate is low. This requirement comes from the low-duty cycle condition required not only by the transmitter, but also by the receiver which collects signals with a time duration determined by the delay spread of the channel. Therefore, the use of chip discrimination requires low data rates, and higher order modulation,

such as M-ary PPM, is used to increase the data rate.

As in the binary case, chip discrimination improves performance of TR UWB systems with M-ary PPM as shown in the second part of Chapter 3. In this chapter, a union bound for the error probability is derived and shown to be tight. The optimal system operation parameters, such as the repetition factor, depend on the value of M and an example is presented for the case $M = 8$. Chip discrimination is shown to result in noise-limited system performance.

While multiple-access interference (MAI) caused by equal-power interfering users for UWB systems is investigated in [33, 27, 13, 14, 15], no explicit and theoretically tractable expressions for the variance of the MAI exist until our work in [55]. In Chapter 4 of this dissertation, the use of the power delay profile (PDP) of the channel simplifies the expression of the variance of the MAI and establishes a theoretical relationship between system parameters. Our analytical results from Chapter 4 give the MA performance of TR UWB systems with M-ary PPM without requiring simulation-based techniques.

Two fundamental issues in communications are addressed in Chapter 4 and the combined effect from both equal-power and high-power users is quantified. System-level trade-offs are carried out for TR systems using the results from Chapter 4, including E_b/N_0, the number of equal-power users, the BEP level, and complexity. The theoretical technique used in deriving the variance of the MAI for TR systems is also applied to slightly frequency-shifted reference (FSR) systems. Multiple access performance between TR and FSR systems is compared.

In Chapter 3 and Chapter 4, synchronization for the desired user is assumed to be established. In Chapter 5, synchronization for conventional UWB systems is investigated

when high-power interfering users are present. The resulting so-called near-far problem causes a very low probability of successful acquisition, shown in our simulations in Chapter 5. The current literature in synchronization for UWB systems assumes power control in the network [44, 45, 46, 47, 48, 49]. In avoiding complex matrix operations such as found in [52] and [53], we proposed an easy-to-implement procedure to suppress the signals from high-power users without requiring their code waveforms. The proposed suppression process effectively reduces the dimension of high-power interfering signals. A subsequent dimension-based detection is proposed to detect the code phase of the desired user as the current energy-based detection fails. Two different methods are proposed in Chapter 5 for setting the threshold required by the dimension detection technique. The methods differ in the amount of prior knowledge of the environment as available to the receiver. Simulation results presented in Chapter 5 verify the proposed suppression and dimension detection procedure and superior performance is observed when compared to the latest technique from the literature.

6.2 Future Work

6.2.1 TR and FSR Synchronization

One natural research direction is to apply the synchronization technique in Chapter 5 to TR UWB systems. The main difficulty encountered in implementing any synchronization technique for TR systems is in the storing of symbols in analog form, especially when multiple symbols are required, which is the case for most systems. To obtain the cross-correlation values between symbols, an analog delay component with a delay time as long

as a symbol interval is required, which is $2N_s$ times the original delay with duration T_d (in the case where $T_f = 2T_d$). Additional effort is required to devise synchronization techniques for TR systems in the presence of high-power users. In this context, synchronization for FSR systems would be easier since no analog delay element is used at the receiver. This leads to another direction of future work – applying the near-far resistant synchronization to FSR UWB systems.

6.2.2 Demodulation Performance

The suppression procedure proposed in Chapter 5 of this dissertation can be used to suppress waveforms from high-power users in the demodulation stage. As suggested by the authors in [49], the by-product in the synchronization stage, the symbol-waveform estimate, can be used as a symbol template in demodulating the information symbols. However, as shown in Chapter 5, the residual waveform that is due to high-power interfering users after the suppression procedure has considerable energy. Therefore, this residual waveform can potentially disturb the demodulation process. While this residual waveform does not cause degradation to the synchronization process, a detailed investigation is needed to quantify its impact on demodulation and detection.

6.2.3 Theoretical Characterization

Another direction of the future work is the full theoretical characterization of the suppression and dimension detection technique. To theoretically calculate the fraction of retaining symbols, the auto-correlation and cross-correlation properties of the spreading codes are required. The difficulty is that the analysis depends on the type of codes used.

A general cross-correlation (or auto-correlation) function for all codes is not likely obtainable. However, for the codes typically used in communications, such as the Gold codes, theoretical expressions can be used to predict the fraction of symbols discarded (or retained). The auto-correlation and cross-correlation functions, together with the thresholds derived in Chapter 5, can then be used to obtain a theoretical expression for the probability of successful acquisition.

Bibliography

[1] FCC First Report and Order: In the Matter of Revision of Part 15 of the Communication's Rules Regardign Ultra-Wideband Transmission Systems. Technical report, FCC 02-48, April 2002.

[2] Moe Z. Win and Robert Scholtz. On the Energy Capture of Ultrawide Bandwidth Signals in Dense Multipath Environments. *IEEE Communications Letters*, 2(9):245–247, September 1998.

[3] Ralph T. Hoctor and Harold W. Tomlinson. An Overview of Delay-Hopped, Transmitted-Reference RF Communications. *GE Research & Development, Technical Information Series*, 2002.

[4] John D. Choi and Wayne E. Stark. Performance of Ultra-Wideband Communications With Suboptimal Receivers in Multipath Channels. *IEEE Journal on Selected Areas in Communications*, 20(9):1754–1766, Dec. 2002.

[5] Quan Hieu Dang, Antonio Trindade, Alle-Jan van der Veen, and Geert Leus. Signal Model and Receiver Algorithms for a Transmitted-Reference Ultra-Wideband Com-

munication System. *IEEE Journal on Selected Areas in Communications*, 24(4):773–779, Apr. 2006.

[6] Yi-Ling Chao and Robert Scholtz. Optimal and Suboptimal Receivers for Ultra-Wideband Transmitted Reference Systems. In *IEEE Global Telecommunications Conference*, volume 2, pages 759–763, Dec. 2003.

[7] Yi-Ling Chao and Robert Scholtz. Ultra-Wideband Transmitted Reference Systems. *IEEE Transaction on Vehicular Technology*, 54(5):1556–1569, Sep. 2005.

[8] Honglei Zhang and Dennis L. Geockel. Generalized Transmitted-Reference UWB Systems. In *IEEE Conference on Ultra Wideband Systems and Technologies*, pages 147–151, Nov. 2003.

[9] Antonio A. D'Amico and Umberto Mengali. GLRT Receivers for UWB Systems. *IEEE Communications Letters*, 9(6):487–489, June 2005.

[10] Stefan Franz and Ulbashi Mitra. Generalized UWB Transmitted Reference Systems. *IEEE Journal on Selected Areas in Communications*, 24(4):780–786, Apr. 2006.

[11] Tony Q. S. Quek and Moe Z. Win. Analysis of UWB Transmitted -Reference Communication Systems in Dense Multipath Channels. *IEEE Journal on Selected Areas in Communications*, 23(9):1863–1874, Sept. 2005.

[12] Lei Fang and Won Namgoong. An Oversampled Channelized UWB Receiver with Transmitted Reference Modulation. *IEEE Transaction on Wireless Communications*, 5(6):1497–1505, June 2006.

[13] K. Witrisal, M. Pausini, and A. Trindade. Multiuser Interference and Inter-frame Interference in UWB Transmitted Reference Systems. In *International Workshop on Joint UWBST & IWUWBS*, pages 96–100, May 2004.

[14] Yi-Ling Chao and Robert A. Scholtz. Multiple Access Performance of Ultra-Wideband Transmitted Reference Systems in Multipath Environments. In *IEEE Wireless Communications and Networking Conference (WCNC)*, volume 3, pages 1788–1793, Mar. 2004.

[15] Zhengyuan Xu and B. M. Sadler. Multiuser Transmitted Reference Ultra-Wideband Communication Systems. *IEEE Journal on Selected Areas in Communications*, 24(4):766–772, Apr. 2006.

[16] C. K. Rushforth. Transmitted-Reference Techniques for Random or Unkown Channels. *IEEE Transactions on Informaiton Theory*, pages 39–42, January 1964.

[17] Ning He and C. Tepedelenlioglu. Performance Analysis of Non-coherent UWB receivers at Different Synchronization Levels. *IEEE Transactions on Wireless Communications*, 5(6):1266–1273, June 2006.

[18] Sandeep Aedudodla, Saravanan Vijayakumaran, and Tan F. Tong. Acquisition of Direct-Sequence Transmitted Reference Ultra-Wideband Signals. *IEEE Journal on Selected Areas in Communications* , 24(4):759–765, April 2006.

[19] Marco Di Renzo, Luca Alfredo Annoni, and Fortunato Santucci. Timing Acquisition for DTR UWB Receivers in Frequecy Selective Multipath Channels. In *IEEE Global*

Telecommunications Conference (GLOBECOM), volume 1, pages 1–6, November 2006.

[20] W. M. Lovelace and J. K. Townsend. The Effects of Timing Jitter and Tracking on the Performance of Impulse Radio. *IEEE J. Select. Areas in Commun.*, 20(9):1646–1651, Dec. 2002.

[21] Zhi Tian and G. B. Giannakis. BEP Sensitivity to Mistiming in Ultra-Wideband Impulse Radios - Part I: Nonrandom Channels. *IEEE Transactions on Signal Processing*, 53(4):1550–1560, April 2005.

[22] Zhi Tian and G. B. Giannakis. BEP Sensitivity to Mistiming in Ultra-Wideband Impulse Radios - Part II: Fading Channels. *IEEE Transactions on Signal Processing*, 53(5):1897–1907, May 2005.

[23] W. M. Lovelace and J. K. Townsend. Chip Discrimination for Large Near Far Power Ratios in UWB Networks. In *IEEE Military Communications Conference*, volume 2, pages 868–873, Oct. 2003.

[24] W. M. Lovelace and J. K. Townsend. Threshhold Discrimination and Blanking for Large Near Far Power Ratios in UWB Networks. *IEEE Transactions on Communications*, 53(9):1447–1450, Sept. 2005.

[25] Jon R. Ward and J. Keith Townsend. Chip Discrimination for UWB Impulse Radio Networks in Multipath Channels. In *IEEE Military Communications Conference (MILCOM)*, pages 1–6, Oct. 2007.

[26] Liping Li, J. Keith Townsend, and Robert Ulman. Performance of Transmitted Reference UWB Communications With Imperfect Power Control. In *IEEE Military Communications Conference (MILCOM)*, pages 1–7, Oct. 2007.

[27] Fernando Ramirez-Mireles. Performance of Ultra Wideband SSMA Using Time Hopping and M-ary PPM. *IEEE Journal on Selected Areas in Communications*, 19(6):1186–1196, June 2001.

[28] Reza Pasand, Saeed Khalesehosseini, John Nielsen, and Abu Sesay. Exact Evaluation of M-ary TH-PPM UWB Systems on AWGN Channels for Indoor Multiple-Access Communications. *IEE Proc.-Commun.*, 153(1):83–92, Feb. 2006.

[29] F. Ramirez-Mireles and R. A. Scholtz. Multiple-Access with Time Hopping and Block Waveform PPM Modulation. In *Proc. IEEE MILCOM '98*, volume 2, pages 529–533, 1998.

[30] Nikos V. Kokkalis, P. Takis Mathiopoulos, George K. Karagiannidis, and Christos S. Koukourlis. Performance Analysis of M-ary PPM TH-UWB Systems in the Presence of MUI and Timing Jitter. *IEEE Journal on Selected Areas in Communications*, 24(4):822–828, Aprial 2006.

[31] Relja Djapic, Geert Leus, Allen-Jan van der Veen, and Antonio Trindada. Blind Synchronization in Asynchronous UWB Networks Based on the Transmit-Reference Scheme. *EURASIP Journal on Wireless Communications and Networking*, pages 1–14, 2006.

[32] Liping Li, J. Keith Townsend, and Robert Ulman. Transmitted Reference Ultra-

Wideband Communications with M-ary PPM . In *IEEE Global Communications Conference (GLOBECOM)*, Dec. 2008.

[33] Robert. A. Scholtz. Multiple Access with Time-Hopping Impulse Modulation. In *Proc. IEEE MILCOM*, Oct. 1993.

[34] Jocelyn Fiorina and Walid Hachem. On the Asymptotic Distribution of the Correlation Receiver Output for Time-Hopped UWB Signals. *IEEE Transactions on Signal Processing*, 54(7):2529–2545, July 2006.

[35] A. R. Forouzan, M. N. Kenari, and J. A. Salehi. Performance Analysis of Time-Hopping Spread-Spectrum Multiple-Access Systems: Ucoded and Coded Schemes. *IEEE Transactions on Wireless Communications*, 1(4):671–681, Oct. 2002.

[36] Matteo Sabattini, Elias Masry, and Laurence B. Milstein. A Non-Gaussian Approach to the Performance Analysis of UWB TH-BPPM Systems. In *IEEE Conference on Ultra Wideband Systems and Technologies*, pages 52–55, Nov. 2003.

[37] Giuseppe Durisi and Giovanni Romano. On the Validity of Gaussian Approximation to Characterize the Multiuser Capacity of UWB TH PPM. In *IEEE Conference on Ultra Wideband Systems and Technologies*, pages 157–162, May 2002.

[38] Norman C. Beaulieu, Hua Shao, and Jocelyn Fiorina. P-Order Metric UWB Receivers Structures with Superior Performance. *IEEE Transactions on Communications*, 56(10):1666–1676, Oct. 2008.

[39] Dennis L. Goeckel and Qu Zhang. Slightly Frequency-Shifted Reference Ultra-

Wideband (UWB) radio. *IEEE Transactions on Communications*, 55(3):508–519, Mar. 2007.

[40] Qu Zhang and Dennis L. Goeckel. Multiple-Access Slightly Frequency-Shifted Reference Ultra-Wideband Communications for Dense Multipath Channels. In *IEEE International Conference on Communications*, pages 1083–1088, June 2007.

[41] T. Q. S. Quek, M. Z. Win, and D. Dardari. Unified Analysis of UWB Transmitted-Reference Schemes in the Presence of Narrowband Interference. *IEEE Transactions on Wireless Communications*, 6(6):2126–2139, June 2007.

[42] Y. D. Alemseged and K. Witrisal. Modeling and Mitigation of Narrowband Interference for Transmitted-Reference UWB Systems. *IEEE Journal of Selected Topics in Signal Processing*, 1(3):456–469, Oct. 2007.

[43] M. Di Renzo, F. Graziosi, and F. Santucci. A Framework for Computing Detection and False Alarm Probabilities for IR-UWB Transmitted-Reference Receivers over Generalized Fading Channels with Tone Interference. In *IEEE ISSSTA*, pages 297–302, Aug. 2008.

[44] Vincenzo Lottici, Aldo D'Andea, and Umberto Mengali. Channel Estimation for Ultra-Wideband Communications. *IEEE Journal on Selected Areas in Communications*, 20(9):1638–1645, Dec. 2002.

[45] S. Gezici, E. Fishler, H. Kobayashi, H.V. Poor, and A.F. Molisch. A Rapid Acquisition Technique for Impulse Radio. In *IEEE Pacific Rim Conference on Communications, Computers and Signal Processing*, volume 2, pages 627–630, Aug. 2003.

[46] D. J. Gargin. A Fast and Reliable Acquisition Scheme for Detecting Wide-Band Impulse Radio Signals in the Presence of Multi-Path and Multiple Access Interference. In *IEEE Conference on Ultra Wideband Systems and Technologies*, pages 106–110, 2004.

[47] A.M. Tonello and R. Rinaldo. A Time-Frequency Domain Approach to Synchronization, Channel Estimation, and Detection for DS-CDMA Impulse-Radio Systems. *IEEE Transactions on Wireless Communications*, 4(6):3018–3030, Nov. 2005.

[48] Xiliang Luo and Georgios B. Giannakis. Low-Complextiy Blind Synchronization and Demodulation for (Ultra-)Wideband Multi-User Ad Hoc Access. *IEEE Transactions on Wireless Communications*, 5(7):1930–1941, July 2006.

[49] Lin Wu, Vincenzo Lottici, and Zhi Tian. Maximum Likelihood Multiple Access Timing Synchronization for UWB Communications. *IEEE Transactions on Wireless Communications*, 7(11):4497–4501, November 2008.

[50] E.G. Strom, S. Parkvall, S.L. Miller, and B.E. Ottersten. Propagation Delay Estimation in Asynchronous Direct-Sequence Code-Division Multiple Access Systems. *IEEE Transactions on Communications*, 44(1):84–93, Jan 1996.

[51] Murat Torlak and Guanghan Xu. Blind Multiuser Channel Estimation in Asynchronous CDMA Systems. *IEEE Transactions on Signal Processing*, 45(1):137–147, January 1997.

[52] Stephen E. Bensley and Behnaam Aazhang. Subspace-Based Channel Estimation

for Code Division Multiple Access Communication Systems. *IEEE Transactions on Communications*, 44(8):1009–1020, Aug. 1996.

[53] Stephen E. Bensley and Behnaam Aazhang. Maximum-Likelihood Synchronization of a Single User for Code-Division Multiple-Access Communication Systems. *IEEE Transactions on Communications*, 46(3):392–399, March 1998.

[54] M. Win and R. A. Scholtz. Ultra-Wide Bandwidth Time-Hopping Spread-Spectrum Impulse Radio for Wireless Multiple-Access Communications. *IEEE Trans. Commun.*, 48(4):679–691, April 2000.

[55] Liping Li, J. Keith Townsend, and Robert Ulman. Multiple-Access Performance of Transmitted Reference UWB Communications with M-ary PPM. In *IEEE Global Communications Conference (GLOBECOM)*, Dec. 2008.

[56] Channel Modeling Sub-committee Report Final. Technical report, IEEE 802.15 SG3a, Nov. 2002.

[57] Andreas F. Molisch, Kannan Balakrishnan, Dajana Cassioli, Chia-Chin Chong, Shahriar Emami, Andrew Fort, Johan Karedal, Juergen Kunisch, Hans Schantz, Ulrich Schuster, and Kai Siwiak. IEEE 802.15.4a Channel Model - Final Report. Technical report, IEEE 802.15 TG4a, 2004.

[58] Minnie Ho, V. Srinivasa Somayazulu, Jeffrey Foerster, and Sumit Roy. A Differential Detector for an Ultra-wideband Communication System. In *IEEE Vehicular Technology Conference*, volume 4, pages 1896–1900, May 2002.

[59] John G. Proakis. *Digital Communications*. Mc Graw-Hill, Inc., 3rd edition, 1995.

[60] Sergio Verdu. *Multiuser Detection.* Cambridge University Press, New York, USA, 1 edition, 1998.

[61] Louis L. Scharf. The SVD and reduced rank signal processing. *Signal Processing,* 25(2):113–133, 1991.

[62] Bernard C. Levy. *Priciples of Signal Detection and Parameter Estimation.* Springer, 2008.

[63] Jack K. Holmes. *Coherent Spread Spectrum Systems*. John Wiley and Sons, 1982.

Appendices

APPENDIX A

Suppose the receiver front-end filter does not distort the signal $g^{(1)}(t) = p(t) * h^{(1)}(t)$, which can be written as

$$\begin{aligned} g^{(1)}(t) &= p(t) * h^{(1)}(t) && (.1) \\ &= X^{(1)} \sum_{l=0}^{L-1} \alpha^{(1)} p(t - \tau_l^{(1)}) && (.2) \end{aligned}$$

The expected energy of $g^{(1)}(t)$ can be calculated as

$$\begin{aligned} \mathop{\mathbb{E}}_{h}\{\varepsilon_1\} &= \mathop{\mathbb{E}}_{h}\left\{ \int_0^{T_I} (X^{(1)})^2 \sum_{l=0}^{L-1} \sum_{l_1}^{L-1} \alpha_l^{(1)} \alpha_{l_1}^{(1)} p(t - \tau_l^{(1)}) p(t - \tau_{l_1}^{(1)}) dt \right\} \\ &\approx \int_0^{T_I} \mathbb{E}\{(X^{(1)})^2\} \sum_{l=0}^{L-1} \mathbb{E}\left\{ \left(\alpha_l^{(1)}\right)^2 \right\} p^2(t - \tau_l^{(1)}) dt && (.3) \end{aligned}$$

The h under the expectation operator $\mathbb{E}$ means the expectation is with respect to the channel h. The approximation in (.3) is made by assuming an independent scattering pattern of the channel, resulting in $\mathbb{E}\{\alpha_l^{(1)} \alpha_{l_1}^{(1)}\} = 0$ for $l \neq l_1$. Suppose T_I is chosen such that almost all energy from the multipath components is collected. With the normalized channel energy ($\sum_{l=0}^{L-1} (\alpha_l^{(1)})^2 = 1$) and the assumption of $\mathbb{E}\{(X^{(1)})^2\} = 1$, we obtain $\mathbb{E}_h\{\varepsilon_1\} = \varepsilon_p = \int_0^{T_p} p^2(t) dt = 1/N_s$.

APPENDIX B

In one symbol (except symbol $i = 0$), N_s correlations are computed and summed to form the decision statistic D_d for DTR receivers. Consider symbol $i = 1$. For easy illustration, denote the signal and noise in the jth frame as g_j and n_j respectively. Here g_j is the channel response of the pulse $p(t)$ and n_j is the jth section of the noise process $n(t)$ defined in Section 2.2.2. The signal and noise terms are shown in Fig. .1 where $g_{-1} + n_{-1}$ from previous symbol is the template for $g_0 + n_0$.

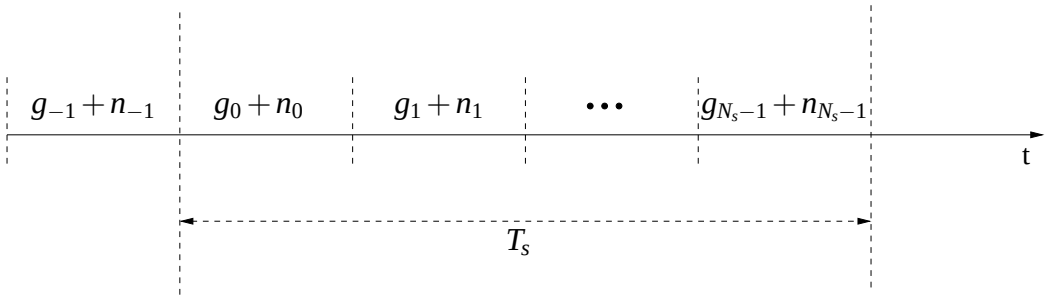

Figure .1: Noise in DTR receivers

Adding the signal $\times$ noise terms from the first two correlations, we have

$$n_d(0) + n_d(1) = g_0 n_{-1} + g_{-1} n_0 + g_1 n_0 + g_0 n_1 \tag{.4}$$

We already see from (.4) that n_0 is used twice. Invoking the assumption that the channel is approximately constant during consecutive symbols, we have $g_{-1} = g_1$. Therefore, the

noise terms are coherently combined, yielding

$$n_d(0) + n_d(1) = g_0 n_{-1} + 2g_1 n_0 + g_0 n_1 \tag{.5}$$

Among the N_s correlations, there are $2N_s$ signal $\times$ noise terms and $2N_s - 2$ of such terms are coherently combined, producing $N_s - 1$ noise signals like the term $2g_1 n_0$ in (.5). The exceptions are the edge noise terms n_{-1} and n_{N_s-1} which only contribute once in forming the decision statistic. The variance of the signal $\times$ noise term n_d is thus given by

$$\begin{aligned} \sigma_d^2 &= (N_s - 1)\left(\frac{E^{(1)}}{N_s}\right) 4\left(\frac{N_0}{2}\right) + 2\left(\frac{E^{(1)}}{N_s}\right)\left(\frac{N_0}{2}\right) \\ &= \frac{2N_s - 1}{N_s} E^{(1)} N_0 \end{aligned} \tag{.6}$$

Note that the symbol energy $E^{(1)}$ is not shown in the derivations until (.6) for easy of illustration.